MIN3P-THCm

A Three-dimensional Numerical Model for Multicomponent Reactive Transport in Variably Saturated Porous Media

Theory Manual

(Draft)

K. Ulrich Mayer, Mingliang Xie and Danyang Su

University of British Columbia

Department of Earth, Ocean and Atmospheric Sciences

Vancouver, BC, Canada V5T 2M1

Kerry MacQuarrie

University of New Brunswick

Department of Civil Engineering

Fredericton, N.B., Canada E3B 5A3

August, 2018

COPYRIGHT NOTICE AND USAGE LIMITATIONS

DISCLAIMER

ACKNOWLEDGEMENTS

The author would like to thank Shawn G. Benner (University of Waterloo, now at Idaho State University, Boise, ID), Frederic Gerard (Eco&Sols, UMR1222, INRA/IRD/SupAgro, Montpellier, France), Sergio Andres Bea (UBC, now at CONICET, IHLLA-Large Plains Hydrology Institute, Buenos Aires, Argentina), and Tom Henderson (UBC, now at Montana Department of Environmental Quality, Helena, MT) for their contributions to earlier versions of this User's Guide.

ABSTRACT

The MIN3P-THCm code is developed as a multicomponent reactive transport model for variably-saturated porous media in one, two or three spatial dimensions with the extension of heat transport, one dimensional hydromechanical coupling, multicomponent diffusion and reactive transport in highly saline solution. Advective-dispersive transport in the aqueous phase, as well as diffusive gas transport can be considered. Darcy velocities are calculated internally using a variably-saturated flow module. The model formulation for reactive transport is based on the global implicit solution approach, which considers reaction and transport processes simultaneously. This formulation enforces a global mass balance between solid, surface, dissolved and gaseous species and thus facilitates the investigation of the interactions of reaction and transport processes. The model can also be used as a batch model for equilibrium speciation problems, kinetic batch problems or for the generation of pC-pH-diagrams.

MIN3P-THCm is characterized by a high degree of flexibility with respect to the definition of the geochemical reaction network to facilitate the application of the model to a wide range of hydrogeological and geochemical problems. Chemical processes included are homogeneous reactions in the aqueous phase, such as complexation and oxidation-reduction reactions, as well as heterogeneous reactions, such as ion exchange, surface complexation, mineral dissolution-precipitation and gas exchange reactions. Reactions within the aqueous phase and dissolution-precipitation reactions can be considered as equilibrium or kinetically-controlled processes.

A new, general framework for kinetically-controlled intra-aqueous and mineral dissolution-precipitation reactions was developed. All kinetically-controlled reactions can be described as reversible or irreversible reaction processes. Different reaction mechanisms for dissolution-precipitation reactions are considered, which can be subdivided into surface- and transport-controlled reactions. This approach allows the consideration of a large number of rate expressions reported in the literature. Related reaction and rate parameters can be incorporated into the model through an accompanying database. The model is primarily designed for problems involving inorganic chemistry, but reactions involving organic chemicals can also be accommodated. Microbially-mediated reactions can be described using a multiplicative Monod approach.

Parallelization of MIN3P-THCm (ParMIN3P-THCm) was achieved through the domain decomposition method based on PETSc (Portable Extensible Toolkit for Scientific Computation) libraries (Balay et al. 1997; Balay et al. 2014a; Balay et al. 2014b).

Contents

LIST OF TABLES

Page

LIST OF FIGURES

Page

1 BACKGROUND: MIN3P-THCM VERSION 1.0

1.1 PROBLEM DEFINITION

Subsurface fluid migration and geochemical conditions may be impacted by a variety of interacting physical and chemical processes, including density-dependent, variably-saturated groundwater flow, heat transport, mass transport, mixing of waters of different geochemical compositions, water-rock interaction, and mechanical loading. Understanding the interactions among these processes is important when investigating contaminant migration in groundwater, natural attenuation processes, or site remediation alternatives, and when assessing the long-term hydrogeological and geochemical stability of rock formations. MIN3P-THCm is a three-dimensional (3D) numerical model that has been developed to simulate the processes that are most relevant to these types of subsurface flow and reactive transport problems.

1.2 SOFTWARE HISTORY

MIN3P-THCm and its precursors have enjoyed widespread acceptance by academic researchers and environmental professionals since the release of the original version of the code (MIN3P) in 1999. The development history of the code is briefly outlined below:

1999: Initial development of MIN3P at the University of Waterloo by U. Mayer as part of his Ph.D. thesis (Mayer, 1999; Mayer et al, 2002). At that time, the code was able to simulate multicomponent reactive transport in variably-saturated porous media. The applications of the code included the generation and fate of acid mine drainage in unsaturated porous media, the in-situ remediation of groundwater contaminated by inorganic (e.g. hexavalent chromium) and organic contaminates (e.g. chlorinated organic compounds).

2006: Dual porosity model (MIN3P-DUAL) added by L. Cheng, (PhD work at University of Sheffield, UK) (Cheng 2006). This model was used in the assessment of the fate and transport of MTBE in a Chalk aquifer. These functions have not; however, been carried forward into the current version of MIN3P-THCm.

2006: Gas exsolution, entrapment and release model (MIN3P-BUBBLE) incorporated by R. Amos (PhD work at the University of British Columbia; Amos and Mayer, 2006). The problems investigated with this version of the code were primarily related to bubble growth and contraction due to in-situ gas production or consumption, bubble entrapment due to water table rise and subsequent re-equilibration of the bubble with ambient groundwater, and permeability changes due to trapped gas phase saturation. These functions have not; however, been carried forward into the current version of MIN3P-THCm.

2007: Multicomponent gas phase diffusion and advection model (MIN3P-DUSTY) added by S. Molins at the University of British Columbia (Molins and Mayer, 2007). The model was used to simulate gas attenuation in partially saturated landfill soil covers, methane production, and oxidation in aquifers contaminated by organic compounds (e.g. an oil spill site) and pyrite oxidation in mine tailings. These functions have not, however, been carried

forward into the current version of MIN3P-THCm.

2009: Density coupling between flow and reactive transport included by T. Henderson as part of his Ph.D. thesis at the University of British Columbia. This code version was named MIN3P-D (Henderson et al., 2009) and was used to simulate permanganate-based remediation under free convection conditions, considering contaminant treatment, and geochemical reactions including the oxidation of naturally occurring organic matter (e.g. DNAPL) using the oxidant ($KMnO_4$), mineral dissolution and precipitation, and ion exchange reactions.

2012: Pitzer equations for activity corrections, energy balance, and a formulation for 1D vertical stress were implemented by Bea et al. (2011, 2012). The resulting code was renamed to MIN3P-THCm.

2013: Great care had been taken during the development of MIN3P-THCm through continued verification and re-verification of all functions. These procedures were further formalized in 2013 by introducing quality control and management procedures in-line with NWMO's requirements. These procedures include documentation, verification, and full version control of MIN3P-THCm.

2014: Multicomponent diffusion to account for the species dependent diffusion coefficient and to maintain local charge balance and multisite ion exchange models were implemented by Rasouli and Xie (Xie et al. 2015; Rasouli, 2016). The code is also parallelized using domain decomposition methods (Su et al. 2015).

In recent years, the code has been used to evaluate redox stability in crystalline rocks of the Canadian shield (Spiessl et al., 2009), to simulate groundwater flow and reactive transport in a hypothetical sedimentary basin subject to a single glaciation/deglaciation event (Bea et al., 2011), to simulate the in-situ borehole diffusion experiments at the Mont Terri underground laboratory (Xie at al. 2014b), to simulate the laboratory experiments of contaminant migration in compacted bentonite (Xie et al. 2014a) and to simulate the reactive transport benchmarks provided by the international SSBENCH community (Steefel et al., 2015; Xie et al. 2015a; Molins et al. 2015; Rassouli e al. 2015; Alt-Epping et al. 2015; Greskowiak et al. 2015, Mayer et al. 2015; Marty et al. 2015; Şengör et al. 2015; Perko et al. 2015).

1.3 OPERATING REQUIREMENTS

MIN3P-THCm is written in FORTRAN 90/95 and can be compiled using the Intel Visual FORTRAN® compiler. Executable files for Microsoft Corporation's Windows as well as Linux operating systems can be generated. The executable file will run without modification on any Microsoft Windows® based PC with sufficient RAM. The output files are in ASCII format. Most output can be viewed using Tecplot postprocessing software developed by Tecplot Inc. (Tecplot, 2005). Section 2 of this documentation describes the governing equations that are solved by MIN3P-THCm.

1.4 REQUIREMENTS SPECIFICATION

MIN3P-THCm is required to solve three-dimensional, variably-saturated, subsurface groundwater flow problems, with coupling to non-reactive and reactive solute transport, heat transport, and one-dimensional hydromechanical coupling. Mass transport processes that must be included are solute transport through advection, dispersion and molecular diffusion. Capabilities must include the ability to simulate solute interactions with the solid phase, such as ion exchange and mineral dissolution-precipitation reactions that affect the groundwater and rock composition, and with the gas phases, such as gas dissolution-exsolution, gas generation and migration. Other requirements include the ability to simulate: mineral dissolution- and precipitation-induced modifications to media properties (e.g. porosity and permeability), possibly providing a feedback to fluid flow; kinetic reactions in the aqueous and solid phases; density-dependent flow; geochemical reactions under highly saline and/or non-isothermal conditions. A detailed description of the governing equations is provided in section 2.1 of this document.

1.5 CAPABILITIES

MIN3P-THCm applies the finite volume approach to solve the Richards equation governing 3D unsaturated/saturated subsurface flows. For the reactive mass transport, the code uses the direct substitution approach (DSA) and employs the global implicit method (GIM) for solution of the multicomponent advection-dispersion equations and the geochemical reactions, which considers reaction and transport simultaneously. Spatial discretization is performed based on the finite volume method and allows conducting simulations in one, two, and three spatial dimensions. To maximize versatility, the model formulation includes a generalized framework for kinetically controlled reactions, which can be specified through a database together with equilibrium processes. The general kinetic formulation includes intra-aqueous and dissolution-precipitation reactions in addition to geochemical equilibrium expressions for hydrolysis, aqueous complexation, oxidation-reduction, ion exchange, surface complexation, and gas dissolution-exsolution reactions. The generalized approach allows consideration of fractional order terms with respect to any dissolved species in terms of species activities or in terms of total concentrations, which facilitates the incorporation of a variety of experimentally derived rate expressions. Monod and inhibition terms can be used to describe microbially mediated reactions or to limit the reaction progress of inorganic reactions. Dissolution-precipitation reactions can be described as surface-controlled or transport-controlled reactions. The formulation also facilitates the consideration of any number of parallel reaction pathways, and reactions can be treated as irreversible or reversible processes. Section 2.2 of this document outlines in more detail the approaches taken for the numerical implementation of the governing equations.

In terms of simulation capability and computational aspects, the code MIN3P-THCm has the following features:

Fluid flow

- 3D unsaturated/saturated single-phase flow

- Transient or steady-state flow
- Coupling of fluid density and viscosity to temperature and/or solute concentration variations
- Free atmospheric boundary conditions
- Physically-based accounting of all components of the subsurface water and gases budget (e.g. gas dissolution/exsolution, evaporation)
- Flow in porous, fractured, and heterogeneous media
- Injection and pumping of fluid

Bio-geochemical Reactions

- Equilibrium reactions including aqueous complexation, gas partitioning between phases, oxidation-reduction, (multisite) ion exchange, and surface complexation
- Kinetically controlled intra-aqueous and dissolution-precipitation reactions
- Dissolution of non-aqueous phase liquids (e.g. NAPLs)
- Pitzer equations for activity corrections and fluid density calculations in highly saline solutions
- Microbially mediated degradation reactions

Heat transport

- Heat transport through the liquid and solid phases in unsaturated/saturated porous media
- Heat transport by convection, conduction and thermal dispersion

Reactive transport

- Advective-diffusive transport in the water phase
- Advective-diffusive transport in the gas phase
- Vapor transport
- Multicomponent non-reactive and reactive transport under saturated/unsaturated conditions in a subsurface flow field
- Coupling and feedback mechanisms between chemical reactions and physical processes involving fluid flow (e.g. concentration dependent density) and/or porous media evolution (e.g. mineral dissolution-precipitation induced porosity and permeability changes)
- Multicomponent diffusion

One-dimensional hydromechanical coupling

- Fluid pressure change due to uniform vertical loads (i.e. loading/unloading due to glaciation)

Numerical methods

- The global implicit method (GIM) and finite volume method (FVM) spatial discretization approach used by the code provides a robust and locally mass-conservative solution scheme
- Fluid and solute mass balance tracking
- Adaptive time-stepping schemes with automatic generation and control of time steps

- Robust and efficient ILU-preconditioned iterative sparse-matrix solver
- Robust and efficient Newton-Raphson linearization

Parallelization of MIN3P-THCm (ParMIN3P-THCm) was achieved through the domain decomposition method based on PETSc (Portable Extensible Toolkit for Scientific Computation) libraries (Su et al. 2016). PETSc is also used as the parallel solver package, and for data structure and message communication. A hybrid MPI and OpenMP parallel programming approach is implemented in the code to take advantage of leadership-class supercomputers that combine both shared memory and distributed memory architectures.

1.6 LIMITATIONS

Version 1.0 of MIN3P-THCm has the following limitations:

- The code cannot simulate coupled hydromechanical deformation. The loading/unloading function is limited to scenarios with purely vertical uniform strain.
- The code cannot simulate the non-isothermal multiphase flow. Gas pressure is considered to be constant for the unsaturated flow simulations and has no effect on the solution of water flow.
- Changes of material properties (e.g. hydraulic conductivity, thermal conductivity) because of ice formation or melting within the porous media are currently not coupled with heat transport.
- NAPL and biomass phases are immobile.
- Multicomponent diffusion model to account for the species dependent diffusion coefficient and to maintain local charge balance is only valid for the aqueous phase.
- The isotope code is not currently capable of simulating isotope partitioning due to intra-aqueous kinetic reaction.

1.7 DOCUMENTATION

This theoretical manual describes the physical, geochemical and mathematical concepts underlying MIN3P-THCm and the implementation in the numerical model. In addition, the user's manual provides the user with instructions and guidance on the application of the code including examples for batch reactions, groundwater flow, reactive transport, and density dependent flow and energy balance problems. The verification and demonstration reports provide benchmarks that are compared to numerical analytical solutions or to results calculated by other code(s), or test examples to demonstrate the functions of the code.

This document is organized into five chapters as outlined below.

Chapter 2 presents the mathematical theory which describes the various physical and chemical processes included in the model (Section 2.1), and shows how it is implemented in the MIN3P-THCm code (Section 2.2).

Other documents which may be of interest include the following NWMO reports:

Spiessl, S.M., K.U. Mayer and K.T.B. MacQuarrie (2009). Reactive Transport Modelling in Fractured Rock – Redox Stability Study, Technical report: NWMO TR-2009-04.

Bea, S.A., K.U. Mayer, K.T.B. MacQuarrie (2011). Modelling Reactive Transport in Sedimentary Rock Environments - Phase II MIN3P-NWMO code enhancements and illustrative simulations for a glaciation scenario. Technical report: NWMO TR-2011-13.

Xie, M., P. Rasouli, K.U. Mayer and K.T.B. MacQuarrie (2015). MIN3P-THCm Code Enhancements for Reactive Transport Modelling in Low Permeability Media, NWMO Technical Report, NWMO-TR-2015-12 October 2015.

Xie, M., P. Rasouli, K.U. Mayer and K.T.B. MacQuarrie (2014). Reactive Transport Modelling in Low Permeability Media – MIN3P-THCm Simulations of EBS TF-C Compacted Bentonite Diffusion Experiments, NWMO Technical Report, NWMO-TR-2014-23, December 2014.

Xie, M., P. Rasouli, K.U. Mayer and K.T.B. MacQuarrie (2014). Reactive Transport Modelling of In-situ Diffusion Experiments for the Mont Terri Project -- MIN3P-THCm Code Enhancement and Numerical Simulations, NWMO Technical Report, NWMO-TR-2014-25, December 2014.

Su, D., K.U. Mayer and K.T.B. MacQuarrie (2015). MIN3P-THCm Parallel Computing Implementation, NWMO Technical Report, NWMO-TR-2015-23.

and the following journal articles and PhD theses:

Bea, S.; Wilson, S.; Mayer, K.; Dipple, G.; Power, I. & Gamazo, P. (2012). Reactive transport modeling of natural carbon sequestration in ultramafic mine tailings Vadose Zone Journal, 11(2), 1-17

Henderson, T. (2009). Numerical modeling of density-driven chemical oxidation of chlorinated solvents, Ph.D. – thesis, Department of Earth and Ocean Sciences, the University of British Columbia, Vancouver, British Columbia, Canada.

Henderson, T., K.U. Mayer, B. Parker and T. Al. (2009). Three-dimensional density-dependent flow and multicomponent reactive transport modeling of chlorinated solvent oxidation by potassium permanganate. Journal of Contaminant Hydrology, 106, 195-211.

Jurjovec, J., D. W. Blowes, C. J. Ptacek, and K. U. Mayer (2004). Multicomponent reactive transport modeling of acid neutralization reactions in mine tailings, Water Resources Research, 40, W11202, doi:10.1029/2003WR002233.

Mayer, K.U. (1999). A numerical model for multicomponent reactive transport in variably-saturated porous media, Ph.D. – thesis, Department of Earth Sciences, University of Waterloo, Waterloo, Ontario, Canada.

Mayer, K.U., Blowes, D.W. and Frind, E.O., (2001). Reactive transport modeling for the treatment of an in situ reactive barrier for the treatment of hexavalent chromium and trichloroethylene in groundwater. Water Resources Research, 37:3091-3103. doi:10:1029/2001WR000862.

Mayer, K.U., Benner, S.G., Frind, E.O., Thornton, S.F., Lerner, D.N., (2001). Reactive

transport modeling of processes controlling the distribution and natural attenuation of phenolic compounds in a deep sandstone aquifer. Journal of Contaminant Hydrology 53 (2001) 341-363.

Mayer, K.U., Frind, E.O., Blowes, D.W., (2002). Multicomponent reactive transport modeling in variably-saturated porous media using a generalized formulation for kinetically controlled reactions. Water Resources Research, Vol. 38, No. 9.

Mayer, K.U. and K.T.B. MacQuarrie (2010). Solution of the MoMaS reactive transport benchmark with MIN3P - model formulation and simulation results, Computational Geosciences 14:405-419.

Bea, S.A., K.U. Mayer and K.T.B. MacQuarrie (2016). Reactive transport and thermo-hydro-mechanical coupling in deep sedimentary basins affected by glaciation cycles: model development, verification, and illustrative example, Geofluids, 16, 279–300

Rasouli, P. (2016). The role of multicomponent diffusion and electrochemical migration for reactive transport in porous media, PhD-thesis, University of British Columbia, in progress.

2 THEORY MANUAL

The conceptual models implemented in MIN3P-THCm can be described in mathematical form by three sets of governing equations: one for groundwater flow under partially saturated conditions (Richards equation) or variable density flow; one for multicomponent reactive transport in variably saturated media; and one for energy balance (i.e. heat storage and transport). MIN3P-THCm's reactive transport equations are based on the global implicit solution method (Steefel and Lasaga, 1994) in combination with a direct substitution approach to minimize the number of primary dependent variables (Yeh and Tripathi, 1989). The reaction network is described by a partial-equilibrium approach (Lichtner, 1985; Sevougian et al., 1993; Steefel and Lasaga, 1994), implying that geochemical reactions that are fast in comparison to transport processes are described by equilibrium relationships, while the generalized formulation for kinetic reactions is employed for reactions characterized by timescales longer than the transport timescales (Bahr and Rubin, 1987; Knapp, 1989; Lichtner, 1993; Steefel and MacQuarrie, 1996). This chapter summarizes the main mathematical formulations and numerical methods based on previously published work (e.g. Mayer 1999; Mayer et al. 2002; Henderson 2009; Mayer and MacQuarrie 2010; Bea et al. 2011).

2.1 MATHEMATICAL FORMULATION

2.1.1 VARIABLY SATURATED GROUNDWATER FLOW EQUATION

The general mass conservation equation for groundwater flow can be written as (Neuman, 1973; Panday et al., 1993)

$$\frac{\partial}{\partial t}(S_a \phi \rho_a) + \nabla \cdot (\rho_a \mathbf{q_a}) = \rho_a Q_a \qquad \text{Equation 2-1}$$

where t is time in [T], ϕ is the porosity [L^3 void L^{-3} bulk], S_a is the saturation of the aqueous phase [L^3 H_2O L^{-3} void], ρ_a being the aqueous phase density [M L^{-3}], Q_a is a source-sink term [T^{-1}], where a positive quantity defines the injection of water, $\mathbf{q_a}$ is the specific discharge vector [L T^{-1}] given by

$$\mathbf{q_a} = \frac{-k_{ra}\,\mathbf{k}}{\mu_a}(\nabla P_a + \rho_a g \nabla z) \qquad \text{Equation 2-2}$$

where P_a is the fluid pressure [M L^{-1} T^{-2}], z is the elevation with respect to datum [L], k_{ra} is the relative permeability of the porous medium with respect to the aqueous phase [-],g [L T^{-2}] is the gravitational acceleration, μ_a [M L^{-1} T^{-1}] is the aqueous phase viscosity, and $\mathbf{k}$ is the intrinsic permeability tensor [L^2] (Bear, 1972). The fluid mass conservation equation for density dependent flow in variably-saturated media can be obtained by combining Equation 2-1 and Equation 2-2:

$$\frac{\partial}{\partial t}(S_a \phi \rho_a) - \nabla \cdot \left(\rho_a \frac{k_{ra}\,\mathbf{k}}{\mu_a}(\nabla P_a + \rho_a g \nabla z) \right) = \rho_a Q_a \qquad \text{Equation 2-3}$$

Under constant fluid density and isothermal conditions, using hydraulic head as the primary dependent variable and adopting the assumptions defined by Neuman (1973) and Huyakorn et al. (1984) (incompressible fluid, no hysteresis, passive air phase), the mass conservation equation (Equation 2-3) for the aqueous phase can be simplified as (Neuman, 1973; Panday et al., 1993; Mayer 1999)

$$S_a S_s \frac{\partial h}{\partial t} + \phi \frac{\partial S_a}{\partial t} - \nabla \cdot [k_{ra} \mathbf{K} \nabla h] - Q_a = 0 \qquad \text{Equation 2-4}$$

where S_s defines the specific storage coefficient [L^{-1}], h is hydraulic head [L], $\mathbf{K} = (\frac{\rho_a g \mathbf{k}}{\mu_a})$ is the hydraulic conductivity tensor [$L\ T^{-1}$].

The nonlinear relationships between aqueous-phase saturation S_a, relative permeability k_{ra}, and aqueous-phase pressure head $\psi_a = h - z$ (with h being the hydraulic head [L]) is expressed by the standard soil hydraulic functions given by Wösten and van Genuchten (1988):

$$S_a = S_{ra} + \frac{1 - S_{ra}}{(1 + \alpha \psi_a^n)^m} \qquad \text{Equation 2-5}$$

$$k_{ra} = S_{ea}^l \left[1 - \left(1 - S_{ea}^{\frac{l}{m}}\right)^m\right]^2 \qquad \text{Equation 2-6}$$

where S_{ra} defines the residual saturation of the aqueous phase, α, n, m and l are soil hydraulic function parameters, with $m = 1 - 1/n$, S_{ea} is the effective saturation of the aqueous phase defined by

$$S_{ea} = \frac{S_a - S_{ra}}{1 - S_{ra}} \qquad \text{Equation 2-7}$$

The gas phase saturations S_g can be calculated based on the water phase saturations S_a obtained from solution of Equation 2-4:

$$S_g = 1 - S_a \qquad \text{Equation 2-8}$$

MIN3P-THCm has the capability for density-dependent flow simulation. The dependence of fluid density on solute concentrations results in the coupling between the movement of fluids and the migration of dissolved species (Voss and Souza, 1987; Oldenburg and Pruess, 1995; Diersch and Kolditz, 2002) and temperature (Voss and Provost, 2008). The density-driven flow formulation implemented in MIN3P-THCm is based on MIN3P-D (Henderson et al., 2009).

The fluid mass accumulation term in Equation 2-1 includes temporal changes in fluid pressure, saturation, the total solute concentration and the temperature (Henderson 2009):

$$\frac{\partial}{\partial t}(S_a \phi \rho_a) = S_a \rho_a S_p \frac{\partial P_a}{\partial t} + \rho_a \phi \frac{\partial S_a}{\partial P_a}\frac{\partial P_a}{\partial t} + S_a \phi \frac{\partial \rho_a}{\partial TDS}\frac{\partial TDS}{\partial t} + S_a \phi \frac{\partial \rho_a}{\partial \mathrm{T}}\frac{\partial \mathrm{T}}{\partial t} \qquad \text{Equation 2-9}$$

In which TDS is the concentration of the total dissolved solids [$M\ L^{-3}$]:

$$TDS = \sum_{i=1}^{N_c} MW_i \, T_i^a \qquad \text{Equation 2-10}$$

Where MW_i is the molecular weight of each component [M mol^{-1}], T_i^a is the total aqueous component concentration for component A_i^c [mol L^{-3} H_2O], and N_c is the number of aqueous components. S_p is the intrinsic specific storage coefficient [M^{-1} L T^2] defined with respect to changes in fluid pressure, it is related to the specific storage coefficient S_s by the following relationship:

$$S_p = \frac{S_s}{\rho_a g} \qquad \text{Equation 2-11}$$

2.1.1.1 Fluid density and viscosity

The relationship between aqueous phase fluid density and solute concentrations has been determined for mixtures of brines, seawater, and freshwater (Millero, 1982), and is typically modelled using empirical relationships (e.g. Frind, 1982; Voss, 1984; Kharaka et al., 1988; Guo and Langevin, 2002; Oldenburg and Pruess, 1995; Frolkovic and Schepper, 2001).

The aqueous phase fluid density (ρ_a) in Equation 2-1 and Equation 2-2 is computed as a function of temperature and concentrations using:

$$\rho_a = \rho_0 + \Delta\rho_C + \Delta\rho_T \qquad \text{Equation 2-12}$$

where ρ_0 is the reference density (e.g. density of pure water at 25 ^{o}C) [M L^{-3}], and $\Delta\rho_C$ and $\Delta\rho_T$ are the density changes due to concentration and temperature, respectively [M L^{-3}].

A commonly employed approach treats fluid density change as a linear function of TDS (total dissolved solids) (Frind, 1982; Voss, 1984; Kharaka et al., 1988; Guo and Langevin, 2002, Henderson et al., 2009):

$$\Delta\rho_C = \frac{\partial\rho_a}{\partial TDS} TDS \qquad \text{Equation 2-13}$$

where $\partial\rho_a / \partial TDS$ [-] is assumed to be constant. Reported values for the constant $\partial\rho_a / \partial TDS$ are 0.688 and 0.714 for geochemical modelling of seawater-freshwater interactions (Kharaka et al., 1988; Guo and Langevin, 2002).

The linear relationship between density and *TDS* is typically assumed when NaCl dominates the salinity (e.g. seawater). However, the presence of $CaCl_2$-enriched brines requires a more sophisticated model for density calculations because density will depend on the elemental composition of the fluids (e.g. McIntosh et al., 2011). MIN3P-THCm allows for the computation of $\Delta\rho_C$ in Equation 2-12 using a non-linear relationship with respect to concentrations. For instance, $\Delta\rho_C$ can be computed as the difference between a

reference density and a density calculated based on Pitzer's equations according to Monnin (1994), implemented following Bea et al. (2010). In this case, density calculations are based on the total volume of the solution that contains 1 kg of water (υ) (Monnin, 1994):

$$V = V_{id} + V_{ex} = 1000\,\upsilon_w + \sum_i m_i \bar{V}_i^o + V_{ex} \qquad \text{Equation 2-14}$$

where V_{id} is the ideal volume based on the molar volume of solutes and V_{ex} represents the total excess volume of a multicomponent electrolyte solution. υ_W is the specific volume of pure water ($L^3\ M^{-1}$), m_i is the molality of the i^{th} aqueous species [mol M^{-1}], and $\bar{V}_i^o$ is the standard partial volume of the solute i (L^3 mol^{-1}). The term V_{ex} in Equation 2-14 can be expressed as a virial expansion of the solute molalities:

$$\frac{V_{ex}}{RT} = f_{DH}^{v}(I) + 2\sum_c \sum_a m_c m_a \left(B_{ca}^{v} + \left(\sum_c m_c z_c \right) C_{ca}^{v} \right) \qquad \text{Equation 2-15}$$

In this expression, R is the ideal gas constant, T the absolute temperature [Θ, in K], m_c the molality of cation c (of charge z_c), and m_a that of anion a. $f_{DH}^{v}(I)$ is the Debye-Hückel term that is a function of the ionic strength, and B_{ca}^{v} and C_{ca}^{v} are the second virial coefficients for the volume that accounts for the interactions among ions. A detailed description of the formulation for fluid density as a function of solution composition is provided in Appendix B.4 in Bea et al. (2011).

In MIN3P-THCm the dependence of density on temperature, $\Delta\rho_T$ in Equation 2-12, can be computed using linear or non-linear relationships. For instance, a linear approximation can be expressed as:

$$\Delta\rho_T \approx \frac{\partial\rho}{\partial T}\Delta T \qquad \text{Equation 2-16}$$

where $\partial\rho/\partial T$ [M L^{-3} Θ^{-1}] is a constant, and ΔT is the temperature change with respect to the reference temperature of the reference density ρ_0. The reference density is typically defined at 25 °C. Alternatively, $\partial\rho/\partial T$ in Equation 2-16 can be computed based on a non-linear relationship.

Groundwater flow as described by the pressure-based form of Darcy's equation (Equation 2-2) is a function of dynamic viscosity (μ_a), which also depends on concentration and temperature according to:

$$\mu_a = \mu_f\, f_T^{\mu}\, f_C^{\mu} \qquad \text{Equation 2-17}$$

where μ_f is the reference viscosity [M L^{-1} T^{-1}] of a reference water with temperature T_f [Θ] and concentration C_f [M L^{-3}], and f_T^{μ} [-] and f_C^{μ} [-] are the correction terms to account

for deviations from reference conditions as a function of temperature and concentration, respectively. These terms are empirically defined and can be computed as (e.g. see Lever and Jackson, 1985; Diersch and Kolditz, 2002):

$$f_C^{\mu} = \frac{1+1.85\omega-4.1\omega^2+44.5\omega^3}{1+1.85\omega_f-4.1\omega_f^2+44.5\omega_f^3} \qquad \text{Equation 2-18}$$

$$f_T^{\mu} = \frac{1+0.7063\,\sigma_f-0.04832\,\sigma_f^3}{1+0.7063\,\sigma-0.04832\,\sigma^3} \qquad \text{Equation 2-19}$$

where ω and ω_f are the solute mass fractions in the fluid for the actual and reference viscosities, respectively, and $\sigma=(T-150)/100$, with T provided in units of ^{o}C. Alternatively, the viscosity-temperature dependence (f_T^{μ}) can be computed based on the expression presented by Voss and Provost (2008):

$$f_T^{\mu} = \frac{10^{\left(\frac{248.37}{T+133.15}\right)}}{10^{\left(\frac{248.37}{T_f+133.15}\right)}} \qquad \text{Equation 2-20}$$

where T_f is the temperature [Θ] of the reference water, with T provided in units of ^{o}C. The temperature corrections presented in Equations 3.11 and 3.12 are both implemented in MIN3P-THCm. If viscosity is assumed constant, then f_T^{μ} and f_C^{μ} in Equation 2-17 are approximated as unity.

2.1.2 VADOSE ZONE FLOW WITH VAPOUR DIFFUSION

Vadose zone flow and vapour diffusion are implemented as follows (Philip and De Vries, 1957; Saito et al., 2006; Bea et al. 2012):

$$\frac{\partial(\phi S_a\rho_a)}{\partial t}+\frac{\partial(\phi S_v\rho_v)}{\partial t}=\nabla\cdot q_a+\nabla\cdot q_v+f_a\xi \qquad \text{Equation 2-21}$$

Where S_v is the vapour saturations [-], ρ_v is the vapour density [M L^{-3}], q_v is the vapour fluxes, [M L^{-2} T^{-1}], f_a is a source/sink term, and ξ is a constant that relates the surface area on the boundary with the volume of the porous medium [L^2 L^{-3}].

The water flux ρ_a is calculated using a modified version of Darcy's law, which incorporates a thermal hydraulic conductivity term (Noborio et al., 1996; Saito et al., 2006; Sakai et al., 2009).

$$q_a = -\rho_a\frac{Kk_r}{\mu_a}\left[(\nabla P_a+\rho_a g)+G_{at}\frac{P_a}{\gamma_0}\frac{\partial\gamma}{\partial T}\nabla T\right] \qquad \text{Equation 2-22}$$

Where, G_{at} is the gain factor that quantifies the temperature dependence of the soil water retention curve [-], γ and γ_0 are the water surface tension and reference water surface tension at 25 °C (71.89 gr s^{-2}) [M T^{-2}], respectively, and T is temperature (°C). A key aspect implied by this equation is that a water flux may be driven by both pressure and temperature gradients.

The water surface tension is a function of temperature and is calculated as (Saito et al., 2006; Sakai et al., 2009):

$$\gamma = 75.6 - 0.1425T - 2.38 \cdot 10^{-4}T^2 \qquad \text{Equation 2-23}$$

The liquid density is dependent on both solution composition and temperature (Equation 2-12).

The vapour flux is calculated according to:

$$\nabla \cdot q_v = \nabla \cdot \phi S_v \tau_v D_w \nabla \rho_v = \nabla \cdot \phi S_v \tau_v D_w \left(\eta \frac{\partial \rho_v}{\partial T} \nabla T + \frac{\partial \rho_v}{\partial P_l} \nabla P_a \right) \qquad \text{Equation 2-24}$$

Where τ_v is the tortuosity factor [-] calculated after Millington (1959), D_w is the vapour diffusion coefficient [L^2 T^{-1}], and η [-] is an enhancement factor to account for the increased thermal vapour flux due to liquid islands and increased temperature gradients in the air (Cass et al., 1984; Saito et al., 2006; Sakai et al., 2009). As evident in Equation 2-24, vapour diffusion is caused by density gradients due to both temperature and pressure effects.

The enhancement factor (η) is determined as:

$$\eta = a + 3S_a - (a-1)e^{-\left[\left(1+\frac{2.6}{\sqrt{f_c}}\right)S_a\right]^4} \qquad \text{Equation 2-25}$$

Where f_c is the fraction by mass of clay in the porous medium [-], and a is an empirical constant [-] (Sakai et al., 2009).

The vapour diffusion coefficient (D_w) is a function of temperature (after Saito et al., 2006):

$$D_w = 2.12 \cdot 10^{-5} \left(\frac{T}{273.15} \right)^2 \qquad \text{Equation 2-26}$$

2.1.3 **ONE-DIMENSIONAL HYDROMECHANICAL COUPLING**

One-dimensional hydromechanical coupling is implemented following the formulation of Neuzil (2003), and its derivation is detailed in Appendix A of Bea et al. (2011). It is valid only for saturated porous media. If surface loading is homogeneous and spatially extensive, a one-dimensional vertical formulation for stress and strain is appropriate. Neuzil (2003) has reviewed the potential errors arising from ignoring lateral strains resulting from non-

uniform loads (e.g. spatially varying ice sheet thickness), and noted that although assessing the errors is difficult, they are probably modest in the context of other uncertainties involved in simulating large-scale hydrogeological systems. The assumption of purely vertical stress has also been invoked previously to simulate groundwater flow in hydrogeological systems affected by large-scale ice sheet loading and unloading (e.g. Bense and Person, 2008; Lemieux et al., 2008; Normani, 2009).

Similar to published work (e.g., Lemieux et al., 2008; Normani, 2009), in MIN3P-THCm, the fluid mass conservation in fully-saturated porous media is described by:

$$\rho_a \frac{S_s}{\rho_{a,f} g}\left(\frac{\partial P_a}{\partial t} - \zeta \frac{\partial \sigma_{zz}}{\partial t}\right) + \phi \frac{\partial \rho_a}{\partial t} - \nabla \cdot (\rho_a \mathbf{q_a}) - \rho_a Q_a = 0 \qquad \text{Equation 2-27}$$

where, ζ is the one-dimensional loading efficiency [-], σ_{zz} is the vertical stress [M L^{-1} T^{-2}], $\rho_{a,f}$ is the freshwater density [M L^{-3}]. As discussed by Normani (2009), the hydromechanical coupling term $\rho_a \frac{S_s}{\rho_{a,f} g}\left(\zeta \frac{\partial \sigma_{zz}}{\partial t}\right)$ in Equation 2-27 effectively links fluid pressure changes with temporal changes in the vertical stress and the porous medium properties S_s and ζ. Geometric deformation of the computational domain to account for land surface movements resulting from vertical stress changes (i.e. lithosphere deflection because of the weight of ice) is not currently considered. Details can be found in Bea et al. (2011).

2.1.4 **ENERGY TRANSPORT**

Energy is transported in the water-solid system by the flow of groundwater and by thermal conduction from higher to lower temperatures through both the fluid and solids. The governing equation for energy transport implemented in MIN3P-THCm represents the balance between energy fluxes and the time rate of change of the amount of energy stored in the solid matrix and fluid. This balance is expressed as follows (Voss and Provost, 2008; Bea et al. 2012):

$$\frac{\partial [\phi \rho_a S_a c_w T]}{\partial t} + \frac{\partial [\phi c_v S_v \rho_v T]}{\partial t} + \frac{\partial [(1-\phi)\rho_s c_s T]}{\partial t} + \frac{\partial [L_w \phi S_v \rho_v]}{\partial t} = \nabla \cdot [\phi \rho_a c_w \mathbf{q}_{\mathbf{a},T} T] - \nabla \cdot [\boldsymbol{\lambda} \nabla T] + \nabla \cdot [\phi \rho_a c_w \mathbf{D}_{\mathbf{a},T} \nabla T] + \rho^* Q c_w T^* + \nabla \cdot [L_w q_v] + f_h \xi \qquad \text{Equation 2-28}$$

where c_w, c_v and c_s are the specific heat capacity for the water, vapor and solid phases, respectively [L^2 T^{-2} Θ^{-1}], ρ_S and ρ_v are the solid and vapor densities, respectively [M L^{-3}], $\boldsymbol{\lambda}$ is thermal conductivity tensor for the porous medium [LM T^{-3} Θ^{-1}], and T and T^* are the temperatures for the porous medium and external water, respectively [Θ].

The time derivative term expresses the total change in energy stored in both the solid matrix and fluid per unit total volume. The term involving $\mathbf{q}_{\mathbf{a},T}$ [L T^{-1}] describes energy transport by convection with the flowing groundwater. The term involving bulk thermal

conductivity, $\boldsymbol{\lambda}$, accounts for heat conduction through groundwater and solids, and the term involving the thermal dispersion tensor, $\mathbf{D}_{\mathbf{a},T}$ [$L^2\ T^{-1}$], approximates the contributions of irregular flows and diffusive mixing, which are not accounted for in the convection term. The term involving Q [T^{-1}], the fluid mass source, accounts for the energy added by an external fluid source with temperature T^* and density ρ^*, f_h is the energy source/sink term [$E\ L^{-2}\ T^{-1}$], and ξ is a constant that relates the surface area on the boundary with the volume of the porous medium [$L^2\ L^{-3}$].

MIN3P-THCm employs a weighted arithmetic mean for bulk thermal conductivity $\boldsymbol{\lambda}$ [$M\ L\ T^{-3}\ \Theta^{-1}$]:

$$\boldsymbol{\lambda} = \phi S_a \boldsymbol{\lambda}_{\mathbf{w}} + (1-\phi)\boldsymbol{\lambda}_{\mathbf{s}} \qquad \text{Equation 2-29}$$

where $\boldsymbol{\lambda}_{\mathbf{w}}$ and $\boldsymbol{\lambda}_{\mathbf{s}}$ are the fluid and solid thermal conductivities [$M\ L\ T^{-3}\ \Theta^{-1}$], respectively. Alternatively, the thermal conductivity is calculated as a function of water saturation (S_l) (Bea et al., 2012; Chung and Horton, 1987; Sakai et al., 2009). The form of the equation is shown below:

$$\boldsymbol{\lambda} = b_1 + b_2 \phi S_a + b_3 (\phi S_a)^{0.5} \qquad \text{Equation 2-30}$$

Where b_1, b_2 and b_3 are constants [$E\ L^{-1}\ T^{-1}\ {}^{o}C^{-1}$].

The latent heat of vapourization (L_w) in Equation 2-28 is defined in MIN3P-THCm as a function of temperature:

$$L_w = 2.501 \times 10^6 - 2369.2 \times T \qquad \text{Equation 2-31}$$

Vapour density is a function of the capillary pressure as related to relative humidity and salinity (Bea et al., 2012; Saaltink et al., 2005):

$$\rho_v = \rho_{sv} H_r a_w \qquad \text{Equation 2-32}$$

Where, ρ_{sv} is the temperature-dependent saturated vapor density [$M\ L^{-3}$], a_w is the activity of water, and H_r is the relative humidity. Relative humidity is a function of pore water pressure and temperature according to (Philip and de Vries, 1957):

$$H_r = e^{-\left(\frac{(P_{atm}-P_a)M_w}{\rho_a RT}\right)} \qquad \text{Equation 2-33}$$

Where P_{atm} is the atmospheric pressure (Pa), R is the universal gas constant (8.314 m^3 Pa $mol^{-1}\ K^{-1}$), and M_w is the molar mass of water (g mol^{-1}).

The saturated vapour density is determined in one of two ways. It can be calculated as a function of vapour pressure based on the psychrometric law (e.g., Edlefson and Anderson, 1943; Olivella et al., 1994; Saaltink et al., 2005):

$$\rho_{sv} = \frac{M_w P_v}{RT}$$ Equation 2-34

Where P_v is the vapour pressure, which is defined by:

$$P_v = 1.36075 \cdot 10^{11} e^{-\frac{5239.7}{T}}$$ Equation 2-35

The above saturated vapour density calculation is the default in MIN3P-THCm. An alternative method to calculate the saturated vapour density is proposed by Saito et al. (2006):

$$\rho_{sv} = 10^{-3} \frac{e^{31.3716 - \frac{6014.79}{T} - 7.92495 \times 10^{-3}}}{T}$$ Equation 2-36

When simulation of water with high salinity is required, the activity of water (a_w) may be updated according to the HMW model (Harvie et al., 1984; Bea et al., 2010b).

Energy production or consumption due to exothermic and endothermic chemical reactions is not implemented in the present version of MIN3P-THCm. In addition, changes in material properties at near-freezing temperatures (e.g. hydraulic conductivity, thermal conductivity) because of ice formation or melting within the porous medium are currently not coupled with energy transport.

2.1.5 **MULTICOMPONENT REACTIVE TRANSPORT**

The reactive transport problem includes the simultaneous solution of advective-dispersive transport of dissolved species, diffusive gas transport, and the contributions from geochemical reactions involving aqueous, gaseous, and mineral species (Lichtner, 1996a).

In the present version of the model, it is assumed that transport of pore gas can be adequately described as a Fickian diffusion process. Thorstenson and Pollock (1989) showed that this assumption is usually a good approximation for reactive gases, such as oxygen and carbon dioxide, if the concentration gradients of nonreactive gases contained in the soil atmosphere, e.g. nitrogen, remain primarily unaffected. However, reaction-induced advective gas fluxes may become important whenever a significant amount of gas is produced or consumed in the subsurface (Thorstenson and Pollock, 1989; Mendoza and Frind, 1990a, 1990b). Advective gas transport may also be driven due to the displacement by changes in water saturation, or due to thermal and/or density gradients in the gas phase. These processes are currently not included. We further assume that water is fully wetting, and that there is no direct contact between the gaseous phase and the solid phase.

In our formulation, intra-aqueous reactions can be described optionally as equilibrium or kinetically controlled reactions, reflecting the vastly different timescales associated with these processes. Dissolution-precipitation reactions are considered as kinetically controlled processes, which can also be used to approximate mineral equilibria, if the reaction rates are sufficiently fast. All remaining reactions are assumed to be rapid in comparison to the transport processes, and are described by equilibrium relationships. The direct substitution

approach allows the mass conservation equations for reactive transport to be expressed in terms of N_c aqueous species, which are defined as components (Yeh and Tripathi, 1989; Steefel and Lasaga, 1994; Lichtner, 1996a). The mass conservation equation for a component A_j^c, written in terms of total component concentration T_j^a, takes the form:

$$\frac{\partial}{\partial t}[S_a\phi T_j^a]+\frac{\partial}{\partial t}[S_g\phi T_j^g]+\frac{\partial T_j^s}{\partial t}=-\nabla\cdot\left[\mathbf{q_a}T_j^a\right]-\nabla\cdot\left[\mathbf{q}_g T_j^g\right]+\nabla\cdot\left[S_a\phi\mathbf{D_a}\nabla T_j^a\right]$$
$$+\nabla\cdot\left[S_g\phi\mathbf{D}_g\nabla T_j^g\right]+Q_j^{a,a}+Q_j^{a,m}+Q_j^{a,ext}+Q_j^{g,ext}\qquad j=1,N_c \qquad \text{Equation 2-37}$$

where T_j^a is the total aqueous component concentration for the component A_j^c [mol L^{-3} H_2O], T_j^g is the total gaseous concentration for the component A_j^c [mol L^{-3} gas], and T_j^s is the total concentration [mol L^{-3} bulk] of the aqueous component A_j^c on the exchanger. $\mathbf{D}_g$ is the dispersion tensor for the gaseous phase. $Q_j^{a,a}$ [mol L^{-3} T^{-1}] and $Q_j^{a,m}$ [mol L^{-3} T^{-1}] are internal source and sink terms from intra-aqueous kinetic reactions and kinetically controlled dissolution-precipitation reactions, and $Q_j^{a,ext}$ and $Q_j^{g,ext}$ [mol L^{-3} T^{-1}] are external source and sink terms for the aqueous and gas phase, respectively (Mayer et al., 2002).

To complete the system of governing equations, an additional set of mass conservation equations has to be defined, which describes the change of mineral quantities over time (Mayer et al., 2002):

$$\frac{\partial V_{f,j}^m}{\partial t}=V_j^m R_j^m \qquad j=1,N_m \qquad \text{Equation 2-38}$$

where $V_{f,j}^m$ [L^3 mineral L^{-3} bulk] is the volumetric fraction for the j^{th} mineral species, V_j^m is its molar volume [L^3 mineral mol^{-1}], and R_j^m is the overall dissolution-precipitation rate for the j^{th} mineral [mol L^{-3} T^{-1}], N_m is the number of minerals.

2.1.5.1 Total concentrations and source-sink terms

Total concentrations in Equation 2-37 are defined as (Mayer et al., 2002):

$$T_j^a=C_j^c+\sum_{i=1}^{N_x}\nu_{ij}^x C_i^x \qquad \text{Equation 2-39}$$

$$T_j^s=\sum_{i=1}^{N_s}\nu_{ij}^s C_i^s \qquad \text{Equation 2-40}$$

$$T_j^g=\sum_{i=1}^{N_g}\nu_{ij}^g C_i^g \qquad \text{Equation 2-41}$$

where N_x, N_g and N_s are the number of aqueous, gaseous complexes and ion-exchange

complexes, respectively. ν_{ij}^{x}, ν_{ij}^{g} and ν_{ij}^{s} are the stoichiometric coefficients for the j^{th} aqueous, gaseous component in the i^{th} aqueous, gaseous complexation and ion exchange reaction, respectively. C_j^c is the concentration of the j^{th} primary species, and C_i^x, C_i^g and C_i^s are the concentrations of the i^{th} aqueous, gaseous complexes and ion-exchanged species, respectively.

The consumption or production of aqueous components due to kinetically controlled intra-aqueous or dissolution-precipitation reactions are calculated from the relevant reaction rates. The source-sink term $Q_j^{a,a}$ defining the consumption or production of aqueous components due to the sum of all kinetically controlled intra-aqueous reactions can be defined as:

$$Q_j^{a,a} = S_a \phi \sum_{i=1}^{N_{a,kin}} \nu_{ij}^a R_i^a \qquad j = 1, N_c \qquad \text{Equation 2-42}$$

where the contributions of the various reaction rates R_i^a [mol L^{-3} H_2O T^{-1}] are scaled to express the source-sink term in the units of the global mass conservation equations [mol L^3 bulk T^{-1}]. The number of intra-aqueous kinetic reactions is defined by $N_{a,kin}$, and ν_{ij}^a is the stoichiometric coefficient of the j^{th} component in the i^{th} intra-aqueous dissolution-precipitation reaction. The source-sink term $Q_j^{a,m}$ defining the consumption or production of aqueous components due to mineral dissolution-precipitation reactions can be defined as

$$Q_j^{a,m} = -\sum_{i=1}^{N_{m,kin}} \nu_{ij}^m R_i^m \qquad j = 1, N_c \qquad \text{Equation 2-43}$$

where R_i^m defines the reaction rate for the i^{th} dissolution-precipitation reaction. The number of dissolution-precipitation reactions is defined by $N_{m,kin}$ and ν_{ij}^m is the stoichiometric coefficient of the j^{th} component in the i^{th} mineral dissolution-precipitation reaction. Any number of parallel reaction pathways can be considered for the dissolution-precipitation reactions.

2.1.5.2 Physical relationships

The Darcy flux vector $\mathbf{q}_a$ [L T^{-1}] can also be obtained from the solution of the Richards equation and is given by Equation 2-2. The hydrodynamic dispersion tensor $\mathbf{D}_a$ [Bear, 1972] uses the notation of Unger et al. [1995]:

$$S_a \phi \mathbf{D}_{a,kl} = (\alpha_l - \alpha_t)\frac{\mathbf{q}_{a,k}\mathbf{q}_{a,l}}{|\mathbf{q}_a|} + \alpha_t |\mathbf{q}_a| \delta_{kl} + S_a \phi \tau_a D_a^* \delta_{kl} \qquad \text{Equation 2-44}$$

where k and l denote the spatial coordinates in the x- y-and z-directions. $|\mathbf{q}_a|$ is the magnitude of the aqueous phase Darcy flux, α_l [L] is the longitudinal dispersivity, and α_t [L] is the transverse dispersivity of the porous medium. The actual implementation distinguishes between horizontal and vertical transverse dispersivities, as proposed by Burnett and Frind (1987), and implemented by Unger et al. (1995). D_a^* is an averaged free-

liquid diffusion coefficient [L^2 T^{-1}] and δ_{kl} defines the Kronecker delta. The tortuosity τ_a [-] can be specified as a constant, or expressed as a function of aqueous phase saturation and porosity based on the semi-empirical expression by Millington (1959):

$$\tau_a = S_a^{7/3}\phi^{1/3} \qquad \text{Equation 2-45}$$

Alternative formulations to describe tortuosity have also been implemented in the code. Gas phase species are assumed to be transported by diffusion only; therefore the corresponding dispersion tensor takes the simple form:

$$S_g\phi\mathbf{D}_{g,kl} = S_g\phi\tau_g D_g^*\delta_{kl} \qquad \text{Equation 2-46}$$

where D_g^* defines an average free-phase diffusion coefficient in air, which, for mathematical convenience, is used for all gaseous species. The definition of gas phase tortuosity τ_g of the gas-filled pore space is analogous to Equation 2-45, but uses gas phase saturation to calculate tortuosity.

2.1.5.3 Geochemical relationships

The following stoichiometric relationships represent the equilibrium and kinetically controlled reactions that are implicitly included in Equation 2-37 and Equation 2-38:

$$A_i^x \leftrightharpoons \sum_{j=1}^{N_c} \nu_{ij}^x A_j^c \qquad i = 1, N_x \qquad \text{Equation 2-47}$$

$$A_i^g \leftrightharpoons \sum_{j=1}^{N_c} \nu_{ij}^g A_j^c \qquad i = 1, N_g \qquad \text{Equation 2-48}$$

$$0 \leftrightharpoons \sum_{j=1}^{N_c} \nu_{ij}^a A_j^c \qquad i = 1, N_{a,kin} \qquad \text{Equation 2-49}$$

$$A_i^m \leftrightharpoons \sum_{j=1}^{N_c} \nu_{ij}^m A_j^c \qquad i = 1, N_{m,kin} \qquad \text{Equation 2-50}$$

where N_x and N_g define the number of equilibrium intra-aqueous reactions and gas dissolution-exsolution reactions, respectively. Because these reactions are treated as equilibrium reactions, N_x and N_g simultaneously define the number of aqueous complexes (including secondary redox master species) and gases. A_i^x and A_i^g are the names of the complexed species and gases, while ν_{ij}^x and ν_{ij}^g define the stoichiometric coefficients of the components A_j^c in the species of concern.

As introduced above, in the generalized reaction network, $N_{a,kin}$ and $N_{m,kin}$ represent the number of kinetically controlled intra-aqueous and dissolution-precipitation reactions, respectively. At this point it must be emphasized that $N_{a,kin}$ and $N_{m,kin}$ do not relate to the number of aqueous components (N_c) or mineral phases (N_m), as is customary for reactive transport formulations based purely on an equilibrium formulation, where reactions are always related to species or phases. One of the major advantages of the generalized formulation is that any number of parallel reaction pathways between aqueous components

and for the dissolution and precipitation of mineral phases can be included.

2.1.5.4 Equilibrium reactions

All equilibrium reactions are described using the law of mass action relationship. The concentrations of aqueous complexes formed by hydrolysis reactions, ion pairing, and equilibrium oxidation-reduction reactions can be described by:

$$C_i^x = (K_i^x \gamma_i^x)^{-1} \prod_{j=1}^{N_c} (\gamma_j^c C_j^c)^{\nu_{ij}^x} \qquad i = 1, N_x \qquad \text{Equation 2-51}$$

where K_i^x is the equilibrium constant for the dissociation of the aqueous complex A_i^x into components as species in solution, γ_i^x is the activity coefficient for the aqueous complex and γ_j^c is the activity coefficient for the component A_j^c as species in solution. The formulation for activity corrections for all dissolved species has been adopted from thermodynamic equilibrium model MINTEQA2 (Allison et al., 1991). Similarly, equilibrium gas dissolution-exsolution reactions can be described by the law of mass action:

$$C_i^g = RT(K_i^g)^{-1} \prod_{j=1}^{N_c} (\gamma_j^c C_j^c)^{\nu_{ij}^g} \qquad i = 1, N_g \qquad \text{Equation 2-52}$$

where K_i^g defines the corresponding equilibrium constant, R is the ideal gas constant [M L^2 T^2 Θ^{-1} mol^{-1}. in units of mol l^{-1} K^{-1} atm^{-1}] and T defines the temperature [Θ, in units of K].

2.1.5.5 Generalized kinetic formulation

The following describes the formulation of the reaction rates used in our reaction network approach to make the model applicable to a wide range of problems subject to kinetically controlled reactions.

2.1.5.5.1 Intra-aqueous kinetic reactions

For modeling purposes, kinetically controlled reactions are often approximated as reversible, elementary processes. These are described by rate expressions based on the principle of detailed balancing (Lasaga, 1998). For intra-aqueous kinetic reactions, such a rate expression can be written as (Lichtner, 1996b; Lasaga, 1998):

$$R_i^a = -k_i^a \prod_{\nu_{ij}^a \neq 0} (\gamma_j^c C_j^c)^{-\nu_{ij}^a} \left[1 - \frac{IAP_i^a}{K_i^a}\right] \qquad \text{Equation 2-53}$$

where k_i^a is the rate constant of the forward reaction, IAP_i^a is the ion-activity product of the reaction, and K_i^a is the equilibrium constant of the intra-aqueous kinetic reaction.

By definition, this rate expression is strictly valid only for elementary reversible reactions (Lasaga, 1998). However, many reactions are complex, and in practice it is often necessary to describe a series of elementary reactions by an overall reaction. The progress of the overall reaction is often limited by the availability of reactants or intermediate species, and

may be slowed not only by the presence of reaction products, but also by other inhibiting species. In addition, the reaction progress may be catalyzed by species which are not directly involved in the reaction. Commonly, laboratory experiments are conducted to determine which species control the reaction progress of an overall reaction and what order the reaction has with respect to each of these species. Furthermore, microbially mediated reactions are frequently described using a multiplicative Monod-type formulation [Borden and Bedient, 1986; MacQuarrie et al., 1990; Tebes-Stevens et al., 1998], which allows consideration of the availability of substrate, electron acceptors and nutrients. Inhibition and toxicity effects due to the presence of other substances can be considered in a similar way (e.g., Schäfer et al., 1998).

In order to be able to apply the model to a wide range of different problems, the kinetic reactions must be formulated in a general way such that the description of the various biogeochemical reaction mechanisms is facilitated in a straightforward and efficient manner. Our formulation is based on a generalization of Equation 2-53 which allows the reaction progress for intra-aqueous kinetic reactions to depend on the total aqueous component concentrations and/or on the activities of any number of dissolved species. The rate expressions can accommodate any reaction order with respect to any of these species. Monod and inhibition terms expressed as functions of total aqueous component concentrations are included and can be used to describe microbially mediated reactions or to dynamically activate or deactivate rate expressions in response to changing geochemical conditions. The rate expression is written as (Mayer et al., 2002):

$$R_i^a = -k_i^a \left[\prod_{\substack{j=1 \\ o_{ij}^{at} \neq 0}}^{N_c} T_j^a \prod_{\substack{j=1 \\ o_{ij}^{ac} \neq 0}}^{N_c} (\gamma_j^c C_j^c)^{o_{ij}^{ac}} \prod_{\substack{j=1 \\ o_{ij}^{ax} \neq 0}}^{N_x} (\gamma_j^x C_j^x)^{o_{ij}^{ax}} \cdot \right.$$

Equation 2-54

$$\left. \prod_{\substack{j=1 \\ K_{ij}^{a,mo} > 0}}^{N_c} \frac{T_j^a}{K_{ij}^{a,mo} + T_j^a} \prod_{\substack{j=1 \\ K_{ij}^{a,in} > 0}}^{N_c} \frac{K_{kj}^{a,in}}{K_{ij}^{a,in} + T_j^a} \right] \left[1 - \frac{IAP_i^a}{K_i^a} \right]$$

where o_{ij}^{at}, o_{ij}^{ac}, and o_{ij}^{ax} define the reaction orders with respect to the total aqueous component concentrations and the activities of the dissolved species, respectively. $K_{ij}^{a,mo}$ define half saturation constants, while $K_{ij}^{a,in}$ is a constant allowing the consideration of inhibition by the component A_j^c. Bacterial growth and die-off is neglected in the present formulation.

The algorithm is designed such that any of the terms in this rate equation, including the affinity term $\left[1 - \frac{IAP_i^a}{K_i^a}\right]$, can be selected by means of keywords to construct a rate expression suitable for a particular problem. Although this formulation includes a large number of terms, very little overhead is carried through the calculations, because all parameters are stored in a compressed data format. In practical terms, this means that entries within the product terms are only stored and evaluated if the reaction order, the half saturation constants, and the inhibition constants assume non-zero values. This approach maximizes

computational efficiency, while maintaining significant model flexibility.

Furthermore, by excluding the affinity term, this rate expression can be used to describe an irreversible reaction, as is often more appropriate for microbially mediated reactions. If all terms, except the rate constant K_i^a, are excluded, the rate expression defined by Equation 2-54 describes a zero-order, irreversible reaction. Reactions that are irreversible, but inhibited when an equilibrium condition is approached, can be approximated by modifying Equation 2-54 to eliminate the backward reaction by means of the switch:

$$R_i^{a,ir} = \min[\, R_i^a, 0] \qquad \text{Equation 2-55}$$

which is controlled by means of a keyword through the database file.

2.1.5.5.2 Dissolution-precipitation reactions

Similarly, a general kinetic formulation can be defined for mineral dissolution-precipitation reactions. These reactions are heterogeneous and take place at the solid-water interface. The progress of these reactions may depend on whether they take place on the mineral surface, in which case they are referred to as ‘‘surface-controlled reactions’’, or by microscale transport processes of reactants or reaction products to or away from the reactive mineral surface (Berner, 1978; Stone and Morgan, 1990; Steefel and Lasaga, 1994), in which case they are referred to as ‘‘transport-controlled reactions’’ (see Figure 2.1). Microscale transport processes encompass the diffusive transport of reactant or product species through a thin stagnant water film (Berner, 1978) covering the mineral surface or through porous surface coatings or alteration rims covering the reactive surface (Murphy et al., 1989; Nicholson et al., 1990; Schnoor, 1990). The reaction is subject to a mixed reaction control if the reaction progress is influenced simultaneously by microscale transport and chemical reaction processes (Stone and Morgan, 1990; Steefel and Lasaga, 1994). The formulation presented here is applicable to purely surface-controlled reactions or to transport-controlled reactions that are exclusively controlled by microscale transport processes through a protective coating covering the mineral surface.

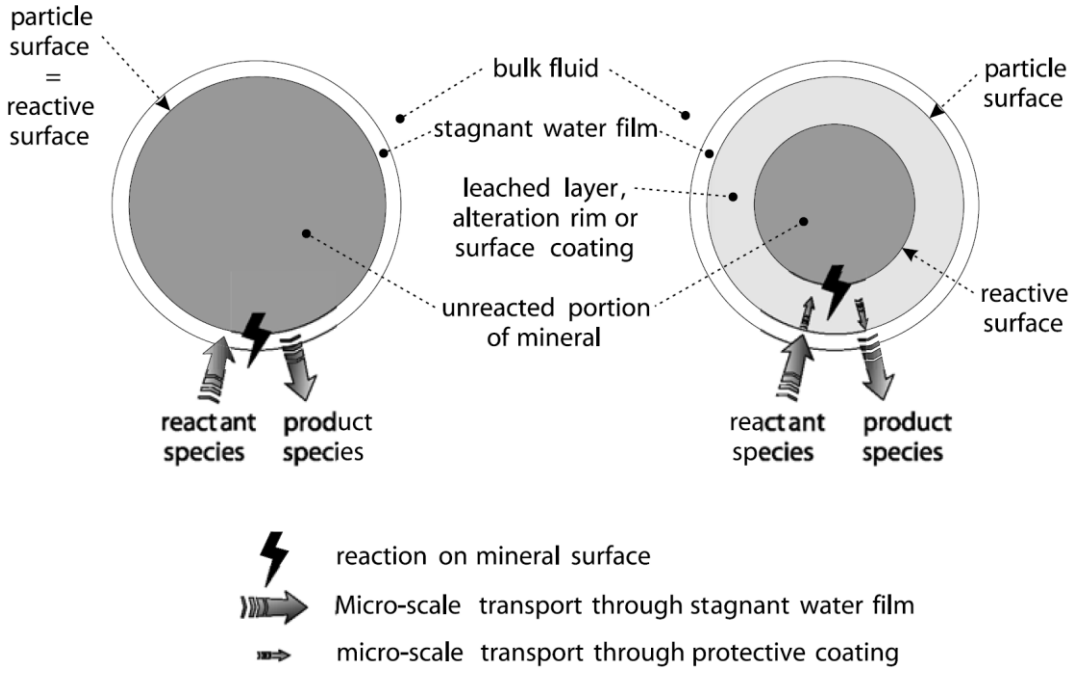

Figure 2.1 Mineral particles with and without protective surface layer (from Mayer et al., 2002)

A general rate expression for surface-controlled dissolution-precipitation reactions can be written as:

$$R_i^{ms} = -S_i k_i^m \left[\prod_{\substack{j=1 \\ o_{ij}^{mt} \neq 0}}^{N_c} \left(T_j^a\right)^{o_{ij}^{mt}} \prod_{\substack{j=1 \\ o_{ij}^{mc} \neq 0}}^{N_c} \left(\gamma_j^c C_j^c\right)^{o_{ij}^{mc}} \prod_{\substack{j=1 \\ o_{ij}^{mx} \neq 0}}^{N_x} \left(\gamma_j^x C_j^x\right)^{o_{ij}^{mx}} \right.$$

$$\left. \prod_{\substack{j=1 \\ K_{ij}^{m,mo} > 0}}^{N_c} \frac{T_j^a}{K_{ij}^{m,mo} + T_j^a} \prod_{\substack{j=1 \\ K_{ij}^{m,in} > 0}}^{N_c} \frac{K_{ij}^{m,in}}{K_{ij}^{m,in} + T_j^a} \left[1 - \frac{IAP_i^m}{K_i^m}\right] \right] \quad \text{Equation 2-56}$$

where R_i^{ms} [mol L^{-3} bulk T^{-1}] defines the reaction rate for the i^{th} surface-controlled dissolution-precipitation reaction. The progress of the reaction is dependent on the reactive surface area S_i corresponding to the mineral phase A_i^m and is given in units of [L^2 mineral L^{-3} bulk]. k_i^m defines the rate constant for the dissolution of the mineral, and o_{ij}^{mt}, o_{ij}^{mc}, and o_{ij}^{mx} are the reaction orders with respect to the total aqueous component concentrations and the activities of the dissolved species, and K_i^m is the equilibrium constant. The remaining parameters $K_{ij}^{m,mo}$ and $K_{ij}^{m,in}$ define the half saturation constants and inhibition constants. As for intra-aqueous kinetic reactions, any of the terms can be selected or excluded, implying that Equation 2-56 can also be used to describe irreversible dissolution or precipitation reactions.

The shrinking core model is used to describe dissolution reactions that are limited by the diffusive mass flux of a single primary reactant through a protective surface coating (Levenspiel, 1972; Davis and Ritchie, 1986; Wunderly et al., 1996), here defined as transport-controlled reactions. In general form, a rate expression for reactions that can be described by the shrinking core model can be written as:

$$R_i^{mt} = -S_i k_i^m \left[\sum_{\substack{j=1 \\ \nu_{ij}^{mt}>0}}^{N_c} \frac{\left(T_j^a\right)^{o_{ij}^{mt}}}{\nu_{ij}^{mt}} + \sum_{\substack{j=1 \\ \nu_{ij}^{mc}>0}}^{N_c} \frac{\left(C_j^a\right)^{o_{ij}^{mc}}}{\nu_{ij}^{mc}} + \sum_{\substack{j=1 \\ \nu_{ij}^{mx}>0}}^{N_c} \frac{\left(T_j^a\right)^{o_{ij}^{mx}}}{\nu_{ij}^{mx}} \right] \qquad \text{Equation 2-57}$$

where R_i^{mt} [mol L^{-3} bulk T^{-1}] defines the reaction rate for the i^{th} transport-controlled dissolution-precipitation reaction, ν_{ij}^{mt}, ν_{ij}^{mc}, and ν_{ij}^{mx} define the stoichiometric coefficients of the primary reactant. To be consistent with the derivation of the shrinking core model, only one of these stoichiometric coefficients can have a nonzero value. The formulation has been generalized by including arbitrary reaction orders with respect to the primary reactants. Although not entirely consistent with the shrinking core model (Levenspiel, 1972), this extension is practical for describing reactions that are subject to passivation, but clearly show no first order dependence on the primary reactant. The rate constant k_i^m can be expressed in terms of the physical parameters controlling the diffusion of the primary reactant. Assuming spherical mineral particles, k_i^m can be expressed as:

$$k_i^m = 10^3 D_i^m \left[\frac{r_i^p}{(r_i^p - r_i^r) r_i^r} \right] \qquad \text{Equation 2-58}$$

where r_i^p [L] is the radius of an average particle and r_i^r [L] is the radius of the unreacted portion of the mineral grain, which is updated with decreasing mineral content. D_i^m [L^2 T^{-1}] is the effective diffusion coefficient of the primary reactant through the protective surface layer and the conversion factor 10^3 [l m^{-3}] is included to yield consistent units with the surface-controlled reaction rates.

The rate expressions defined by Equation 2-56 and Equation 2-57 are scaled by the reactive surface area S_i [L^2 mineral L^{-3} bulk], which defines the mineral surface that is actively participating in dissolution-precipitation reactions. The algorithm provides the choice between a constant reactive surface area or a variable surface area that is updated, while the mineral dissolves or precipitates, according to the two-thirds power-relationship (Lichtner, 1996a):

$$S_i = S_i^0 \left[\frac{\phi_i}{\phi_i^0} \right]^{2/3} \qquad \text{Equation 2-59}$$

Alternatively, the product of reactive surface area S_i and the rate constant k_i^m may be replaced by an effective rate constant $k_i^{m,eff}$ (Mayer, 1999).

For a full description of the formulation of these reactions the reader is referred to Mayer et al. (2002).

2.1.5.6 Multicomponent diffusion model

Diffusion is commonly simulated as a part of the hydrodynamic dispersion term (Bear 1972; Mayer et al. 2002), with the diffusion coefficients and tortuosity of all species assumed to be identical. However, for clayey materials (e.g. compacted bentonite) mass transport is dominated by more complex phenomena such as anion exclusion, species-dependent diffusion, and interlayer/surface diffusion. To account for these processes, alternative and enhanced model formulations are required (Shackelford and Moore 2013). Different approaches have been reported in the literature to address the complex phenomena for reactive diffusion in dense clayey materials (Bourg et al. 2003; Steefel et al. 2005). Giambalvo et al. (2002) applied a multicomponent diffusion model to simulate fluid-sediment interactions considering species dependent diffusion coefficients and electromigration to ensure maintenance of local charge balance. This function is also implemented in MIN3P-THCm (Xie et al. 2014a; Rasouli 2015).

The general equation for diffusion-dominated reactive solute transport in fully saturated porous media can be expressed as:

$$\frac{\partial\left(\phi_e T_j^a\right)}{\partial t} + \frac{\partial T_j^s}{\partial t} + \nabla \cdot J_i^a = Q_j^{a,a} + Q_j^{a,m} + Q_j^{a,ext} \qquad j = 1, N_c \qquad \text{Equation 2-60}$$

subject to the following definitions:

T_j^a total aqueous component concentration of the j^{th} component in [mol L^{-3} H_2O], defined as:

$$T_j^a = C_j^c + \sum_{i=1}^{N_x} \nu_{ij}^x C_i^x$$

T_j^s total concentration [mol L^{-3} porous medium] of the j^{th} aqueous component on the exchanger;

$Q_j^{a,a}$ internal source and sink terms from intra-aqueous kinetic reactions [mol L^{-3} porous medium T^{-1}];

$Q_j^{a,m}$ source-sink term due to mineral dissolution/precipitation reactions [mol L^{-3} porous medium T^{-1}];

$Q_j^{a,ext}$ external source and sink term [mol L^{-3} porous medium T^{-1}];

C_j^c concentrations of the components as species in solution [mol L^{-3} H_2O];

C_i^x concentrations of complexed species in solution [mol L^{-3} H_2O];

ν_{ij}^x stoichiometric coefficients of the j^{th} component in the i^{th} complexed species;

ϕ_e effective porosity [-];

N_x number of aqueous complexes.

J_j^a total diffusive flux of the j^{th} component [M L^{-3} T^{-1}], described by the extended Nernst-Planck equation (Giambalvo et al. 2002):

$$J_j^a = -\left[\tau_e \phi_e \left(D_{0,j}^c \nabla C_j^c + \sum_i^{N_x} D_{0,i}^x \nu_{ij}^x \nabla C_i^x \right) - T_j^\varepsilon \frac{\sum_l^{N_c} z_l \left(\tau_e \phi_e D_{0,k}^c \nabla C_l^c + \sum_i^{N_x} \nu_{li}^x \tau_e \phi_e D_{0,i}^x \nabla C_i^x \right)}{\sum_k^{N_c} z_k T_k^\varepsilon} \right] \qquad \text{Equation 2-61}$$

where:

$D_{0,j}^c$ free diffusion coefficient of the j^{th} component as species in solution [L^2 T^{-1}],

$D_{0,i}^x$ free diffusion coefficient of the i^{th} complexed species in solution [L^2 T^{-1}],

ϕ_e effective porosity [-];

τ_e effective tortuosity [-],

z_j charge number [-]

The variables T_j^ε (equally applicable for index k) in Equation 2-61 are defined as (Giambalvo et al. 2002):

$$T_j^\varepsilon = \tau_e \phi_e D_{0.j}^c z_j C_j^c + \sum_{i=1}^{N_x} \tau_e \phi_e D_{0,i}^x \nu_{ij}^x z_i C_i^x \qquad \text{Equation 2-62}$$

The formulation outlined in Equation 2-60 through Equation 2-62 assumes that the effective porosity and the effective tortuosity are identical for all species.Hybrid multicomponent diffusion model

Further development of a hybrid multicomponent diffusion (hMCD) approach combines the multicomponent diffusion module with modified equations for species-dependent effective porosity and tortuosity. In essence, correction factors are introduced for the effective porosity and tortuosity for each individual species to capture the net effect of processes such as anion exclusion and interlayer/surface diffusion. While this is an empirical approach that requires calibration of the individual correction factors to experimental results, it does allow for the efficient simulation of several processes that may influence solute migration in low permeability, clay rich media. Applying this approach consistently to Equation 2-60 through Equation 2-62 leads to:

$$\frac{\partial T_j^{\varepsilon,s}}{\partial t} + \frac{\partial T_j^s}{\partial t} + \nabla \cdot J_j^a = Q_j^{a,a} + Q_j^{a,m} + Q_j^{a,ext} \qquad j = 1, N_c \qquad \text{Equation 2-63}$$

with

$$T_j^{\varepsilon,s} = f_{\phi,j}^c \phi_e C_j^c + \sum_{i=1}^{N_x} f_{\phi,i}^x \phi_e \nu_{ij}^x C_i^x \qquad \text{Equation 2-64}$$

$$J_j^a = -\left[\begin{array}{l} (f_{\phi,j}^c \phi_e f_{\tau,j}^c \tau_e D_{0.j}^c \nabla C_j^c + \sum_{i=1}^{N_x} f_{\phi,i}^x \phi_e f_{\tau,i}^x \tau_e D_{0,i}^x \nu_{ij}^x \nabla C_i^x) - \\ T_j^{\varepsilon,d} \dfrac{\sum_{l=1}^{N_c} z_l (f_{\phi,l}^c \phi_e f_{\tau,l}^c \tau_e D_{0,l}^c \nabla C_l^c + \sum_{i=1}^{N_x} f_{\phi,i}^x \phi_e f_{\tau,i}^x \tau_e D_{0,i}^x \nu_{li}^x \nabla C_i^x)}{\sum_{k=1}^{N_c} z_k T_k^{\varepsilon,d}} \end{array} \right] \quad \text{Equation 2-65}$$

and

$$T_j^{\varepsilon,d} = f_{\tau,j}^c \tau_e f_{\phi,j}^c \phi_e D_{0.j}^c z_j C_j^c + \sum_{i=1}^{N_x} f_{\tau,i}^x \tau_e f_{\phi,i}^x \phi_e D_{0,i}^x \nu_{ij}^x z_i C_i^x \quad \text{Equation 2-66}$$

Equation 2-64 and Equation 2-66 are species-normalized total concentration terms for the mass storage term and diffusive transport terms, respectively, accounting for species-dependent effective porosities, effective tortuosities and free phase diffusion coefficients. Species-dependent effective tortuosities and porosities are expressed relative to a reference value using the correction factors $f_{\tau,j}^c$, $f_{\phi,j}^c$, $f_{\tau,i}^x$ and $f_{\phi,i}^x$, which are defined as:

$f_{\tau,j}^c$ effective tortuosity correction factor for the j^{th} component as species in the solution [-];

$f_{\phi,j}^c$ effective porosity correction factor for the j^{th} component as species in solution [-];

$f_{\tau,i}^x$ effective tortuosity correction factor for the i^{th} complexed species in solution [-];

$f_{\phi,i}^x$ effective porosity correction factor for the i^{th} complexed species in solution [-];

2.1.5.7 Extension of MCD and hMCD Models for Radial or Cylindrical Coordinates

The above equations are expressed in general terms, and apply to a Cartesian coordinate system. For a two-dimensional cylindrical coordinate system, the gradient terms in Equation 2-61 and Equation 2-65 must be replaced with the following term (Istok 1989):

$$\nabla^2 C_i^c = \frac{\partial^2 C_i^c}{\partial r^2} + \frac{1}{r}\frac{\partial C_i^c}{\partial r} + \frac{\partial^2 C_i^c}{\partial z^2} = \frac{1}{r}\frac{\partial}{\partial r}\left(r \frac{\partial C_i^c}{\partial r} \right) + \frac{\partial^2 C_i^c}{\partial z^2} \quad \text{Equation 2-67}$$

$$\nabla^2 C_i^x = \frac{\partial^2 C_i^x}{\partial r^2} + \frac{1}{r}\frac{\partial C_i^x}{\partial r} + \frac{\partial^2 C_i^x}{\partial z^2} = \frac{1}{r}\frac{\partial}{\partial r}\left(r \frac{\partial C_i^x}{\partial r} \right) + \frac{\partial^2 C_i^x}{\partial z^2} \quad \text{Equation 2-68}$$

For a one-dimensional radial coordinate system, the gradient terms in Equation 2-61 and Equation 2-65 must be replaced with the following term:

$$\nabla^2 C_i^c = \frac{\partial^2 C_i^c}{\partial r^2} + \frac{1}{r}\frac{\partial C_i^c}{\partial r} = \frac{1}{r}\frac{\partial}{\partial r}\left(r\frac{\partial C_i^c}{\partial r}\right) \qquad \text{Equation 2-69}$$

$$\nabla^2 C_i^x = \frac{\partial^2 C_i^x}{\partial r^2} + \frac{1}{r}\frac{\partial C_i^x}{\partial r} = \frac{1}{r}\frac{\partial}{\partial r}\left(r\frac{\partial C_i^x}{\partial r}\right) \qquad \text{Equation 2-70}$$

in which *r* denotes the radial axis. For simplicity, only the MCD and hMCD models for radial coordinate systems are described below. Both models can be obtained in the same manner for cylindrical coordinates.

Combining Equation 2-61, Equation 2-69, and Equation 2-70, the diffusion term for the one- dimensional radial coordinate MCD model can be obtained:

$$J_j^a = -\left[\tau_e\phi_e(D_{0,j}^c\nabla^2 C_j^c + \sum_i^{N_x} D_{0,i}^x \nu_{ij}^x \nabla^2 C_i^x) - T_j^\varepsilon \frac{\sum_l^{N_c} z_l(\tau_e\phi_e D_{0,k}^c \nabla^2 C_l^c + \sum_i^{N_x} \nu_{li}^x \tau_e\phi_e D_{0,i}^x \nabla^2 C_i^x)}{\sum_k^{N_c} z_k T_k^\varepsilon}\right] \qquad \text{Equation 2-71}$$

$$= -\left\{\tau_e\phi_e\left[D_{0,j}^c \frac{1}{r}\frac{\partial}{\partial r}\left(r\frac{\partial C_j^c}{\partial r}\right) + \sum_i^{N_x} D_{0,i}^x \nu_{ij}^x \frac{1}{r}\frac{\partial}{\partial r}\left(r\frac{\partial C_i^x}{\partial r}\right)\right] - T_j^\varepsilon \frac{\sum_l^{N_c} z_l\left[\tau_e\phi_e D_{0,k}^c \frac{1}{r}\frac{\partial}{\partial r}\left(r\frac{\partial C_j^c}{\partial r}\right) + \sum_i^{N_x} \nu_{li}^x \tau_e\phi_e D_{0,i}^x \frac{1}{r}\frac{\partial}{\partial r}\left(r\frac{\partial C_i^x}{\partial r}\right)\right]}{\sum_k^{N_c} z_k T_k^\varepsilon}\right\}$$

All other terms remain the same as defined for the Cartesian coordinate system (Equation 2-60).

Similarly, combining Equation 2-65, Equation 2-69, and Equation 2-70, the diffusion term for the one-dimensional radial coordinate hMCD model can be obtained:

$$J_j^a = -\left[\begin{array}{l} (f_{\phi,j}^c \phi_e f_{\tau,j}^c \tau_e D_{0.j}^c \nabla^2 C_j^c + \sum_{i=1}^{N_x} f_{\phi,i}^x \phi_e f_{\tau,i}^x \tau_e D_{0,i}^x \nu_{ij}^x \nabla^2 C_i^x) - \\ T_j^{\varepsilon,d} \dfrac{\sum_{l=1}^{N_c} z_l (f_{\phi,l}^c \phi_e f_{\tau,l}^c \tau_e D_{0,l}^c \nabla^2 C_l^c + \sum_{i=1}^{N_x} f_{\phi,i}^x \phi_e f_{\tau,i}^x \tau_e D_{0,i}^x \nu_{li}^x \nabla^2 C_i^x)}{\sum_{k=1}^{N_c} z_k T_k^{\varepsilon,d}} \end{array} \right]$$

$$= -\left\{ \begin{array}{l} \left[f_{\phi,j}^c \phi_e f_{\tau,j}^c \tau_e D_{0.j}^c \dfrac{1}{r} \dfrac{\partial}{\partial r} \left(r \dfrac{\partial C_j^c}{\partial r} \right) + \sum_{i=1}^{N_x} f_{\phi,i}^x \phi_e f_{\tau,i}^x \tau_e D_{0,i}^x \nu_{ij}^x \dfrac{1}{r} \dfrac{\partial}{\partial r} \left(r \dfrac{\partial C_i^x}{\partial r} \right) \right] - \\ T_j^{\varepsilon,d} \dfrac{\sum_{l=1}^{N_c} z_l \left[f_{\phi,l}^c \phi_e f_{\tau,l}^c \tau_e D_{0,l}^c \dfrac{1}{r} \dfrac{\partial}{\partial r} \left(r \dfrac{\partial C_l^c}{\partial r} \right) + \sum_{i=1}^{N_x} f_{\phi,i}^x \phi_e f_{\tau,i}^x \tau_e D_{0,i}^x \nu_{li}^x \dfrac{1}{r} \dfrac{\partial}{\partial r} \left(r \dfrac{\partial C_i^x}{\partial r} \right) \right]}{\sum_{k=1}^{N_c} z_k T_k^{\varepsilon,d}} \end{array} \right\}$$

Equation 2-72

In a geochemical system dominated by primary species, effective porosity and tortuosity corrections for the secondary species can be neglected.

2.1.5.8 Multisite ion exchange

A multisite modelling approach for cation exchange processes on illite has been successfully applied in predicting Cs^+ sorption under various conditions of pH and ionic strength (e.g. Zachara et al. 2002; Bradbury and Baeyens, 2011). This model well described the different sorption properties of the various sites (e.g. planar and edge sites).

Multicomponent cation exchange can be formulated using the Gaines-Thomas activity convention (Appelo and Postma 2005). Written in general form, cation exchange between the cations A_k^d and A_j^d multisite exchanger can be expressed as:

$$\frac{A_k^d}{Z_k^d} + \frac{A_{ij}^d \sim (X_i)_{Z_j^d}}{Z_j^d} \leftrightarrow \frac{A_{ik}^d \sim (X_i)_{Z_k^d}}{Z_k^d} + \frac{A_j^d}{Z_j^d}, \qquad i = 1, N_{ex}$$

Equation 2-73

where Z_k^d and Z_j^d define the charge of the cations A_k^d and A_j^d in [meq mmol^{-1}], while $(Z_k^d)^{-1}$ and $(Z_j^d)^{-1}$ can be interpreted as the stoichiometric coefficients of the reaction equation. X_i is the i^{th} exchange site and N_{ex} is the number of exchange sites. To simplify the description, it is convenient to redefine the ion-exchange species as:

$$\mathrm{A_{ij}^s} = \mathrm{A_{ij}^d} \sim (\mathrm{X_i})_{\mathrm{Z_j^d}}$$

Equation 2-74

$$\mathrm{A_{ik}^s} = \mathrm{A_{ik}^d} \sim (\mathrm{X_i})_{\mathrm{Z_k^d}}$$

Equation 2-75

Substituting Equation 2-74 and Equation 2-75 into Equation 2-73 leads to:

$$\frac{A_k^d}{Z_k^d} + \frac{A_{ij}^s}{Z_j^d} \leftrightarrow \frac{A_{ik}^s}{Z_k^d} + \frac{A_j^d}{Z_j^d}, \; i = 1, N_{ex}$$

Equation 2-76

Equation 2-76 can be rearranged to obtain a stoichiometric relationship with a unit stoichiometric coefficient for the cation exchange species A_{ij}^s:

$$A_{ij}^s \leftrightarrow \frac{z_j^d}{z_k^d} A_{ik}^s + A_j^d - \frac{z_j^d}{z_k^d} A_k^d,\ i = 1, N_{ex} \qquad \text{Equation 2-77}$$

The stoichiometric relationship in Equation 2-77 expresses cation exchange reactions in a general way involving any pair of dissolved cations on the exchange site X_i. This formulation has to be adjusted to facilitate its incorporation into the existing model equations. In this context, ion-exchange reactions are limited to exchange reactions involving cations, which are defined in the geochemical system as components. Equation 2-77 can be further generalized for any pair of ion-exchange reactions as:

$$A_{ij}^s \leftrightarrow v_{ij}^s A_{ik}^s + \sum_{l=1}^{N_c} v_{ijl}^s A_l^d,\ i = 1, N_{ex};\ j = 1, N_i^s \qquad \text{Equation 2-78}$$

where v_{ij}^s is the stoichiometric coefficient of the ion-exchanged species A_{ik}^s in the j^{th} ion exchange reaction on the i^{th}exchange site, which is defined by the ratio of the charge of the two competing cations. The parameters v_{ijl}^s are the stoichiometric coefficients of the components, in the j^{th} ion exchange reaction on the i^{th}exchange site. N_{ex} is the number of ion exchange site types. N_i^s is the number of the ion-exchanged species on the i^{th} exchange site. The cations in dissolved form A_l^d can be expressed by the corresponding component concentration. However, since A_{ij}^s cannot be expressed exclusively in terms of aqueous components, but is dependent on the ion-exchanged species A_{ik}^s on each cation exchange site, one of the ion-exchanged species has to be chosen to represent A_{ik}^s. Based on the stoichiometry defined in Equation 2-78, the law of mass action can be applied to obtain a relationship that defines the fractions of the ion-exchanged species A_{ij}^s in terms of equivalent fractions:

$$\beta_{ij}^s = \left[K_{ij}^s\right]^{-1} [\beta_{ik}^s]^{v_{ij}^s} \prod_{l=1}^{N_c} (\gamma_l^c C_l^c)^{v_{ijl}^s},\ i = 1, N_{ex};\ j = 1, N_i^s \qquad \text{Equation 2-79}$$

where β_{ij}^s and β_{ik}^s are the fractions of the ion-exchanged species A_{ij}^s and A_{ik}^s on the i^{th} exchange site in [meq meq^{-1}] and K_{ij}^s refers to the selectivity coefficient for the j^{th} ion-exchange reaction on the i^{th} ion-exchange site. Equation 2-79 provides only an explicit relationship for the calculation of β_{ij}^s, if the fraction β_{ik}^s of the ion-exchanged species A_{ik}^s is known. It is not possible to determine β_{ik}^s using Equation 2-79. Therefore, an additional relationship is needed. This relationship can be defined as the sum of the fractions of all ion-exchanged species on the exchange site X_i, which equals 1 for each type of ion exchange site (Appelo and Postma 1993):

$$1 = \sum_{j=1}^{N_i^s} \beta_{ij}^s,\ i = 1, N_{ex} \qquad \text{Equation 2-80}$$

Equation 2-79 and Equation 2-80 constitute the set of equations defining the ion-exchange sub-problem for the multisite cation exchange model.

If the number of ion exchange sites equals to one, it can be simplified as the traditional ion exchange model.

2.1.5.9 Surface complexation

Surface complexation reactions are essential because it allows for the treatment of sorption as influenced by variable chemical conditions. In this approach, the sorbing solid surfaces are assumed to possess surface function groups (e.g. –OH) that can form complexes analogues to the formation of aqueous complexes in solution (Steefel et al. 2014). The surface complexation reactions include proton exchange, cation binding and anion binding via ligand exchange at surface hydroxyl sites. For example, the sorption of a metal (M with a valence z+) could be described as:

$$\equiv X\bullet OH + M^{z+} \rightleftharpoons \equiv X\bullet OM^{(z-1)+} + H^{+} \qquad \text{Equation 2-81}$$

where $\equiv X\bullet OH$ represents the binding site with ligand exchange at the function group hydroxyl. The mass action equation for this surface complexation reaction is given by

$$K_{eq} = \frac{[\equiv X\bullet OM^{(z-1)+}][H^{+}]}{[\equiv X\bullet OH][M^{z+}]} \qquad \text{Equation 2-82}$$

Where K_{eq} is the equilibrium constant, the square brackets refers to the activities.

2.1.5.10 Activity corrections

Ion interactions are neglected in dilute solution models, such as Debye-Hückel (DH) and its variants which are appropriate for dilute solutions with ionic strengths up to 0.7 mol l^{-1}. Activity coefficients γ_i^d for all charged dissolved species A_i^d, where A_i^d can be either a component as species in solution or an aqueous complex, are calculated based on the modified Debye-Hückel equation if ion-specific parameters are available (Parkurst, 1990; Allison et al., 1991):

$$log\gamma_i^d = \frac{-A_d Z_i^2 \sqrt{I}}{1 + B_d a_i \sqrt{I}} + b_i I \qquad \text{Equation 2-83}$$

where A_d and B_d are constants, a_i and b_i are ion-specific fit parameters. If a_i is available, but not b_i, Equation 2-83 is used with $b_i = 0$. Otherwise the Davies equation is used as an approximation when a_i cannot be provided (Allison et al., 1991):

$$log\gamma_i^d = -A_d Z_i^2 \left[\frac{\sqrt{I}}{1 + \sqrt{I}} - 0.24I\right] \qquad \text{Equation 2-84}$$

Activity corrections for neutral species excluding water is calculated as described by Allison et al. (1991):

$$log\gamma_i^d = 0.1I \qquad \text{Equation 2-85}$$

The activity correction for water is defined by (Allison et al., 1991):

$$\gamma_{H_2O} = 1 - 0.017 \sum_{i=1}^{N_d} C_i^d \qquad \text{Equation 2-86}$$

In more concentrated electrolyte solutions, short-range, non-electrostatic interactions have to be considered as well. One possible way is suggested based on the specific ion interaction theory (SIT theory), which was first suggested by Brønsted (1922), and further developed by Guggenheim (1955), Scatchard (1936) and Ciavatta (1980). Based on this theory, the activity coefficient (γ_i) is basically corrected through the addition of a linear term to the DH expression (Sipos 2008):

$$log\gamma_i = \frac{-AZ_i^2\sqrt{I}}{1+B\sqrt{I}} + \sum_k \varepsilon(i,k)\, m_k \qquad \text{Equation 2-87}$$

In which, A is the limiting DH law slop (0.509 $kg^{1/2}$ $mol^{1/2}$ at 25 degC), B is the empirical constant ($kg^{1/2}$ $mol^{1/2}$), m_k is the molality of the ion k, and $\varepsilon(i,k)$ is an aqueous species interaction coefficient representing the specific short-range interactions between the aqueous species I and k. For uncharged species, or ions of the same charge, $\varepsilon(i,k)$ is assumed to be 0.0. In general, $\varepsilon(i,k)$ is an empirical parameter, which has to be determined through experiment. The accuracy of the SIT theory is well accepted when the ionic strength is between 0.5 to 3.5 mol kg^{-1} (Grenthe et al. 2013).

In highly saline solutions and brines, however, the interaction between individual ions can be better described by Pitzer equation. Simulating geochemical processes under these conditions are based on the Pitzer equations (Pitzer, 1973, 1991; Pitzer and Kim, 1974), which entail summation of all possible binary and ternary short-range interaction terms as well as mixing terms. Parameters have been derived for major ions (e.g. Harvie et al., 1982; Reardon, 1988; Haung, 1989; Christov and Möller, 2004). The Pitzer model is appropriate for solutions with ionic strengths up to 20 mol l^{-1} and has been applied successfully to simulate geochemical reactions in brines in various hydrogeologic settings (e.g. Eugster et al., 1980; He and Morse, 1993; Ayora et al., 1994; Krumgalz, 2001; Marion, 2002; Marion et al., 2003; Tosca et al., 2005).

The Pitzer equations have been implemented using the standard Harvie-Moller-Weare (HMW) formulation (Harvie et al., 1984) into the MIN3P-THCm code. The HMW model consists of a set of polynomial equations for water activity (a_w), the osmotic coefficient (ϕ), the activity coefficients of cations ($\boldsymbol{\gamma}_C$), anions ($\boldsymbol{\gamma}_A$), and neutral species ($\boldsymbol{\gamma}_N$). These equations are expressed in compact matrix form, which eliminates the need to discriminate between cations, anions, and neutral species (see Bea et al., 2010).

The vector of species molalities ($\mathbf{m}$) is the input for this algorithm. The vector of activity coefficients ($\boldsymbol{\gamma}$) is computed according to:

$$\ln\boldsymbol{\gamma} = \left(\ln\gamma_{DH} + q'\right)\mathbf{z^2} + q^c\mathbf{z} + \left(2\mathbf{Q} + Z\mathbf{C}\right)\mathbf{m} + \mathbf{m}^t\mathbf{T}\mathbf{m} \qquad \text{Equation 2-88}$$

$\mathbf{z}$ and $\mathbf{z^2}$ are the vectors of electric charge and squared electric charge, respectively. The modified Debye-Hückel terms (γ_{DH}), in Equation 2-88, are defined according to Harvie et al. (1984):

$$\ln \gamma_{DH} = -A^{\phi}\left[\frac{\sqrt{I}}{1+b\sqrt{I}} + \frac{2}{b}\ln\left(1+b\sqrt{I}\right)\right] \qquad \text{Equation 2-89}$$

where A^{ϕ} is the one third Debye-Hückel slope (A^{ϕ}=0.392 at 25°C, Pitzer and Mayorga, 1973), I is ionic strength, and b is a Debye-Hückel parameter (for all electrolytes b=1.2).

The activity of water (a_w) is computed from the osmotic coefficient ϕ (Felmy and Weare, 1986):

$$\ln a_w = -\phi MW \qquad \text{Equation 2-90}$$

where W is the molecular weight of water [M mol^{-1}]. The osmotic coefficient is defined as:

$$\phi = \frac{2}{M}\left(f'(I) + q^{\phi} + Zq^{c} + q^{L} + t\right) + 1 \qquad \text{Equation 2-91}$$

Ionic strength (I) and Z account for the effect of the electric charge in the electrolytic solution and are computed according to:

$$I = \frac{1}{2}\mathbf{z}_2^{\mathbf{t}}\mathbf{m} \qquad \text{Equation 2-92}$$

$$Z = \mathbf{z}_{\mathbf{abs}}^{\mathbf{t}}\mathbf{m} \qquad \text{Equation 2-93}$$

where $\mathbf{z}_2^{\mathbf{t}}$ and $\mathbf{z}_{\mathbf{abs}}^{\mathbf{t}}$ are the transpose of the square and absolute electric charge vectors, respectively. The total molar mass of solutes (M) in the water activity expression in Equation 2-89 is calculated as:

$$M = \mathbf{1}_{\mathbf{N_{aq}}}^{\mathbf{t}}\mathbf{m} \qquad \text{Equation 2-94}$$

where $\mathbf{1}_{\mathbf{N_{aq}}}^{\mathbf{t}}$ is the unity vector of dimension $_{\mathrm{N_{aq}}}$. Scalars q', q^{ϕ}, q^{c} and q^{L} in Equation 2-88 and Equation 2-91 represent the contributions of binary interactions. They are computed from:

$$q' = \mathbf{m}^{\mathbf{t}}\mathbf{Q}'\mathbf{m} \qquad \text{Equation 2-95}$$

$$q^{\phi} = \mathbf{m}^{\mathbf{t}}\mathbf{Q}^{\phi}\mathbf{m} \qquad \text{Equation 2-96}$$

$$q^{c} = \mathbf{m}^{\mathbf{t}}\mathbf{C}\mathbf{m} \qquad \text{Equation 2-97}$$

$$q^{L} = \mathbf{m}^{\mathbf{t}}\mathbf{Q}^{\mathbf{L}}\mathbf{m} \qquad \text{Equation 2-98}$$

The last term in Equation 2-88 and the scalar t in Equation 2-91 account for ternary interactions. The scalar t is given by:

$$t = \mathbf{m}^{\mathbf{t}}\mathbf{T}\mathbf{m}$$ Equation 2-99

Matrices $\mathbf{Q}$, $\mathbf{Q}'$, $\mathbf{Q}^{\phi}$, $\mathbf{Q}^{\mathbf{L}}$ and $\mathbf{C}$ are square and symmetric $[N_{aq} \times N_{aq}]$.These matrices include submatrices for interactions between cations (c), anions (a) and neutral species (n). Additional details on the mathematical and numerical formulations of the Pitzer equations are described in Bea et al. (2011). The Pitzer database developed for use with the chemical modelling code EQ3/6 (Worley 1992), as part of the Yucca Mountain project (USDOE, 2007), was used in the simulations presented in the verification report in section 'Pitzer equation - chemical speciation of Dead Sea water' and section 'Reactive transport in highly saline solution'.

2.1.6 **ATMOSPHERIC BOUNDARY CONDITION**

An atmospheric boundary condition for flow and energy transport has been implemented in MIN3P-THCm (Bea et al., 2012), which facilitate the code with an adequate description of evaporation under varying climate conditions. It consists of two parts: the flow boundary condition, and the energy boundary condition

2.1.6.1 Atmospheric flow boundary condition

Evaporation, rainfall, and surface runoff are considered as part of the atmospheric boundary and comprise a source/sink term in the vadose zone flow equation (Equation 2-21; f_a):

$$f_a = P + E + J_{sr}$$ Equation 2-100

where J_{sr} is the surface runoff. The rate of evaporation is dependent on the flow of vapour to the ground surface, the subsequent transfer of vapor from the ground surface to the atmosphere, as well as the exchange of heat between the ground surface and the atmosphere (Bea et al., 2012). This relationship is represented in MIN3P-THCm by the following equation:

$$E = \frac{(\rho_v^{atm} - \rho_v)}{r_s + r_h}$$ Equation 2-101

Where ρ_v^{atm} is the atmospheric vapour density [M L^{-3}], and r_s is the resistance of the porous medium surface to vapour flow. Equation 2-101 is an integrated form of Fick's law for vapour diffusion that equates the evaporation rate to the difference in vapor density between the soil surface and the atmosphere divided by the resistance to flow provided by both the atmospheric boundary-layer (r_h) and porous medium surface (r_s) [T L^{-1}] (Bea et al., 2012).

Two formulations are available for calculation of the porous medium resistance to flow (r_s), including that of Bitelli et al. (2008):

$$r_s = 3.5\left(\frac{1}{S_a}\right)^{2.3} + 33.5$$ Equation 2-102

The formulation of Simunek et al. (2009) can also be employed:

$$r_s = r_{s0} e^{36.5\phi(S_a - S_{a0})}$$ Equation 2-103

Where r_s is the soil resistance, r_{s0} is the soil resistance at the soil surface [T L^{-1}], S_a is the water saturation, and S_{a0} is the residual saturation.

The surface runoff (J_{sr}) term is activated if the pore water pressure exceeds atmospheric pressure at the ground surface. Runoff will therefore occur when the porous medium is saturated at the ground surface:

$$J_{sr} = \gamma_l(P_l - P_{atm}); \qquad P_l > P_{atm}$$ Equation 2-104

Where γ_l is a leakage coefficient [T L^{-1}] that is defined in the MIN3P-THCm input '.dat' file.

The precipitation rate (P) is calculated from values provided by the user, as described in detail in the MIN3P-THCm user manual section 3.9.

2.1.6.2 Atmospheric energy boundary condition

The energy source/sink in Equation 2-28 is defined by the energy balance at the surface of the domain (atmospheric boundary) as follows (Saaltink et al., 2005; Saito et al., 2006):

$$f_h = H_s + L_w E + c_a P T^{atm} + R_n$$ Equation 2-105

Where R_n is the net solar radiation [E L^{-2} T^{-1}], H_s is the sensible heat flux [E L^{-2} T^{-1}], and T^{atm} is the temperature of the atmosphere (°C). The latent heat term ($L_w E$) in Equation 2-105 accounts for the energy source or sink due to the latent heat of evaporation and condensation. The term $c_a P T^{atm}$ accounts for the internal energy of rainfall, which may be important when rain is of a different temperature than the pore fluid.

The solar radiation (R_n) can be provided as an external input in the 'atmospheric' input file (.atm), or is calculated internally based on latitude and climate data that are entered in the .dat file. The required inputs for these calculations are described in Section 3.9 of the user manual. If calculated internally using values defined in the .dat file, the net solar radiation (R_n) is calculated according to the following (Saaltink et al., 2005):

$$R_n = (1 - A_l)R_g + \varepsilon R_a - \varepsilon\sigma T^4$$ Equation 2-106

Where, A_l is the albedo [-], R_g is the direct short wave solar radiation [E L^{-2} T^{-1}], ε is the emissivity [-], R_a is the long wave atmospheric radiation [E L^{-2} T^{-1}], and σ is the Stefan-

Boltzmann constant. The albedo and emissivity are calculated as a function of water saturation (S_a):

$$A_l = A_d + (A_d - A_w)(S_a^2 - 2S_a) \quad \text{Equation 2-107}$$

Where A_d and A_l are the albedo of a dry and wet ground surface, respectively.

The emissivity ε is determined as:

$$\varepsilon = 0.90 + 0.05S_a \quad \text{Equation 2-108}$$

The direct short wave solar radiation (R_g) depends on the time of year, the time of day, and the latitude of the location. It can be calculated internally according to:

$$R_g = \frac{\pi R_G}{2d_s} sin\left(\frac{(t - t_m + 0.5d_s)\pi}{d_s}\right) \quad \text{Equation 2-109}$$

Where d_s is the number of daylight hours, and t_m is the time at noon, and R_G is the daily solar radiation. This equation is valid when $t_m - 0.5d_s \leq t \leq t_m + 0.5d_s$, otherwise $R_g = 0$. R_G is calculated according to:

$$R_G = R_A(0.29cos\kappa + 0.521I_n) \quad \text{Equation 2-110}$$

Where κ is the latitude, I_n is the cloud index, and R_A is the daily solar radiation in absence of the atmosphere. R_A is determined as follows:

$$R_A = S_0 r_e \left[\frac{d_d}{\pi} cos\kappa \cdot cos\delta \cdot sin\left(\frac{\pi d_s}{d_d}\right) + d_s \cdot sin\kappa \cdot sin\delta\right] \quad \text{Equation 2-111}$$

Where S_0 is the solar constant equal to 1376 J m^{-2} s^{-1}, d_d is the duration of a day, δ is the declination of the sun, and r_e is the relationship between the average distance between the earth and the sun and this distance at a particular moment in time. The number of daylight hours (d_s) is calculated by:

$$d_s = \frac{d_d}{\pi} acos(-tan\kappa \cdot tan\delta) \quad \text{Equation 2-112}$$

The solar declination is calculated as:

$$\delta = -\delta_{max} sin\left(2\pi \frac{t - t_s}{d_a}\right) \quad \text{Equation 2-113}$$

Where d_a is the duration of a year (i.e., 365.241 days), t_s is the time when autumn starts (e.g., September 21 in the northern hemisphere, March 21 in the southern hemisphere), and δ_{max} is the maximum declination of the sun (0.4119 rad or 23.26°).

The relationship between the average distance between the Earth and the sun and this

distance at a particular moment in time (r_e) is determined by the following:

$$r_e = 1.00011 + 0.03422cos\left(2\pi\frac{t - t_0}{d_a}\right) + 0.00128sin\left(2\pi\frac{t - t_0}{d_a}\right) + 0.000179cos\left(4\pi\frac{t - t_0}{d_a}\right) + 0.000077sin\left(2\pi\frac{t - t_0}{d_a}\right) \quad \text{Equation 2-114}$$

Where t_0 is the time of January 1.

The sensible heat flux (H_s) is calculated by the following:

$$H_s = \rho_g^{atm} c_g \frac{\left(T^{atm} - T\right)}{r_h} \quad \text{Equation 2-115}$$

Where is the r_g^{atm} density of the atmospheric air [M L^{-3}], and c_g is the heat capacity of air [E M^{-1} °C^{-1}], and r_h is the aerodynamic resistance to vapour flow in the atmospheric boundary layer [T L^{-1}]. Aerodynamic resistance (r_h) is calculated as (Saito et al., 2006; Bittelli et al., 2008):

$$r_h = \frac{\left[ln\left(\frac{z_a + z_0}{z_0}\right) + \theta\right]^2}{k^2 v_a} \quad \text{Equation 2-116}$$

Where k is the Von Karman's constant (≈0.4), θ is a stability factor [-], v_a is the wind velocity [L T^{-1}], z_0 is the roughness length [L], and z_a is the elevation above ground surface at which v_a and the atmospheric vapour density are measured.

2.1.7 **BIOMASS GROWTH AND DECAY**

Microorganisms play an important role in many subsurface environment, in particular, bioremediation for the immobilization of redox-sensitive contaminants through amendment with organic substrates. Two pathways involve in the mocrobially mediated redox reactions. One of them is the catabolic pathway used for energy production. The other one is the anabolic pathway used for cell synthesis. According to the approach of Rittmann and McCarty (2001) based on the stoichiometry of the reaction, microorganisms appear as a product and catalyst of the reactions, in which a portion of the electrons from the substrate (f_e^0) is transferred to the electron acceptor. The energy produced in this reaction is used for the conversion of other portion of electrons (f_s^0) into microbial cells, satisfying $f_e^0 + f_s^0 = 1$. The overall stoichiometry of the microbially mediated reaction is thus a sum of the both pathways weighted by the corresponding portions (Molins et al., 2015):

$$0 = \sum_{k=1}^{N_c} (f_e^0 \nu_{jk}^e + f_s^0 \nu_{jk}^s) A_k = \sum_{k=1}^{N_c} \nu_{jk}^b A_k \quad \text{Equation 2-117}$$

Where $N_c$is the number od primary species; A_k is the chemical formula of the primary

species; ν_{jk}^{e} and ν_{jk}^{s} represent the stoichiometric coefficients of the primary species in the catabolic and anabolic pathways, respectively, for the *j*th reaction. ν_{jk}^{b} are the stoichiometric coefficients of the overall redox reactions.

A monod-type expression is used to calculate the rate for the microbially mediated reactions:

$$r_j = \mu_j B \frac{c_D}{c_D + K_D} \frac{c_A}{c_A + K_A} \frac{K_I}{c_I + K_I} F_T \qquad \text{Equation 2-118}$$

In which r_j is the rate of the *j*th reaction (mol L^{-1} s^{-1}); μ_j is the specific rate constant (mol $cell^{-1}$ s^{-1}), B is the biomass concentration (cells L^{-1}); c_D, c_A and c_I are the concentration of the electron donor, acceptor and inhibitor (mol L^{-1}), respectively; K_D, K_A and K_I are the half-saturation constants for the electron donor, acceptor and inhibitor (mol L^{-1}), respectively; F_T is the thermodynamic limitation term (Jin and Bethke, 2005).

The biomass decay can be simulated in a first-order rate expression:

$$r_{decay} = -bB \qquad \text{Equation 2-119}$$

Biomass is assumed to be present only as immobile species; thus, biomass decay, if considered, is the only process that accounts for biomass removal.

2.1.8 **GAS REACTIONS**

Reactions with a discrete gas phase can be included in MIN3P-THCm with either an equilibrium or kinetic treatment. In the equilibrium case, mass action equations for gas are analogous to those for the aqueous complexes. The only difference lies in the definitions of gas concentration in fugacity and activity corrections. The fugacity of a gas species can be written as (Steefel et al., 2014):

$$f_l = K_l^{-1} \prod_{j=1}^{N_c} (\gamma_j C_j)^{\nu_{lj}} \qquad \text{Equation 2-120}$$

In which f_l is the fugacity of the *l*th gas; K_l is the equilibrium constant of the reaction; γ_j is the activity coefficient of the *j*th component; C_j is the concentration of the primary species; ν_{lj} is the number of moles of the *j*th primary species in *l*th gas reaction; and N_c is the number of primary species. The fugacity of the gas is related to the partial pressure of the *l*th gas (P_l) through the fugacity coefficient, φ_l:

$$P_l = \frac{f_l}{\varphi_l} \qquad \text{Equation 2-121}$$

The concentration of the gas species can be calculated from the ideal gas law:

$$\frac{n_l}{V} = \frac{P_l}{RT}$$ Equation 2-122

In which n_l is the number of moles of the lth gas; V is the total volume of gas; R is the gas constant; T is the temperature.

2.1.9 **ISOTOPE GEOCHEMISTRY**

Stable isotopes are widely used to identify the hydrogeochemical processes in the hydrosphere (Clark and Fritz 1997). One of the important models in the isotope geochemistry is the Rayleigh fractionation model. However, the application of the model in a complex geochemical environment may not be appropriate because the Rayleigh model neglects secondary transformations such as mineral precipitation and oxidation as well as transport effects such as dispersion and mixing. To solve these problems, the isotope fractionation factor is incorporated into the reactive transport code MIN3P-THCm to account for the secondary effect and obtain a fractionation factor that is more representative of the geochemical systems. Details of the model and applications can be found in Gibson et al. (2011) and Jamieson-Hanes et al. (2012).

Gibson et al. (2010) extended MIN3P to simulate isotope fractionation in a two-isotope sulfur system. Jamieson-Haines et al. (2012) provided a generalized formulation allowing for an unlimited number of isotopes for any element to be tracked. The four-isotope Cr system is used as an example (Jamieson-Haines et al. 2012).

The reduction of chromate by organic carbon (represented as CH_2O) can be described as:

$$3CH_2O + 4\,CrO_4^{2-} + 6\,H^+ \xrightarrow{k_{eff}} 4\,Cr(OH)_2^+ + 3\,CO_3^{2-} + 2\,H_2O$$ Equation 2-123

where k_{eff} is the effective rate constant. To simulate mass-dependent isotope effects, Eqn. 1 is expressed in terms of the four isotopes of Cr:

$$3CH_2O + 4\,{}^{50}CrO_4^{2-} + 6\,H^+ \xrightarrow{{}^{50}k} 4\,{}^{50}Cr(OH)_2^+ + 3\,CO_3^{2-} + 2\,H_2O$$ Equation 2-124

$$3CH_2O + 4\,{}^{52}CrO_4^{2-} + 6\,H^+ \xrightarrow{{}^{52}k} 4\,{}^{52}Cr(OH)_2^+ + 3\,CO_3^{2-} + 2\,H_2O$$ Equation 2-125

$$3CH_2O + 4\,{}^{53}CrO_4^{2-} + 6\,H^+ \xrightarrow{{}^{53}k} 4\,{}^{53}Cr(OH)_2^+ + 3\,CO_3^{2-} + 2\,H_2O$$ Equation 2-126

$$3CH_2O + 4\,{}^{54}CrO_4^{2-} + 6\,H^+ \xrightarrow{{}^{54}k} 4\,{}^{54}Cr(OH)_2^+ + 3\,CO_3^{2-} + 2\,H_2O$$ Equation 2-127

For a given isotope, the mass-dependent rate constants ${}^{x}k$, where *x* refers to the mass number of the isotope, can be described as a function of the kinetic isotope fractionation factor, α_x, the isotope ratio of the substrate, ${}^{x}R_s$ xR_s, and the isotope ratio of the instantaneously derived product, ${}^{x}R_p$:

$$^{53}R_p = \frac{^{53}k_p}{^{52}k_p} = \frac{-^{53}k_s}{-^{52}k_s} = \alpha_{53}\ ^{53}R_s \qquad \text{Equation 2-128}$$

An analogous equation can be derived for the 50Cr and 54Cr isotopes. Employing a mass balance approach:

$$k_{eff} = {}^{50}k + {}^{52}k + {}^{53}k + {}^{54}k \qquad \text{Equation 2-129}$$

the rate constants for each isotope reaction can be derived:

$$^{50}k = \frac{k_{eff}\alpha_{50/52}R_{50/52}}{1 + \alpha_{50/52}R_{50/52} + \alpha_{53/52}R_{53/52} + \alpha_{54/52}R_{54/52}} \qquad \text{Equation 2-130}$$

$$^{52}k = \frac{k_{eff}}{1 + \alpha_{50/52}R_{50/52} + \alpha_{53/52}R_{53/52} + \alpha_{54/52}R_{54/52}} \qquad \text{Equation 2-131}$$

$$^{53}k = \frac{k_{eff}\alpha_{53/52}R_{53/52}}{1 + \alpha_{50/52}R_{50/52} + \alpha_{53/52}R_{53/52} + \alpha_{54/52}R_{54/52}} \qquad \text{Equation 2-132}$$

$$^{54}k = \frac{k_{eff}\alpha_{54/52}R_{54/52}}{1 + \alpha_{50/52}R_{50/52} + \alpha_{53/52}R_{53/52} + \alpha_{54/52}R_{54/52}} \qquad \text{Equation 2-133}$$

2.1.10 **SALINITY DEPENDENT SRB REACTION**

Sulfur water is widely found in groundwater at intermediate depths of sedimentary basins, including regions of the Michigan basin in southeastern Ontario (Carter 2012). However, the mechanisms responsible for the occurrence and controlling factors of these brackish sulfur waters are not fully understood. Anaerobic microbial sulfate reduction is a common process resulting in the formation of sulfur water and has been intensively investigated in various fields of environmental science and engineering (Brown 1982), and by the oil and gas industry (Tang et al. 2009). Sulfate reduction rates depend on many factors including the concentrations of sulfate, the abundance of organic substances, redox conditions, temperature, salinity and the type of sulfate reducing bacteria (SRB) (Brandt et al. 2001). It is well known that the efficiency of sulfate reduction decreases with increasing salinity.

Sulfate reduction by SRB can be generally described by the following reaction (Gibson et al. 2011):

$$CH_2O + 0.5\,SO_4^{2-} = CO_3^{2-} + 0.5H_2S + H^+ \qquad \text{Equation 2-134}$$

in which CH_2O represents organic substances in simplified form. This reaction can be treated in the same way as mineral dissolution and precipitation reactions, and can be modeled as a kinetically controlled irreversible reaction. Experiments have demonstrated that many factors exert strong inhibition effects on hydrogen sulfide generation, such as the concentrations of dissolved oxygen and hydrogen sulfide, and the salinity of the solution (Brandt et al. 2001; Brown 1982; Carter 2012; Tang et al. 2009). To take these

factors into account, sulfate reduction is simulated using a simplified Monod-type rate expression of the form:

$$R = -k_{sal} k_{sulf} \left[\frac{[SO_4^{2-}]}{k_s + [SO_4^{2-}]}\right]\left[\frac{K_{H_2S}^{in}}{K_{H_2S}^{in} + [H_2S(aq)]}\right]\left[\frac{K_{O_2}^{in}}{K_{O_2}^{in} + [O_2(aq)]}\right] \quad \text{Equation 2-135}$$

in which R is the rate of sulfate reduction, k_s is the half-saturation constant, and $[SO_4^{2-}]$, $[H_2S(aq)]$ and $[O_2(aq)]$ represent the concentrations of sulfate, hydrogen sulfide and oxygen, respectively. $K_{H_2S}^{in}$ and $K_{O_2}^{in}$ are the inhibition constants for $[H_2S(aq)]$ and $[O_2(aq)]$, respectively. k_{sulf} is the maximum rate constant and k_{sal} is the salinity inhibition factor between 0.0 and 1.0, which can be calculated according to the following equation based on experimental data:

$$k_{sal} = \sum_{i=0}^{n} f_i S^i \quad \text{Equation 2-136}$$

in which f_i is the coefficients [-], and S is the salinity in [g/L].

2.2 NUMERICAL IMPLEMENTATION

2.2.1 OVERVIEW

This section summarizes the numerical techniques used for the solution of the governing equations described in section 2.1. These equations are nonlinear and require an iterative solution. For the non-isothermal variably-saturated flow and reactive transport equations without density driven flow, Newton's methods are used. In such cases, the flow Equation 2-4 is independent of the reactive transport Equation 2-37 and thus can be solved separately. With the addition of more complex processes, Newton's and/or Picard's methods are employed for the solution of the equations depending on the problems to be solved.

The finite volume method (Patankar 1980) is used for spatial discretization. This method is locally mass-conservative, which is a necessary requirement for the solution of reactive transport using the global implicit solution method. Fully implicit time weighting is employed for the temporal discretization of the governing equations. To increase the accuracy, efficiency and robustness of the model, several numerical technics have been used or developed including spatial weighting schemes (van Leer 1974; Unger et al. 1996), adaptive time stepping and update modification algorithm, activity update techniques, sparse matrix data structure and the treatment of finite mineral phases (Mayer, 1999).

2.2.2 SPATIAL AND TEMPORAL DISCRETIZATION

Obtaining solutions to the governing equations describing the movement of variable

density fluids in fully- or variably-saturated media requires discretization in space and time.

2.2.2.1 Isothermal variably-saturated flow with constant density

Spatial and temporal discretization of the mass conservation equation for isothermal variably-saturated flow of fluid with constant density (e.g. Equation 2-4) using the finite volume technique leads to (Mayer, 1999):

$$\left[S_{a,k}^{N+1} S_{s,k} \frac{h_k^{N+1} - h_k^N}{\Delta t} + \phi_k \frac{S_{a,k}^{N+1} - S_{a,k}^N}{\Delta t}\right] V_k$$
$$- \sum_{l \in \eta_k} k_{ra,kl}\, \gamma_{kl} [h_l^{N+1} - h_k^{N+1}] - Q_{a,k}^{N+1} = 0 \qquad k = 1, N_v$$

Equation 2-137

where the subscript k refers the k^{th} control volume, and η_k refers to the number of adjacent control volumes, which can vary from one for the boundary control volume in case of a 1D problem to six for an internal control volume (assuming blocks) in the case of 3D spatial discretization. The subscript l identifies the adjacent control volumes, Δt is the time increment, $N+1$ represents the new time level and N defines the old time level. V_k is the volume of the k^{th} control volume. N_v defines the number of control volumes in the solution domain. $k_{ra,kl}$ is the representative relative permeability used for the flux calculation between control volumes k and l. γ_{kl} is the influence coefficient that can be calculated as:

$$\gamma_{kl} = \frac{A_{kl}}{d_{kl}} K_{kl} \qquad \text{Equation 2-138}$$

where A_{kl} is the interfacial area between the control volumes k and l. d_{kl} is the distance between the centroids of the control volumes k and l. K_{kl} defines the representative hydraulic conductivity used for the flux calculation between control volumes k and l, and can be calculated based on the distance-weighted harmonic mean (Mayer, 1999):

$$K_{kl} = \frac{2 K_{i,k} K_{i,l} d_{kl}}{K_{i,k} d_{i,l} + K_{i,l} d_{i,k}}, \qquad \text{Equation 2-139}$$

where $K_{i,k}$ and $K_{i,l}$ are the hydraulic conductivities of the control volumes k and l, respectively, perpendicular to the interfacial area A_{kl}. The subscript i identifies here the spatial coordinates x, y and z. $d_{i,l}$ and $d_{i,k}$ define the spatial extent of the two adjacent control volumes perpendicular to the interfacial area A_{kl}.

2.2.2.2 Density dependent flow

The fluid mass conservation equations for density dependent flow are formulated using an implicit time weighting scheme. Using the Picard iterative approach, time step and Picard iteration indices must be specified for all dynamic variables. Using the superscripts $N+1$ and N to indicate current and previous timelevels, and superscripts $i+1$ and i to indicate current and previous Picard iterations, the following fluid mass conservation equation is implemented:

$$
\begin{aligned}
&[\,S_p^{N+1,i} S_{a,k}^{N+1,i+1} \rho_{a,k}^{N+1,i} \frac{P_{a,k}^{N+1,i+1} - P_{a,k}^{N}}{\Delta t} + \phi_k^N \rho_{a,k}^{N+1,i} \frac{S_{a,k}^{N+1,i+1} - S_{a,k}^{N}}{\Delta t} \\
&+ S_{a,k}^{N+1,i+1} \phi_k^N \frac{\partial \rho_a}{\partial TDS} \frac{TDS_k^{N+1,i} - TDS_k^{N}}{\Delta t} + S_{a,k}^{N+1,i+1} \phi_k^N \frac{\partial \rho_a}{\partial T} \frac{T_k^{N+1,i} - T_k^{N}}{\Delta t}]V_k \\
&- \sum_{l \in \eta_k} k_{ra,kl}\, \mathrm{K}_{kl} \frac{\rho_{a,kl}^{N+1,i}}{\mu_{a,kl}^{N+1,i}} \frac{A_{kl}}{d_{kl}} [(P_{a,l}^{N+1,i+1} - P_{a,k}^{N+1,i+1}) \\
&+ \rho_{a,kl}^{N+1,i} g(z_l - z_k)] = -\rho_{a,s} Q_{a,k}^{N+1} \qquad k = 1, N_v
\end{aligned}
$$

Equation 2-140

where $S_p = S_s/(\rho g)$ is the one-dimensional pressure-based specific storage coefficient in [M^{-1} L T^2] for the relationship between pressure-based specific storage coefficient and specific storage coefficient S_s), ρ_a is the aqueous phase density in [M L^{-3}], $\rho_{a,s}$ is the aqueous phase density of external sources/sinks [M L^{-3}], g is the gravity constant [L T^{-2}], S_a is the aqueous phase saturation [-], P_a represents the aqueous phase pressure, ϕ is the porosity [-], K_{kl} is the representative hydraulic conductivity used for the flux calculation between control volumes k and l, z is the elevation [L], μ_a is the viscosity of the aqueous phase [M L^{-1} T^{-1}], and Q_a is the volumetric aqueous phase source/sink term [T^{-1}].

A detailed description of the density dependent flow model and implementation can be found in Henderson (2009).

2.2.2.3 One-dimensional hydromechanical coupling

Similarly, the fluid mass conservation equations (Equation 2-27) including 1D hydromechanical coupling for saturated porous media is discretized as (Bea et al., 2011):

$$
\begin{aligned}
&[\,S_p^{N+1} \rho_{a,k}^{N+1} \left(\frac{P_{a,k}^{N+1} - P_{a,k}^{N}}{\Delta t} - \zeta_k \frac{\sigma_{zz}^{N+1} - \sigma_{zz}^{N}}{\Delta t}\right) \\
&+ \phi_k^{N+1} \frac{\rho_{a,k}^{N+1} - \rho_{a,k}^{N}}{\Delta t}]V_k - \sum_{l \in \eta_k} \mathrm{K}_{kl} \frac{\rho_{a,kl}^{N+1}}{\mu_{a,kl}^{N+1}} \frac{A_{kl}}{d_{kl}} [(P_{a,l}^{N+1} - P_{a,k}^{N+1}) \\
&+ \rho_{a,kl}^{N+1} g(z_l - z_k)] = -\rho_{a,s} Q_{a,k}^{N+1}
\end{aligned}
$$

Equation 2-141

Where ζ is the one-dimensional efficiency loading coefficient [-] (Neuzil, 2003), σ_{zz} is the vertical stress [M L^{-1} T^{-2}]. A detailed description can be found in Bea et al. (2011).

2.2.2.4 Energy transport

In MIN3P-THCm, the energy balance equation is fully coupled with the fluid mass conservation equation and solved at the same time. Thus, the Newton-Raphson method is used to linearize the system of equations. Coupling among fluid flow, solute and energy transport results from the solute concentration and temperature dependence of fluid density and viscosity, and thus Darcy velocities.

The energy conservation equations (Equation 2-28) are discretized in space using the finite volume technique and by applying fully implicit time weighting. The discretized equations can be written as (Bea et al., 2011):

$$\frac{c_w V_k}{\Delta t}\left[\phi_k^{N+1}\rho_{a,k}^{N+1}T^{N+1}-\phi_k^{N}\rho_{a,k}^{N}T^{N}\right]+$$
$$\frac{c_{s,k}\rho_{s,k}V_k}{\Delta t}\left[(1-\phi_k^{N+1})T^{N+1}-(1-\phi_k^{N})T^{N}\right]=$$
$$-c_w\sum_{l\in\eta_k}\rho_{a,kl}^{N+1}q_{a,kl}T_{kl}^{N+1}-\sum_{l\in\eta_k}\gamma_{kl}^{c,N+1}\Delta T_{kl}^{N+1}+$$
$$\sum_{l\in\eta_k}\phi_{kl}^{N+1}\rho_{a,kl}^{N+1}\gamma_{kl}^{d,N+1}\Delta T_{kl}^{N+1}+c_w\rho^{*}A_kQ^{*}T^{*}$$

Equation 2-142

where c_w is the heat capacity for water [L^2 T^{-2} $^oC^{-1}$], V_k is the volume of the k^{th} cell [L^3], Δt is the time increment [T], ϕ is the porosity [-], ρ_a [M L^{-3}] is the aqueous phase density, and T is temperature [Θ]. c_s and ρ_s are the heat capacity [L^2 T^{-2} Θ^{-1}] and density [M L^{-3}] of the solid, respectively. $q_{a,kl}$ is the volumetric fluid flux between control volumes *k* and *l* [L^3T^{-1}] used for the advective flux calculations across the interface between the control volumes *k* and *l* with T_{kl}^{N+1}[^{o}C] and ρ_{kl}^{N+1} [M L^{-3}] defining the temperature and fluid density at the interface, respectively. γ_{kl}^{c} is the influence coefficient for the conduction flux [M L^2 T^{-3} $^oC^{-1}$] and γ_{kl}^{d} is the influence coefficient for the dispersive flux [L^5T^{-3} $^oC^{-1}$]. ΔT_{kl}^{N+1} [Θ] represents the temperature difference between cells *k* and *l*. T^* and ρ^* are the external temperature [Θ] and fluid density [M L^{-3}] when fluid mass flux is entering the system, or the temperature and fluid density corresponding to an adjacent cell at the boundary when fluid mass exits the system. Q^* is the volumetric flux per unit of surface area at the boundary [L^3 L^{-2} T^{-1}] and A_k is the surface area of the boundary cell [L^2].

The influence coefficient γ_{kl}^{c} for the conduction flux is defined by:

$$\gamma_{kl}^{c}=\frac{A_{kl}}{d_{kl}}\lambda_{kl}$$

Equation 2-143

where A_{kl}, d_{kl} and λ_{kl} [M L T^{-3} Θ^{-1}] are the interfacial area, distance and thermal conductivity of the porous medium between cells *k* and *l*, respectively. Thermal conductivity of the porous medium is computed according to:

$$\lambda_k=\phi_k\lambda_{w,k}+(1-\phi_k)\lambda_{s,k}$$

Equation 2-144

where λ_w and λ_s are thermal conductivities for water and solid, respectively.

λ_{kl} is the representative thermal conductivity used for the flux calculation between control volumes *k* and *l*, and can be calculated based on the distance-weighted harmonic mean:

$$\lambda_{kl}=\frac{\lambda_k\lambda_l d_{kl}}{\lambda_k d_k+\lambda_l d_l}$$

Equation 2-145

where λ_k and λ_l are thermal conductivities of the control volumes *k* and *l*, respectively,

perpendicular to the interfacial area A_{kl} .

Thermal dispersive term (γ_{kl}^{d}) is computed as:

$$\gamma_{kl}^{d} = \frac{A_{kl}}{d_{kl}} c_w \phi_{kl} D_{a,kl} \qquad \text{Equation 2-146}$$

where $D_{a,kl}$ [L^2 T^{-1}] defines the effective dispersion coefficient in the aqueous phase between control volumes k and l.

2.2.2.5 Reactive transport

The global mass conservation equations (Equation 2-37) for the components A_j^c ($j=1, N_c$) are discretized in space using the finite volume technique and applying fully implicit time weighting (Mayer et al., 2002):

$$\begin{aligned}
&\frac{\phi_k V_k}{\Delta t}\left[S_{a,k}^{N+1} T_{j,k}^{a,N+1} - S_{a,k}^{N} T_{j,k}^{a,N}\right] + \frac{\phi_k V_k}{\Delta t}\left[S_{g,k}^{N+1} T_{j,k}^{g,N+1} - S_{g,k}^{N} T_{j,k}^{g,N}\right] \\
&+ \frac{V_k}{\Delta t}\left[T_{j,k}^{s,N+1} - T_{j,k}^{s,N}\right] + \sum_{l\in\eta_k} q_{a,kl}\, T_{j,kl}^{a,N+1} \\
&- \sum_{l\in\eta_k} \gamma_{a,kl}^{d}\left[T_{j,l}^{a,N+1} - T_{j,k}^{a,N+1}\right] - \sum_{l\in\eta_k} \gamma_{g,kl}^{d}\left[T_{j,l}^{g,N+1} - T_{j,k}^{g,N+1}\right] \qquad \text{Equation 2-147} \\
&- Q_{j,k}^{a,a,N+1} V_k - Q_{j,k}^{a,m,N+1} V_k - Q_{j,k}^{a,ext,N+1} V_k \\
&- Q_{j,k}^{g,ext,N+1} V_k = 0 \qquad\qquad k = 1, N_v
\end{aligned}$$

where $q_{a,kl}$ is the aqueous phase flux between control volumes k and l, accounting for the interfacial area between the adjacent cells, $\gamma_{a,kl}^{d}$ are the influence coefficients for the dispersive flux in the aqueous phase, and $\gamma_{g,kl}^{d}$ are the influence coefficients for the diffusive gas flux in the gaseous phase. $T_{j,kl}^{a,N+1}$ are the total aqueous component concentrations used for the advective flux calculations across the interface between the control volumes k and l, which are determined by upstream or centered weighting, or by a flux limiter scheme.

The influence coefficients $\gamma_{a,kl}^{d}$ for the dispersive flux terms are defined by:

$$\gamma_{a,kl}^{d} = \frac{A_{kl}}{d_{kl}} S_{a,kl}^{N+1} \phi_{kl} D_{a,kl} \qquad \text{Equation 2-148}$$

where $D_{a,kl}$ is the effective dispersion coefficient in the aqueous phase between control volumes k and l. The computation of the dispersion coefficient is based on the implementation by Forsyth et al. (1998). $S_{a,kl}^{N+1}$ and ϕ_{kl} are the harmonic average aqueous phase saturation and porosity between control volumes k and l. Influence coefficients $\gamma_{g,kl}^{d}$ for the diffusive gas flux between control volumes k and l are determined similarly.

As for minerals, it is generally assumed that mineral parameters change slowly compared to those of aqueous species (Lichtner, 1988). Therefore, the volume fractions of the minerals are updated after completion of a time step by discretizing Equation 2-38 explicitly in time and solving for the volume fractions at the new time level:

$$V_{f,j}^{m,N+1} = V_{f,j}^{m,N} + V_j^m R_j^{m,N+1} \Delta t, \qquad j = 1, N_m \qquad \text{Equation 2-149}$$

The advantage of this approach is that the number of primary unknowns at each control volume are reduced by N_m. When using this approach, however, special provisions have to be made to ensure mass conservation especially in the case of finite mineral volume, because the computed rates do not implicitly depend on the mineral parameters. In MIN3P-THCm, the reaction rates are adjusted such that mineral concentrations cannot become negative if a mineral phase dissolves entirely from a particular cell (see section 2.2.6).

Details of the numerical implementation of the reactive transport models for low permeability porous media such as the multicomponent diffusion model (MCD), the hybrid multicomponent diffusion model (hMCD) and the multisite ion exchange model (MIE) is referred to Xie et al. (2014).

2.2.3 **MASS BALANCE CALCULATIONS**

The present mode1 formulation includes detailed mass balance calculations for variably-saturated flow and reactive transport. This is specifically useful for the reactive transport simulations, because it facilitates the evaluation of the interactions between aqueous, and gaseous species, as well as solid phases. Mass balance calculations include absolute and relative mass balance errors per time step and the corresponding cumulative errors. Mass balance calculations also include the total mass of the species contained in the solution domain, the total mass gain and mass loss due to fluxes across the boundaries, change in storage, and mass transfer between the phases in the case of reactive transport. Mass balance calculations for variably-saturated flow are formulated in a standard way. Detailed formulations can be found in Mayer (1999).

2.2.4 **SOLUTION METHOD**

The solution of the entire system of equations consists of the solution of the variably-saturated flow and energy balance equations, with the subsequent solution of the reactive transport problem based on the fluxes and phase saturations obtained from the flow solution.

The system of algebraic nonlinear equations for the isothermal variably-saturated flow (Equation 2-4), energy balance (Equation 2-28) and reactive transport (Equation 2-37) are linearized using Newton's method. The coupling between fluid density and solute concentrations (Equation 2-3, Equation 2-9 and Equation 2-37) is resolved using the Picard iterative approach (Putti and Paniconi 1995). This method linearizes the combined set of flow and reactive transport equations by computing fluid density and solving the fluid conservation equations using chemical concentrations computed during the previous Picard iteration (Voss 1984). The Picard approach is conceptually straightforward, and is widely used for simulating density dependent flow and mass transport problems (Voss 1984; Diersch 2002; Langevin and Guo 2006; Henderson 2009). A representative flow diagram is depicted in Figure 2.2 for the numerical solution of multicomponent reactive transport problems including density driven flow and energy transport.

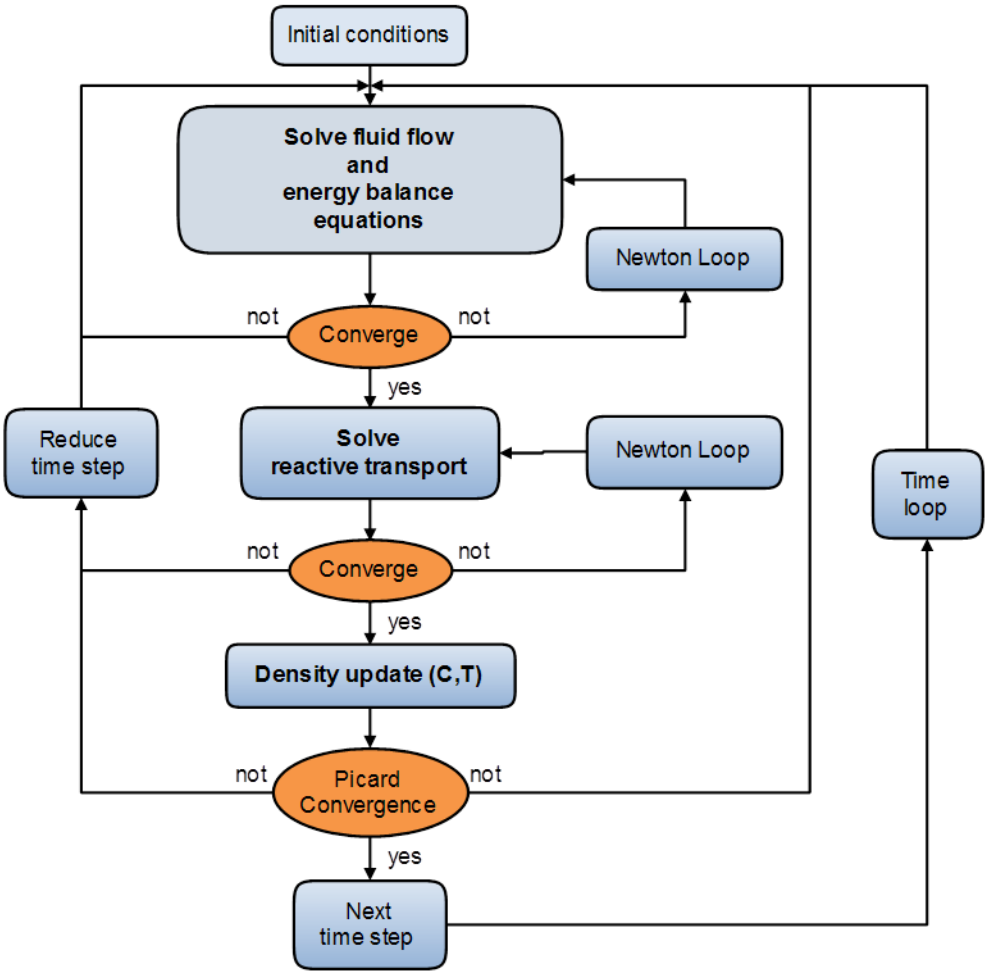

Figure 2.2 Flow diagram of the equation solution process implemented in MIN3P-THCm. Time step reductions occur when the maximum number of Newton or Picard iterations have been reached and the convergence criteria have not been achieved (Bea et al., 2011)

The Newton-linearization for the variably-saturated flow and energy balance equations is implemented following standard techniques (e.g. Paniconi and Putti, 1994) and is therefore not repeated here. For density-dependent flow, updates in fluid density provide the criterion to evaluate the convergence of the Picard iterations. The Picard iteration method has also been implemented in other codes (e.g.: Guo and Langevin, 2002).

Special techniques are employed; however, to solve the systems of algebraic non-linear equations for reactive transport problems, because the primary unknowns can vary over tens of orders of magnitude during the course of a simulation (Mayer and MacQuarrie, 2010). This may result in Jacobian matrices that are often numerically singular (Holm, 1989). The systems of algebraic non-linear equations for reactive transport (Equation 2-37) are linearized using the Newton–Raphson method:

$$\frac{\partial F(C_j^c)}{\partial C_i^c}\Delta C_i^c = -F(C_j^c) \qquad \text{Equation 2-150}$$

where $F(C_j^c)$ is defined by Equation 2-37 and ΔC_i^c is the update for the primary unknowns C_i^c. Although Equation 2-37 does not explicitly contain the primary unknown C_i^c, the primary unknows are contained in the mass balance equations (Equation 2-39 - Equation 2-41), law of mass cation relationships (Equation 2-51 and Equation 2-52), and rate expressions (Equation 2-53 - Equation 2-57), which are all directly substituted into Equation 2-37. The concentrations at the new iteration level are obtained from:

$$C_j^{c,N+1,I+1} = C_j^{c,N+1,I} + \Delta C_j^{c,I+1} \qquad \text{Equation 2-151}$$

where the superscript *I* defines the old iteration level and *I + 1* defines the new iteration level.

The standard Newton–Raphson method is modified for the solution of reactive transport problems by solving the system of equations in terms of concentration increments defined on a logarithmic scale (e.g. Steefel and Lasaga, 1994):

$$\frac{\partial F(C_j^c)}{\partial \ln(C_i^c)}\Delta\ln(C_i^c) = -F(C_j^c) \qquad \text{Equation 2-152}$$

This modification greatly reduces the condition number of the Jacobian matrix (Holm 1989), and often leads to better convergence properties (Steefel and Lasaga, 1994). The concentrations at the new iteration level are obtained from:

$$\ln[C_j^{c,N+1,I+1}] = \ln[C_j^{c,N+1,I}] + \Delta\ln[C_j^c] \qquad \text{Equation 2-153}$$

The solution for one time step consists of a series of iterations and is considered complete if all updates are smaller than a prescribed tolerance. This tolerance is also expressed on a logarithmic scale to account for the poor scaling properties:

$$\Delta\ln(C_{act}^c) = \varepsilon \qquad \text{Equation 2-154}$$

where ε is the prescribed tolerance and $\Delta\ln(C_{act}^c)$ is the actual maximum update in the solution domain for all components defined by:

$$\Delta\ln(C_{act}^c) = \max\left[\Delta\ln(C_{j,k}^c), \Delta\ln(C_{act}^c)\right], \quad k = 1, N_v, j = 1, N_c \qquad \text{Equation 2-155}$$

The partial derivatives in Equation 2-152 can be obtained using numerical differentiation, which is particularly advantageous for complex nonlinear functions (Mayer, 1999).

The set of algebraic relationships given by Equation 2-37 leads to a large Jacobian matrix that is solved using the sparse iterative solver package WATSOLV (Van der Kwaak et al., 1997).

2.2.5 COMPRESSED DATA STRUCTURE FOR REACTION MATRICES

A compressed data structure, which stores only non-zero entries, is not only applied for the Jacobian matrices resulting from the discretization of the variably-saturated flow and reactive- transport problems, but also for the geochemical reaction matrices. These matrices contain the stoichiometric coefficients of the components in the secondary species, but are also used to store the reaction orders of the reactant species in the case of kinetically-controlled reactions. Compressed storage in general has the advantage of minimizing the memory requirements and the number of floating point operations when performing matrix operations. Memory savings is not an issue in the case of reaction matrices; however, the computational effort might be decreased significantly (Mayer, 1999).

2.2.6 TREATMENT OF FINITE MINERAL PHASES

One of the major difficulties for the solution of the reactive transport equations is that the masses of minera1 phases are finite. This is a particular problem when minerals are treated as secondary unknowns, even though dissolution-precipitation reactions are formulated as kinetically-controlled reactions. The reactive surface area term and all other mineral parameters in reaction expressions are defined at the old time level when calculating the reaction rate for the solution at the new time level. Therefore, the solution of Equation 2-37 does not indicate the depletion of a mineral phase during a time step and it is possible that non-physical negative mineral volume fractions may be obtained when updating the mineral volume fractions with Equation 2-149.

The general idea to solve this problem is to check whether a sufficient amount of a mineral C_i^m is available to sustain the computed dissolution rate during a particular time step. If this is not the case, the reaction rate has to be adjusted in order to just deplete the particular mineral phase. This reaction rate can then be inserted in the right-hand-side vector as a known source-sink term. An appropriate algorithm is given by:

$$\Delta C_i^m = R_i^{m,N+1}\Delta \mathrm{t}$$
$$\text{if } \left(C_i^{m,N} + \Delta C_i^m < 0\right) \text{ then}$$
$$R_i^{m,N+1} = -\frac{C_i^{m,N}}{\Delta t} \qquad \text{Equation 2-156}$$
$$\text{end if}$$

The depletion of a mineral phase results in a discontinuity in the system of governing equations and time step reductions may occur as a result of the manipulations described above (Mayer 1999).

2.2.7 ADAPTIVE TIME STEPPING AND UPDATE MODIFICATION SCHEMES

In order to ensure a reliable and robust solution of the linearized equations, adaptive time stepping must be employed. In the present formulation, the size of the time increment is

based on the change in aqueous concentrations ("update-based") and/or the number of Newton–Raphson iterations ("iteration-based"). The update-based and iteration-based time increment adjustments can be used simultaneously or as stand-alone schemes. A flow chart of the time stepping schemes for reactive transport is summarized in Table 2.1.

Table 2.1 Adaptive time stepping scheme for solution of reactive transport equations (Mayer, 1999)

No.	Description	Mathematic equation
1.	Set maximum new time increment	$\Delta t^{N+1} = min[\Delta t_{max}, \alpha_{inc}\Delta t^{N}]$
2.	Determine maximum actual update $\Delta\log(C^{c}_{act})$	$for\ k = 1, N_v$ $for j = 1, N_c$ $\Delta\log(C^{c}_{act}) = max[\Delta\log(C^{c}_{j,k}), \Delta\log(C^{c}_{act})]$ end for end for
3.	Determine new time increment based on anticipated and maximum actual update	$\Delta t^{N+1} = min[\Delta\log(C^{c}_{ant})/\Delta\log(C^{c}_{act})\Delta t^{N}, \Delta t^{N+1}]$
4.	Determine new time increment based on anticipated and actual number of iterations	$\Delta t^{N+1} = min[f(N^{act}_{it}, N^{ant}_{it})\Delta t^{N}, \Delta t^{N+1}]$
5.	Limit decrease of time increment	$\Delta t^{N+1} = max[\Delta t^{N+1}, \alpha_{dec}\Delta t^{N}]$
6.	Lower bound – minimum time increment	$\Delta t^{N+1} = max[\Delta t_{min}, \alpha_{inc}\Delta t^{N}]$

The time increment for the next time step is initially limited by the minimum of the user-specified maximum time increment Δt^{N+1}, and the previous time increment multiplied by a factor α_{inc}, which determines the maximum tolerable time increment increase. In the following the new time increment is estimated based on the geochemical changes which have occurred during the previous time step using a method similar to the one proposed by Forsyth and Sammon (1986). Employing a first order scheme, the new time increment can be based on the maximum actual update $\Delta\log(C^{c}_{act})$, which is determined based on the local updates for all components in the entire solution domain, and an user-specified anticipated update $\Delta\log(C^{c}_{j,k})$. These updates have to be defined on a logarithmic scale to account for the large concentration ranges characteristic for reactive transport problems. A second possibility is to base the new time increment on the number of Newton-iterations N^{act}_{it}

which were required for the solution of the previous time step and an anticipated number of Newton-iterations N_{it}^{ant}. Various functional relationships between these parameters can be employed to yield a rapid adjustment towards the anticipated time increment. The new time increment can now be defined as the minimum of the estimated time increments. The time increment is finally checked against a maximum tolerable decrease in comparison to the previous time increment, defined by the factor α_{dec}, and a user-specified minimum time increment.

Despite these provisions, it is possible that convergence cannot be achieved; in this case, the time step is restarted with a reduced time increment.

In addition, it is also important to ensure that a non-convergent solution is not induced during the early stages of the Newton–Raphson iteration loop, when quadratic convergence behavior is not yet encountered. If intermediate updates assume unrealistic values, the successful solution of the model equations may be jeopardized. It is therefore necessary to constrain the updates within specified limits in order to force the solution into the zone of quadratic convergence (Leeming et al., 1998). The MIN3P-THCm code makes use of local update corrections, which limit the concentration updates to a user specified number of log cycles:

$$\begin{aligned}
&\Delta\log(C_{j,k}^{c}) = min\left[\Delta\log(C_{j,k}^{c}), \Delta\log(C_{max}^{c})\right], \\
&\qquad k = 1, N_v, j = 1, N_c, if\ \Delta\log(C_{j,k}^{c}) > 0 \\
&\Delta\log(C_{j,k}^{c}) = max\left[\Delta\log(C_{j,k}^{c}), -\Delta\log(C_{max}^{c})\right], \\
&\qquad k = 1, N_v, j = 1, N_c, if\ \Delta\log(C_{j,k}^{c}) < 0
\end{aligned} \qquad \text{Equation 2-157}$$

Where $\Delta\log(C_{max}^{c})$ is the user specified maximum update. Investigations by Leeming et al. (1998) have shown that more sophisticated techniques, such as line search methods, do not lead to a significant improvement of the convergence behavior in comparison to simple local update modification schemes implemented in MIN3P-THCm.

The present time stepping scheme does not limit the maximum time step size based on a Courant (CFL) constraint, because fully implicit time integration is used and a Courant criterion does not have to be obeyed to warrant numerical stability (Unger et al., 1996). The time stepping scheme also does not include an error control as provided by more sophisticated methods included in DAE solvers such as DASSL or DASPK (Hindmarsh and Petzold, 1995). However, the accuracy of the solution can be controlled by the user specified maximum time increment. Further details on the adaptive time stepping and update modification schemes can be found in Mayer (1999) and Mayer and MacQuarrie (2010).

2.2.8 **INITIAL AND BOUNDARY CONDITIONS**

2.2.8.1 Flow

Boundary conditions (BCs) for subsurface flow include Dirichlet (specified hydraulic head/pressure), Cauchy (specified flux), free exit conditions, and seepage faces BC.

Initial hydraulic conditions (ICs) and boundary conditions may be assigned in units of fluid

pressure, pressure heads, hydraulic heads, or freshwater heads (positive for saturated flow, negative for unsaturated flow). Initial fluid pressures are assigned to the model grid using the following relationships:

$$P_{a,k} = \psi_k |g| \rho_{a,k} \quad \text{Equation 2-158}$$

$$P_{a,k} = \left(h_f - z_{ivol}\right) g |\rho_{a,f} \quad \text{Equation 2-159}$$

$$P_{a,k} = \left(h_k - z_k\right) g |\rho_{a,k} \quad \text{Equation 2-160}$$

Where *k* stands for the control volume to be assigned for IC and/or BC, ψ is the pressure head [L], |g| is the magnitude of gravitational acceleration [L T^{-2}], h_f and h represent freshwater and hydraulic heads [L], $\rho_{a,f}$ is the freshwater density [M L^{-3}] and the density ρ_a [M L^{-3}] is calculated using Equation 2-12.

Initial and boundary conditions specified for the geochemical system are read and assigned to the model grid before initial and boundary conditions are assigned to the flow system. This order of execution allows the density of fluids at assigned model boundaries to be computed, and facilitates the calculation of internal initial fluid pressures. A hydrostatic fluid pressure profile may be assigned to a vertical interval in the model domain containing a uniform solute concentration using the following relationship (Henderson, 2009):

$$P_{a,k} = P_{a,0} + |g| \rho_{a,k} \left[z_0 - z_k\right] \quad \text{Equation 2-161}$$

where $P_{a,0}$ [M L^{-1} T^{-2}] and z_0 [L] represent the fluid pressure and the elevation at the top of the interval. This calculation provides an efficient mechanism to assign initial fluid pressures when dense fluids are present and ensures that their distribution is consistent with solute concentrations and fluid densities.

Specified fluid head, pressure or Darcy flux boundary conditions may be assigned to the exterior boundaries of the model domain. Time dependent flow conditions can be assigned through separate input file.

2.2.8.2 Reactive transport

Boundary conditions for solute transport include Dirichlet (specified concentration), Cauchy (specified mass flux), free exit conditions, and seepage faces. In the Dirichlet formulation, concentrations are specified at the boundary or internal nodes. In the Cauchy formulation, fluids entering the model domain are assigned user-specified chemical concentrations. Concentrations can be specified as total concentrations. In addition, pH, Eh, and partial gas pressures can be defined. The latter option is useful to define the saturation state of recharge with respect to oxygen.

Injection of solutes into an interior node of the model domain can be simulated using a point source boundary condition. The fluid boundary condition requires that a volumetric injection or extraction rate is specified. When fluids are added to a model cell, a Cauchy (specified mass flux) boundary condition is used to assign solute concentrations to the

injected fluids. When fluids are removed from the model cell, a free exit boundary condition is applied to simulate an extraction well. Boundary conditions, including fluid injection/extraction rates and locations, may be modified throughout a simulation (Henderson 2009).

2.2.8.3 Heat transport

Boundary conditions for energy balance equations include Dirichlet (specified temperature), Cauchy (specified heat flux), and free exit conditions. In the Dirichlet formulation, temperature is specified at boundary or internal nodes. In the Cauchy formulation, heat fluxes entering the model domain are assigned by the user.

The initial conditions for temperature can be defined in a similar manner as the boundary conditions.

REFERENCES

Abrams, R. H., K. Loague and D. B. Kent (1998). Development and testing of a compartmentalized reaction network model for redox zones in contaminated aquifers, *Water Resources Research*, 34(6), 1531–1541, doi:10.1029/98WR00485.

Ackerer, P., A. Younes and R. Mose (1999). Modeling variable density flow and solute transport in porous medium: 1. Numerical model and verification. Transport in Porous Media, 35, 345-373.

Allison, J. D., W. Brown and K.J. Novo-Gradac (1991). MINTEQA2/PRODEFA2, A geochemical assessment model for environmental systems: version 3.0 User's Manual. Environmental research laboratory, U.S Enviromentla protection Agency, EPA/600/3-91/021.

Alt-Epping, P., C. Tournassat, P. Rasouli, C. I. Steefel, K. U. Mayer, A. Jenni, U. Mäder, S. S. Sengor and R. Fernández. 2015. Benchmark reactive transport simulations of a column experiment in compacted bentonite with multispecies diffusion and explicit treatment of electrostatic effects, Computational Geosciences 19(3): 535. doi:10.1007/s10596-014-9451-x.

Amos, R. T. and K. U. Mayer (2006). Investigating the role of gas bubble formation and entrapment in contaminated aquifers: Reactive transport modeling, Journal of Contaminant Hydrology, 87:123-154.

Appelo, C.A.J. and D. Postma (2005). Geochemistry. Groundwater and Pollution, Sec. Ed., Leiden, The. Netherlands (Balkema Publishers).

Appelo, C.A.J., A. Vinsot, S. Mettler and S. Wechner (2008). Obtaining the porewater composition of a clay rock by modelling the in- and out-diffusion of anions and cations from an in-situ experiment. Journal of Contaminant Hydrology, 101, 67-76.

Ayora, C., J. Garcia-Veigas and J. Pueyo (1994). The chemical and hydrological evolution of an ancient potash-forming evaporite basin as constrained by mineral sequence, fluid inclusion composition, and numerical simulation. Geochimica et Cosmochimica Acta, 58, 3379-3394.

Balay, S., S. Abhyankar, M.F. Adams, J. Brown, P. Brune, K. Buschelman, V. Eijkhout, W.D. Gropp, D. Kaushik, M.G. Knepley, L.C. McInnes, K. Rupp, B.F. Smith and H. Zhang (2014a). PETSc Web page. http://www.mcs.anl.gov/petsc.

Balay, S., S. Abhyankar, M.F. Adams, J. Brown, P. Brune, K. Buschelman, V. Eijkhout, W.D. Gropp, D. Kaushik, M.G. Knepley, L.C. McInnes, K. Rupp and B.F. Smith and H. Zhang (2014b). PETSc Users Manual. http://www.mcs.anl.gov/petsc.

Balay, S., W.D. Gropp, L.C. McInnes and B.F. Smith (1997). Efficient Management of Parallelism in Object Oriented Numerical Software Libraries, in Modern Software Tools in Scientific Computing (editors Arge, E., Bruaset, A. M. and Langtangen, H. P.), 163-202, Birkhauser Press.

Bahr, J. M. and J. Rubin (1987). Direct comparison of kinetic and local equilibrium formulations for solute transport affected by surface reactions, Water Resources Research, 23, 438– 452.

Bea, S.A., J. Carrera, C. Ayora and F. Batlle (2010). Pitzer Algortithm: Efficient implementation of Pitzer equations in geochemical and reactive transport models. Computers & Geosciences, 36, 526-538.

Bea, S.A., K.U. Mayer, K.T.B. MacQuarrie (2011). Modelling Reactive Transport in Sedimentary Rock Environments - Phase II, MIN3P-THCm code enhancements and illustrative simulations for a glaciation scenario. Technical report: NWMO TR-2011-13.

Bea, S., S. Wilson, K.U. Mayer, G. Dipple, I. Power and P. Gamazo, (2012). Reactive transport modeling of natural carbon sequestration in ultramafic mine tailings, Vadose Zone Journal, 11(2), 1-17

Bear, J. (1972). Dynamics of Fluids in Porous Media, Elsevier Sci., New York.

Bennett, T.A. (1997). An in-situ reactive barrier for the treatment of hexavalent chromium and trichloroethylene in groundwater, M.Sc. thesis, University of Waterloo, Waterloo, Onterio, Canada.

Berner, R. A. (1978). Rate control of mineral dissolution under earth surface conditions, Am. J. Sci., 278, 1235–1252.

Bitelli M., F. Ventura, G.S. Campbell, R.L. Snyder, F. Gallegati and P.R. Pisa (2008) Coupling of heat, water vapor, and liquid water fluxes to compute evaporation in bare soils, Journal of Hydrology 362, 191-205

Bolt, G.H., M.E. Summer and A. Kamphorst. (1963). A study of the equilibrium between three categories of potassium in an illitic soil. Soil Science Society of America, Proceedings 27, 294-299.

Borden, R. C. and P. B. Bedient (1986). Transport of dissolved hydrocarbons influenced by oxygen-limited biodegradation, 1, Theoretical development, Water Resources Research, 22, 1973– 1982.

Bourg, I.C., A.C.M. Bourg and G. Sposito (2003). Modeling diffusion and adsorption in compacted bentonite: a critical review. Journal of Contaminant Hydrology, 61, 293-302.

Bradbury, M. H. and B. Baeyens (2000). A generalized sorption model for the concentration dependent uptake of caesium by argillaceous rocks, Journal of Contaminant Hydrology, 42, 141-163.

Bradbury, M. H. and B. Baeyens (2011). Predictive sorption modelling of Ni(II), Co(II), Eu(III), Th(IV) and U(VI) on MX-80 bentonite and Opalinus Clay: A “bottom-up” approach, Applied Clay Science, 52, 27-33.

Brandt, K., F. Vester, A.N. Jensen and K. Ingvorsen (2001). Sulfate reduction dynamics and enumeration of sulfate-reducing bacteria in hypersaline sediments of the Great Salt Lake (Utah, USA). Microbial Ecology, 41(1):1-11.

Brønsted, J.N. (1922). "Studies on solubility IV. The principle of the specific interaction of ions". J. Am. Chem. Soc. 44: 877–898. doi:10.1021/ja01426a001

Brouwer, E., B. Baeyens, A. Maes and A. Cremers (1983). Cesium and rubidium ion equilibria in illite clay, Journal of Physical Chemistry, 87, 1213-1219.

Brown, K. A. (1982). Sulphur in the environment: a review. Environmental Pollution

Series B, Chemical and Physical, **3**(1):47-80.

Carter, T.R. (2012). Regional groundwater systems in southern Ontario. Ontario Oil & Gas: 44-48.

Cheng, L. (2006). Dual porosity reactive transport modeling, PhD thesis, University of Sheffield, UK.

Chou, L., R.M. Garrels and R. Wollast (1989). Comparative study of the kinetics and mechanisms of dissolution of carbonate minerals. Chemical Geology, 78, 269–282.

Christov, C. and N. Moller (2004). A chemical equilibrium model of solution behavior and solubility in the H-Na-K-Ca-OH-Cl-HSO4-SO4-H2O system to high concentration and temperature. Geochimica et Cosmochimica Acta, 68, 3717-3739.

Ciavatta, L. (1980). "The specific interaction theory in the evaluating ionic equilibria". Ann. Chim. (Rome). 70: 551–562.

Clark, I.D. and P. Fritz. 1997. Environmental Isotopes in Hydrogeology, CRC Press, 328p.

Crank, J. (1975). The Mathematics of Diffusion (Second Edition), Claredon Press, ISBN 0-19-853344-6, England.

Davis, L. A. and S. P. Neuman (1983), Documentation and user's guide: UNSAT2 - Variably saturated flow model, Final Rep., WWL/TM-1791-1, Water, Waste & Land, Inc.

Diersch H. J. G. (2002). FEFLOW finite element subsurface flow and transport simulation system user's manual/reference manual/ white papers. Release 5.0. WASY Ltd.

Diersch, H. and O. Kolditz (1998). Coupled groundwater flow and transport: 2. Thermaohaline and 3D convection systems. Advances in Water Resources, 21, 401-425.

Diersch, H. and O. Kolditz (2002). Variable-density flow and transport in porous media: approaches and challenges. Advances in Water Resources, 25, 899-944.

Elder, J.W. (1967). Transient convection in a porous medium. Journal of Fluid Mechanics, 27, 609-623.

Eugster, H.P., C.E. Harvie and J.H. Weare (1980). Mineral equilibria in a six-component seawater system, Na-K-Mg-Ca-SO4-Cl-H2O, at 25^{o}C. Geochimica et Cosmochimica Acta, 44, 1335-1347.

Felmy, A.R. and J.H. Weare (1986). The prediction of borate mineral equilibria in natural waters: Application to Searles Lake, California. Geochimica et Cosmochimica Acta, 50, 2771-2783.

Forsyth, P. A. and P. H. Sammon (1986). Practical considerations for adaptive implicit methods in reservoir simulation, Journal of Computational Physics, 62, 265-281.

Forsyth, P. A., Y.S. Wu and K. Pruess. (1995). Robust numerical methods for saturated-unsaturated flow with dry initial conditions in heterogeneous media, Advances in Water Resources, 18, 25-38.

Frolkovic, P. and H.D. Schepper (2001). Numerical modeling of convection dominated transport with density driven flow in porous media. Advances in Water Resources, 24, 63-72.

Galindez, J.M., C.I. Steefel and U. Maeder (2011). Continuum model for diffusive transport in the electrical double layer and clay interlamellæ. Proceedings at the Goldschmidt 2011 Conference, Prague, Czech Republic, August 14-19, 2011.

Giambalvo, E.R., C.I. Steefel, A.T. Fisher, N.D. Rosenberg and C.G. Wheat (2002). Effect of fluid-sediment reaction on hydrothermal fluxes of major elements, eastern flank of the Juan de Fuca Ridge. Geochimica et Cosmochimica Acta, 66 (10), 1739–1757.

Gibson, B., R.T. Amos and D.W. Blowes (2011) $^{34}S/^{32}S$ fractionation during sulfate reduction in groundwater treatment systems: Reactive transport modeling. *Environmental Science & Technology* 45, 2863–2870.

Greskowiak, J., J. Gwo, D. Jacques, J. Yin and K. U. Mayer. 2015. A benchmark for multi-rate surface complexation and 1D dual-domain multi-component reactive transport of U(VI), Computational Geosciences 19(3): 585. doi: 10.1007/s10596-014-9457-4

Greenberg, J.P. and N. Möller (1989). The prediction of mineral solubilities in natural-waters - A chemical-equilibrium model for the Na-K-Ca-Cl-SO_4-H_2O system to high-concentration from 0º to 250ºC. Geochimica et Cosmochimica Acta, 53, 2503-2518.

Grenthe, I., F. Mompean, K. Spanhiu and H. Wanner (2013). TDB-2: Guidelines for the extrapolation to zero ionic strength, OECD Nuclear Energy Agency, Data Bank, Issy-les-Moulineaux (France).

Guggenheim, E.A.; Turgeon, J.C. (1955). "Specific interaction of ions". Trans. Faraday Soc. 51: 747–761. doi:10.1039/TF9555100747

Guo, W. and C. Langevin (2002). User's Guide to SEAWAT: a computer program for simulation of three-dimensional variable density ground-water flow, U.S. Geological Survey Open File Report 01-434.

Harvie, C.E., H.P. Eugster and J.H. Weare (1982). Mineral equilibria in the six-component seawater system, Na-K-Mg-Ca-SO4-Cl-H2O at 25ºC. II: Compositions of the saturated solutions. Geochimica et Cosmochimica Acta, 46, 1603-1618.

Harvie, C.E., N. Moller and J.H. Weare (1984). The prediction of mineral solubilities in natural waters: The Na-K-Mg-Ca-H-Cl-SO_4-OH-HCO_3-CO_3-CO_2-H_2O system to high ionic strengths at 25ºC. Geochimica et Cosmochimica Acta, 48, 723-751.

Haverkamp, R., M. Vauclin, J. Touma, P.J. Wierenga and G. Vachaud (1977). A comparison of numerical-simulation models for one-dimensional infiltration, Soil science society of America journal, 41, 285-294.

He, S. and J.W. Morse (1993). Prediction of halite, gypsum, and anhydrite solubility in natural brines under subsurface conditions. Computers & Geosciences, 19, 1-22.

Henderson, T. (2009). Numerical modeling of density-driven chemical oxidation of chlorinated solvents, PH.D. – thesis, Department of Earth and Ocean Sciences, the University of British Columbia, Vancouver, British Columbia, Canada.

Henderson, T., K.U. Mayer, B. Parker and T. Al. (2009). Three-dimensional density-dependent flow and multicomponent reactive transport modeling of chlorinated solvent oxidation by potassium permanganate. Journal of Contaminant Hydrology, 106, 195-211.

Henry, H.R. (1964). Effects of dispersion on salt encroachment in coastal aquifers. U.S. Geological Survey Water Supply Paper, 1613-C, 70-84.

Henry, H. and J. Hilleke (1972). Exploration of multiphase fluid flow in a saline aquifer system affected by geothermal heating. Bureau of Engineering Research, Report No. 150-118, University of Alabama, U.S. Geological Survey Contract No. 14-08-0001-12681, National Technical Information Service Publication No. PB234233, 105 pp.

Hindmarsh, A.C. and L.R. Petzold (1995). Algorithms and software for ordinary differential equations and differential/algebraic equations, Part I: Euler methods and error estimation. Comp. Physiol. 9, 34–41.

Hobbs, M., S. Frape, O. Shouakar-Stash and L. Kennell (2011). Regional Hydrogeochemistry, Southern Ontario. Nuclear Waste Management Organization Report. NWMO DGR-TR-2011-12 R000. Toronto, Canada.

Holm, T.R. (1989). Comment on "Computing the equilibrium composition of aqueous systems: an iterative solution at each step in Newton–Raphson". Environmental Science & Technology 23, 1531–1532.

Hughes, J. and W. Sanford (2004). SUTRA-MS: A Version of SUTRA Modified to Simulate Heat and Multiple-Solute Transport U.S. Department of the Interior. U.S. Geological Survey.

Huyakorn, P. S., S. D. Thomas, and B. M. Thompson (1984). Techniques for making finite elements competitive in modeling flow in variably-saturated media, Water Resources Research, 20, 1099– 1115.

Hoopes, J. A. and D. R. F. Harleman (1967). Dispersion in radial flow from a recharge well, Journal of Geophysical Research, 72(14) 3595-3607.

Hsieh, P.A. (1986). A new formula for the analytical solution of the radial dispersion problem, Water Resources Research, 22(11), 1597–1605.

Jamieson-Hanes, J.H., R.T. Amos and D.W. Blowes (2012). Reactive Transport Modeling of Chromium Isotope Fractionation during Cr(VI) Reduction. Environmental Science & Technology, **46**, 13311–13316.

Jin, Q. and C.M. Bethke (2005). Predicting the rate of microbial respiration in geochemical environments. Geochimica et Cosmochimica Acta, **69**, 1133–1143.

Kadioglu, S.Y., R.R. Nourgaliev and V.A. Mousseau (2008). A Comparative Study of the Harmonic and Arithmetic Averaging of Diffusion Coefficients for Non-linear Heat Conduction Problems, Technical report INL/EXT-08-13999, DOI:10.2172/928087.

Kipp, K.L. (1986). HST3D-A computer code for simulation of heat solute transport in three-dimensional ground-water flow systems. U.S. Geological Survey Water-Resources Investigations Report 86-4095.

Knapp, R. B. (1989). Spatial and temporal scales of local equilibrium in dynamic fluid-rock systems, Geochimica et Cosmochimica Acta, 53, 1955 – 1964.

Krumgalz, B.S. (2001). Application of the Pitzer ion interaction model to natural hypersaline brines. Journal of Molecular Liquids, 91, 3-19.

Langevin, C. D. and W. Guo. (2006). MODFLOW/MT3DMS-based simulation of variable-density ground water flow and transport, Ground Water 44(3), 339-351.

Lemieux, J.M., E.A. Sudicky, W.R. Peltier and L. Tarasov (2008). Simulating the impact of glaciations on continental groundwater flow systems: 1. Relevant processes and model formulation. Journal of Geophysical Research-Earth Surface, 113, Article No. F03017, 12 p.

Levenspiel, O. (1972). Chemical Reaction Engineering, Wiley, New York.

Lichtner, P. C. (1985). Continuum model for simultaneous chemical reactions and mass transport in hydrothermal systems, Geochimica et Cosmochimica Acta, 49, 779– 800.

Lichtner, P.C. (1988). The quasi stationary state approximation to coupled mass transport and fluid–rock interaction in a porous medium. Geochimica et Cosmochimica Acta 52, 143–165.

Lichtner, P. C. (1993). Scaling properties of time-space kinetic mass transport equations and the local equilibrium limit, Am. J. Sci., 293, 257– 296.

Lichtner, P. C. (1996a). Continuum formulation of multicomponent-multiphase reactive transport, in Reactive Transport in Porous Media, Reviews in Mineralogy, 34, 1 – 81.

Lichtner, P. C. (1996b). Modeling of reactive flow and transport in natural systems, paper presented at the Rome Seminar on Environmental Geochemistry, Castelnuovo di Porto, Rome.

Marion, G.M. (2002). A molal-based model for strong acid chemistry at low temperatures (< 200 to 298 K). Geochimica et Cosmochimica Acta, 66, 2499-2516.

Marion, G.M., D.C. Catling and J.S. Kargel (2003). Modeling aqueous ferrous iron chemistry at low temperatures with application to Mars. Geochimica et Cosmochimica Acta, 67, 4251-4266.

Marty, N.C.M., O. Bildstein, P. Blanc, F. Claret, B. Cochepin, E.C. Gaucher, D. Jacques, J.-E. Lartigue, S. Liu, K.U. Mayer, J.C.L. Meeussen, I. Munier, I. Pointeau, D. Su, C.I. Steefel. 2015. Benchmarks for multicomponent reactive transport across a cement/clay interface, Computational Geosciences 19(3): 635. doi:10.1007/s10596-014-9463-6

Mayer, K.U. (1999). A numerical model for multicomponent reactive transport in variably-saturated porous media, Ph.D. – thesis, Department of Earth Sciences, University of Waterloo, Waterloo, Ontario, Canada.

Mayer, K.U., P. Alt-Epping, D. Jacques, B. Arora and C. I. Steefel. 2015. Benchmark problems for reactive transport modeling of the generation and attenuation of acid rock drainage, Computational Geosciences 19(3): 599. doi:10.1007/s10596-015-9476-9.

Mayer, K.U., D.W. Blowes and E.O. Frind (2001). Reactive transport modeling for the treatment of an in situ reactive barrier for the treatment of hexavalent chromium and trichloroethylene in groundwater. Water Resources Research, 37:3091-3103. doi:10:1029/2001WR000862

Mayer, K.U., E.O. Frind and D.W. Blowes (2002). Multicomponent reactive transport

modeling in variably-saturated porous media using a generalized formulation for kinetically controlled reactions. Water Resources Research, 38(9).

Mayer, K.U. and K.T.B. MacQuarrie (2010). Solution of the MoMaS reactive transport benchmark with MIN3P- model formulation and simulation results, Computational Geosciences 14:405-419.

MacQuarrie, K. T. B., E. A. Sudicky and E. O. Frind (1990). Simulation of biodegradable organic contaminants in groundwater: 1. Numerical formulation in principal directions, Water Resources Research, 26, 207 – 222.

Mendoza, C. A. and E. O. Frind (1990a). Advective-dispersive transport of dense organic vapours in the unsaturated zone, 1, Model development, Water Resources Research, 26, 379– 387.

Mendoza, C. A. and E. O. Frind (1990b). Advective-dispersive transport of dense organic vapours in the unsaturated zone, 2, Sensitivity analysis, Water Resources Research, 26, 388– 398.

Millington, R. J. (1959). Gas diffusion in porous media. *Science*, 130:100-102.

Millington, R.J. and J.P. Quirk (1961). Permeability of porous solids. *Trnas. Faraday Soc.* 57, 1200 – 1207.

Mizayaki, T (1976). Condensation and movement of water vapor in sand under temperature gradient (In Japanese), Transactions of the Japanese Society of Irrigation, Drainage and Reclamation Engineering, 61, 1-8.

Molins, S. and K. U. Mayer (2007). Coupling between geochemical reactions and multicomponent gas diffusion and advection – A reactive transport modeling study, Water Resources Research, 43, W05435, doi:10.1029/2006WR005206.

Molins, S., J. Greskowiak, C. Wanner and K.U. Mayer. 2015. A benchmark for microbially mediated chromium reduction under denitrifying conditions in a biostimulation column experiment, Computational Geosciences 19(3): 479. doi:10.1007/s10596-014-9432-0

Müller, B. (1993). MacμQL, V 1.2, A Program to calculate chemical Speciation and. Adsorption; EAWAG, Dübendorf, Switzerland.

Murphy, W. M., E. H. Oelkers, and P. C. Lichtner (1989). Surface reaction versus diffusion control of mineral dissolution and growth rates in geochemical processes, Chem. Geol., 78, 357– 380.

Neuman, S. P. (1973). Saturated-unsaturated seepage by finite elements, J. Hydraul. Div. Am. Soc. Civ. Eng., 99(HY12), 2233–2250.

Nicholson, R. V., R. W. Gillham and E. J. Reardon (1990). Pyrite oxidation in carbonate-buffered solution, 2, Rate control by oxide coatings, Geochimica et Cosmochimica Acta, 54, 395–402.

Ogata, A. and R.B. Banks (1961). A solution of the differential equation of longitudinal dispersion in porous media: U.S. Geological Survey Professional Paper 411-A.

Oldenburg, C. and K. Pruess (1995). Radionuclide Transport for TOUGH2. Lawrence

Berkeley National Laboratory Report LBL-34868.

Oltean, C. and A. Buès (2001). Coupled groundwater flow and transport in porous media. A conservative or non-conservative form? Transport in Porous Media, 44, 219-246.

Oswald, S.E. and W. Kinzelbach (2004). Three-dimensional physical benchmark experiments to test variable-density flow models. Journal of Hydrology, 290, 22-42.

Panday, S., P. S. Huyakorn, R. Therrien and R. L. Nichols, Improved three dimensional finite-element techniques for field simulation of variably-saturated flow and transport, Journal of Contaminant Hydrology, 12, 3, 1993.

Paniconi, C. and M. Putti (1994). A comparison of Picard and Newton iteration in the numerical solution of multidimensional variably-saturated flow problems, Water Resources Research, 30 (12), 3357-3374.

Parkhurst, D.L. (1990). Ion-association models and mean-activity coefficients of various salts. In Bassett, R.L. and Melchior, D. eds., Chemical modeling in aqueous systems II: Washington D.C., American Chemical Society Symposium Series 416. chap. 3, p. 30-43.

Parkhurst, D., K. Kipp, P. Engesgaard and S. Charlton (2005). PHAST-A program for simulating ground-water flow, solute transport, and multicomponent geochemical reactions. Geochimica et Cosmochimica Acta, 69, A156-A156.

Patankar, S.V. (1980). Numerical Heat Transfer and Fluid Flow, Taylor & Francis.

Philip, J. and De Vries, D. (1957). Moisture movement in porous materials under temperature gradient. Transactions American Geophysical Union, 38:222-232.

Pitzer, K.S. (1973). Thermodynamics of electrolytes. I. Theoretical basis and general equations. Journal of Physical Chemistry, 77, 268-277.

Pitzer, K. S. 1991. Ion interaction approach: theory and data correlation. In Activity Coefficients in Electrolyte Solutions (ed. K. S. Pitzer). CRC Press, Boca Raton.

Pitzer, K.S., J.-J. Kim. 1974. Thermodynamics of electrolytes. IV. Activity and osmotic coefficients for mixed electrolytes. J. Am. Chem. Soc., 96, p. 5701

Perko, J., K.U. Mayer, G. Kosakowski, L. De Windt, J. Govaerts, D. Jacques, D. Su and J.C.L. Meeussen. 2015. Decalcification of cracked cement structures, Computational Geosciences 19(3): 673 doi:10.1007/s10596-014-9467-2.

Putti, M., Paniconi, C. (1995). Picard and Newton linearization for the coupled model of saltwater intrusion in aquifers, Advances in Water Resources 3, 159-170.

Rasouli, P. (2016). The role of multicomponent diffusion and electrochemical migration for reactive transport in porous media, PhD-thesis, University of British Columbia, in progress.

Rasouli, P., C.I. Steefel and K.U. Mayer. 2015. Benchmarks for multicomponent diffusion and electrochemical migration, Computational Geosciences 19(3): 523. doi:10.1007/s10596-015-9481-z

Reardon, E.J. (1988). Ion interaction parameters for $AlSO_4$ and application to the prediction of metal sulfate solubility in binary salt systems. Journal of Physical Chemistry, 92, 6426-6431.

Rittmann, B. and P. McCarty (2001). Environmental biotechnology: principles and applications, McGraw-Hill series in water resources and environmental engineering. McGraw-Hill, London.

Saaltink, M. W., C. Ayora and S. Olivella (2005). User's guide for RetrasoCodeBright (RCB). Department of Geotechnical Engineering and Geo-Sciences, Technical University of Catalonia (UPC), Barcelona, Spain.

Saito, H., J. Šimůnek and B.P. Mohanty. 2006. Numerical analysis of coupled water, vapor, and heat transport in the vadose zone. Vadose Zone Journal 5:784–800

Scatchard, G. (1936). "Concentrated solutions of strong electrolytes". Chem. Rev. 19: 309–327. doi:10.1021/cr60064a008

Schäfer, D., W. Schäfer and W. Kinzelbach (1998). Simulation of reactive processes related to biodegradation in aquifers, 1. Structure of the three dimensional reactive transport model, Journal of Contaminant Hydrology, 31, 167–186.

Şengör, S.S., K.U. Mayer, J. Greskowiak, C. Wanner, D. Su and H. Prommer. 2015. Benchmarks for multicomponent reactive transport across a cement/clay interface, Computational Geosciences 19(3): 569. doi: 10.1007/s10596-015-9480-0

Shackelford, C.D. and S.M. Moore (2013). Fickian diffusion of radionuclides for engineered containment barriers: Diffusion coefficients, porosities, and complicating issues, Engineering Geology, 152(1):133–147, DOI: 10.1016/j.enggeo.2012.10.014.

Schnoor, J. L. (1990). Kinetics of chemical weathering: A comparison of laboratory and field weathering rates, in Aquatic Chemical Kinetics, Reaction Rates of Processes in Natural Waters, edited by W. Stumm, John Wiley, New York.

Sevougian, S. D., R. S. Schechter and L. W. (1993). Lake, Effect of partial local equilibrium on the propagation of precipitation/dissolution waves, Ind. Eng. Chem. Res., 32, 2281– 2304.

Simpson, M. J. and T.P. Clement (2003). Theoretical analysis of the worthiness of Henry and Elder problems as benchmarks of density-dependent groundwater flow models. Advances in Water Resources, 26, 17-31.

Simpson, M.J. and T.P. Clement (2004). Improving the worthiness of the Henry problem as a benchmark for density-dependent groundwater flow models. Water Resources Research, 40(1), W01504, doi:10.1029/2003WR002199.

Sipos, P. (2008). Application of the Specific Ion Interaction Theory (SIT) for the ionic products of aqueous electrolyte solutions of very high concentrations. Journal of Molecular Liquids, 143(1), 13-16. DOI: 10.1016/j.molliq.2008.04.003

Spiessl, S.M., K.T.B. MacQuarrie and K.U. Mayer (2008). Identification of key parameters controlling dissolved oxygen migration and attenuation in fractured crystalline rocks. Journal of Contaminant Hydrology 95, 141–153

Steefel, C. I. and A. C. Lasaga (1994). A coupled model for transport of multiple chemical species and kinetic precipitation/dissolution reactions with application to reactive flow in single phase hydrothermal systems, Am. J. Sci., 294, 529– 592.

Steefel, C. I. and K. T. B. MacQuarrie (1996). Approaches to modeling of reactive transport in porous media, in Reactive Transport in Porous Media, Rev. Mineral., 34, 83–129.

Steefel, C.I, D.J. DePaolo and P.C. Lichtner (2005). Reactive transport modeling: An essential tool and a new research approach for the Earth sciences, Earth and Planetary Science Letters 240 (2005) 539– 558.

Steefel, C.I., Appelo, C.A.J., Arora, B., Jacques, D., Kalbacher, T., Kolditz, O., Lagneau, V., Lichtner, P.C., Mayer, K.U., Meeussen, J.C.L., Molins, S., Moulton, D., Shao, H., Šimůnek, J., Spycher, N., Yabusaki, S.B., Yeh, G.T. (2015). Reactive transport codes for subsurface environmental simulation, Computational Geosciences, 19(3), 445-478 DOI: 10.1007/s10596-014-9443-x

Stone, A. T. and J. J. Morgan (1990). Kinetics of chemical transformations in the environment, in Aquatic Chemical Kinetics, Reaction Rates of Processes in Natural Waters, edited by W. Stumm, John Wiley, New York.

Stumm, W. and J. J. Morgan (1996). Aquatic Chemistry, John Wiley, New York.

Tang, K., V. Baskaran and M. Nemati (2009). Bacteria of the sulphur cycle: an overview of microbiology, biokinetics and their role in petroleum and mining industries. Biochemical Engineering Journal, 44(1):73-94.

Su, D., K.U. Mayer and K.T.B. MacQuarrie (2015). Parallelization of the Reactive Transport Code MIN3P-THCm, NWMO Technical Report NWMO-TR-2015-23 October 2015.

Su, D. K. U. Mayer and K. T. B. MacQuarrie (2017) Parallelization of MIN3P-THCm: a high performance computational framework for subsurface flow and reactive transport simulation, Environmental Modelling & Software, 95, 271- 289.

Tebes-Stevens, C., A. J. Valocchi, J. M. VanBriesen and B. E. Rittmann (1998). Multicomponent transport with coupled geochemical and mirobiological reactions: Model description and example applications, Journal of Hydrology, 209, 8 –26.

Tecplot, Inc. (2005). Tecplot User's manual, version 10, Tecplot,, Inc. Bellevue, Washington March, 2005.

Thorstenson, D. C. and D. W. Pollock (1989). Gas transport in unsaturated porous media: The adequacy of Fick's law, Rev. Geophys., 27, 61–78.

Tosca, N., S. McLennan, B. Clark, J. Grotzinger, J. Hurowitz, A. Knoll, C. Schroder and S. Squyre (2005). Geochemical modeling of evaporation processes on Mars: Insight from the sedimentary record at Meridiani Planum. Earth and Planetary Science Letters, Sedimentary Geology at Meridiani Planum, Mars, 240, 122-148.

Unger, A.J.A., P.A. Forsyth and E.A. Sudicky (1996). Variable spatial and temporal weighting schemes for use in multi-phase compositional problems. Advances in Water Resources 19, 1–27

USDOE (United States Department of Energy), (2007). In-drift precipitates/salts model. Argonne National Laboratory Report EBS-MD-000045 REV 03. Chicago, USA.

Valocchi, A. J., R.L. Street and P.V. Roberts (1981) Transport of ion- exchanging solutes

in groundwater – chromatographic theory and field simulation, *Water Resources Research*, 17(5):1517-1527. DOI: 10.1029/WR017i005p01517.

van de Griend, A. A. and M. Owe (1994). Bare soil surface resistance to evaporation by vapor diffusion under semiarid conditions, Water Resources Research, 30, 181-188.

van der Kwaak, J.E., P.A. Forsyth, K.T.B. MacQuarrie and E.A. Sudicky. (1997). WatSolv—Sparse Matrix Iterative Solver, User's Guide for Version 2.16. University of Waterloo, Waterloo, Canada.

van Genuchten, M. Th. (1980). A closed form equation for predicting the hydraulic conductivity of unsaturated soils. Soil Science Society of America Journal44: 892–898.

Van Leer, B. (1974). Towards the ultimate conservative scheme. II Monotonicity and conservation combined in a second order scheme. Journal of Computational Physics, 14, 361-370.

Vauclin, M., D. Khanji and G. Vachaud. (1979). Experimental and numerical study of a transient, two-dimensional unsaturated-saturated water table recharge problem, Water Resources Research, 15(5), 1089-1101.

Voss, C. I. (1984). A finite-element simulation model for saturated-unsaturated, fluid-densitydependent ground-water flow with energy transport or chemically-reactive single-species solute transport: U.S. Geological Survey Water-Resources Investigation Report 84-4369.

Voss, C. and A. Provost, (2008). SUTRA-A model for saturated-unsaturated, variable-density ground-water flow with solute or energy transport. U.S. Geological Survey Water-Resources Investigations Report 02-4231, 250p.

Voss, C. and W. Souza, (1987). Variable density flow and solute transport simulation of regional aquifers containing a narrow freshwater-saltwater transition zone. Water Resources Research, 23, 1851-1866.

Weatherill, D., C.T. Simmons, C. Voss and N. Robinson (2004). Testing density-dependent groundwater models: Two-dimensional steady state unstable convection in infinite, finite and inclined porous layers. Advances in Water Resources, 27, 547-562.

Wersin, P. E, E. Curti and C.A.J. Appelo (2004). Modelling bentonite–water interactions at high solid/liquid ratios: swelling and diffuse double layer effects, Applied Clay Science, 26(1–4), 249–257.Westall, J.C. (1979). MICROQL-I: A chemical equilibrium program in BASIC, EAWAG report, Dübendorf, Switzerland.

Westall, J.C. (1979). MICROQL-I: A chemical equilibrium program in BASIC, EAWAG report, Dübendorf, Switzerland.

Wollast, R. and L. Chou. (1985). Kinetic study of the dissolution of albite with a continuous flow-through fluidized bed reactor. In: The Chemistry of Weathering. (eds Drever, J.I.) NATO ASI series C149, pp.75-96, Reidel, Dordrecht/Boston/Lancaster.

Wolery, T.J. (1992). EQ3/6, A Software Package for Geochemical Modeling of Aqueous Systems: Package Overview and Installation Guide (Version 7.0). UCRL-MA-110662 PT I. Livermore, California: Lawrence Livermore National Laboratory. TIC: 205087.

Wösten, J. H. M. and M. T. van Genuchten (1988). Using texture and other soi1 properties to predict the unsaturated soi1 hydraulic functions, Soi1 Sci. Soc. Am. J., 52, 1762-1770.

Wunderly, M.D., D.W. Blowes, E.O. Frind and C.J. Ptacek (1996). Sulfide mineral oxidation and subsequent reactive transport of oxidation products in mine tailings impoundments: A numerical model. Water Resources Research, 32 (10): 3173-3187.

Stumm, W. and J.J. Morgan. (1996). Aquatic Chemistry. 3rd Ed. John Wiley and Sons Inc.

Xie, M., K.U. Mayer, F. Claret, P. Alt-Epping, D. Jacques, C. Steefel, Ch. Chiaberge and J. Simunek. (2015) Benchmark of implementation and evaluation of permeability-porosity relationships linked to mineral dissolution-precipitation, Journal of computational geosciences, 19(3) 655-671, DOI 10.1007/s10596-014-9458-3.

Xie, M., P. Rasouli, K.U. Mayer and K.T.B. MacQuarrie (2014a). Reactive Transport Modelling of Diffusion in Low Permeable Media – MIN3P-THCm Simulations of EBS TF-C Compacted Bentonite Diffusion Experiments, NWMO Technical Report, NWMO-TR-2014-23.

Xie, M., P. Rasouli, K.U. Mayer and K.T.B. MacQuarrie (2014b). Reactive Transport Modelling of In-situ Diffusion Experiments for the Mont Terri Project, NWMO Technical Report, NWMO-TR-2014-25.

Xie, M., P. Rasouli, K.U. Mayer and K.T.B. MacQuarrie (2015a). MIN3P-THCm Code Enhancements for Reactive Transport Modelling in Low Permeability Media, NWMO Technical Report, NWMO-TR-2015-12.

Yeh, G. T. and V. S. Tripathi (1989). A critical evaluation of recent developments in hydrogeochemical transport models of reactive multichemical components, Water Resources Research, 25, 93– 108.

Zachara, J. M., S. C. Smith, C. Liu, J. P. McKinley, R. J. Serne and P. L. Gassman (2002). Sorption of Cs^+ to micaceous subsurface sediments from the Hanford site, USA. Geochimica et Cosmochimica Acta, 66, 193-211.

Appendixes

CONTENTS

APPENDIX A: NOMWNCLATURE

A NOMENCLATURE

A.1. NOMENCLATURE FOR SECTION 2.1

Symbol	Definition	Unit
a_i	Ion size parameter for the modified Debye-Hückel equation	[-]
a_w	Activity of water	[-]
A_d	Constant that depends on the dielectric constant and temperature for the modified Debye-Hückel equation	[-]
A_k	Chemical formula of the kth component	[-]
A_i^c	Name of the ith component	[-]
A_i^g	Name of the ith complexed gas	[-]
A_i^m	Name of the ith mineral	[-]
A_i^x	Name of the ith complexed species	[-]
A^ϕ	Debye-Hückel slope parameter for Pitzer model	[-]
b	Biomass first-order decay constant	[T^{-1}]
B	Concentration of biomass	[cells L^{-3}]
b_i	Ion specific parameter that accounts for the decrease in solvent concentration in concentrated solutions for the modified Debye-Hückel equation	[-]
B_{ca}^v	Second virial coefficients accounting for the interactions between ions – Pitzer equations	[-]
B_d	Constant that depends on the dielectric constant and temperature for the modified Debye-Hückel equation	[-]
C	Coefficient matrix (Pitzer model)	-
c_A	Concentration of the acceptor	[mol L^{-3} H_2O]

c_D	Concentration of the donor	[mol L^{-3} H_2O]
c_I	Concentration of the inhibitor	[mol L^{-3} H_2O]
C_i^d	Concentration of the i^{th} dissolved species	[mol L^{-3} H_2O]
C_i^g	Concentration of the i^{th} gaseous complexes	[mol L^{-3} gas]
C_i^s	Concentration of the i^{th} ion-exchanged species	[mol L^{-3} H_2O]
C_i^x	Concentration of the i^{th} aqueous complexes	[mol L^{-3} H_2O]
C_j	Concentration of the primary species	[mol L^{-3} H_2O]
C_j^c	Concentration of the j^{th} primary species	[mol L^{-3} H_2O]
c_w	Specific heat capacity for the aqueous phase	[L^2 T^{-2} Θ^{-1}]
c_s	Specific heat capacity for the solid phase	[L^2 T^{-2} Θ^{-1}]
C_{ca}^v	Second virial coefficients accounting for the interactions between ions – Pitzer equations	[-]
$\mathbf{C_f}$	Concentration	[M L^{-3}]
$\mathbf{D_a}$	Dispersion tensor for the aqueous phase	[L^2 T^{-1}]
D_a^*	Averaged free-phase diffusion coefficient in the aqueous phase	[L^2 T^{-1}]
$\mathbf{D}_{\mathbf{a},T}$	Dispersion tensor for the aqueous phase at temperature T	[L^2 T^{-1}]
$\mathbf{D}_g$	Dispersion tensor for the gaseous phase	[L^2 T^{-1}]
D_g^*	Average free-phase diffusion coefficient in the gas phase	[L^2 T^{-1}]
D_i^m	Effective diffusion coefficient of the primary reactant through a protective surface layer (mineral dissolution-precipitation)	[L^2 T^{-1}]
$f_{DH}^v(I)$	Debye-Hückel term that is a function of the ionic strength	[-]
f_e^0	The portion of the electrons from the substrate	[-]

	transferred to the electron acceptor	
f_i	the coefficients (f_i) of a function to calculate the salinity inhibition factor k_{sal}	[-]
f_l	Fugacity of the *l*th gas	[M L^{-1} T^{-2}]
f_s^0	The portion of the electrons into microbial cells	[-]
F_T	Thermodynamic limitation term	[-]
g	Gravitational acceleration	[L T^{-2}]
h	Hydraulic head	[L]
I	Ionic strength	[mol L^{-3}]
IAP_i^a	Ion-activity product of the i^{th} intra-aqueous kinetic reaction	[-]
k_{ra}	Relative permeability of the porous medium with respect to the aqueous phase	[-]
k	Intrinsic permeability tensor	[L^2]
K	Hydraulic conductivity tensor	[L T^{-1}]
K_D	Half-saturation constant of the donor	[mol L^{-3} H_2O]
K_A	Half-saturation constant of the acceptor	[mol L^{-3} H_2O]
K_I	Half-saturation constant of the inhibitor	[mol L^{-3} H_2O]
K_i^g	Equilibrium constant for the i^{th} equilibrium gas dissolution-exsolution reactions	[-]
k_i^a	Rate constant of the forward reaction for the i^{th} intra-aqueous kinetic reaction	[varied]
K_i^a	Equilibrium constant of the i^{th} intra-aqueous kinetic reaction	[varied]
k_i^m	Rate constant for the dissolution of the i^{th} mineral	[varied]
$k_i^{m,eff}$	Effective rate constant for the dissolution of the i^{th} mineral	[varied]
K_i^x	Equilibrium constant for the dissociation of the aqueous	[varied]

	complex A_i^x into components as species in solution	
$K_{ij}^{a,in}$	Inhibition constant of intra-aqueous kinetic reactions	[mol L^{-3}]
$K_{ij}^{a,mo}$	Half saturation constants of intra-aqueous kinetic reactions	[mol L^{-3}]
$K_{ij}^{m,in}$	Inhibition constant of surface-controlled dissolution-precipitation reactions	[mol L^{-3}]
$K_{ij}^{m,mo}$	Half saturation constants of surface-controlled dissolution-precipitation reactions	[mol L^{-3}]
K_l	Equilibrium constant of the chemical reaction	[-]
k_{sal}	Salinity inhibition factor	[-]
l	Soil hydraulic function parameters (van Genuchten model)	[-]
m	Soil hydraulic function parameters (van Genuchten model)	[-]
$\mathbf{m}$	Vector of species molalities (Pitzer model)	[mol M^{-1}]
$\mathbf{m}^t$	Transpose of species molalities vector (Pitzer model)	[mol M^{-1}]
m_a	molality of anion a (of charge z_c)	[mol M^{-1}]
m_c	molality of cation c (of charge z_c)	[mol M^{-1}]
m_i	molality of the i^{th} aqueous species	[mol M^{-1}]
$\mathbf{M}$	The sum of molality of all solutes: cations, anions and neutrals	[mol M^{-1}]
MW_i	Molecular weight of each component	[M mol^{-1}]
$\mathbf{S}$	Salinity	[g L^{-1}]]
$\mathbf{W}$	Molecular weight of water	[M mol^{-1}]
n	Soil hydraulic function parameters (van Genuchten model)	[-]
n_l	Number of moles of the *l*th gas	[mol]

$\boldsymbol{N_{a,kin}}$	Number of intra-aqueous kinetic reactions	[-]
$\boldsymbol{N_{m,kin}}$	Number of dissolution-precipitation reactions	[-]
N_c	Number of aqueous components	[-]
N_d	Number of dissolved species	[-]
$\boldsymbol{N_g}$	Number of gaseous species	[-]
N_m	Number of minerals	[-]
$\boldsymbol{N_s}$	Number of ion-exchange complexes	[-]
$\boldsymbol{N_x}$	Number of aqueous complexes	[-]
$\boldsymbol{o_{ij}^{ac}}$	Reaction order of intra-aqueous kinetic reactions with respect to the activity of dissolved primary species	[-]
$\boldsymbol{o_{ij}^{at}}$	Reaction order of intra-aqueous kinetic reactions with respect to the total aqueous component concentration	[-]
$\boldsymbol{o_{ij}^{ax}}$	Reaction order of intra-aqueous kinetic reactions with respect to the activity of dissolved complexes	[-]
$\boldsymbol{o_{ij}^{mc}}$	Reaction order of surface-controlled dissolution-precipitation reactions with respect to the activity of dissolved primary species	[-]
$\boldsymbol{o_{ij}^{mt}}$	Reaction order of surface-controlled dissolution-precipitation reactions with respect to the total aqueous component concentration	[-]
$\boldsymbol{o_{ij}^{mx}}$	Reaction order of surface-controlled dissolution-precipitation reactions with respect to the activity of dissolved complexes	[-]
P_a	Aqueous phase pressure	[M L^{-1} T^{-2}]
$\boldsymbol{P_l}$	Partial pressure of the *l*th gas	[M L^{-1} T^{-2}]
$\mathbf{q}_a$	Specific discharge vector or Darcy flux vector	[L T^{-1}]
$\mathbf{q}_{\mathbf{a},T}$	Energy transport vector due to advection with flowing groundwater	[L T^{-1}]

q'	Scalar term for Pitzer model	-
q^c	Scalar term for Pitzer model	-
q^L	Scalar term for Pitzer model	-
q^ϕ	Scalar term for Pitzer model	-
$\mathbf{Q}$	Matrix (Pitzer model)	-
$\mathbf{Q}'$	Matrix (Pitzer model)	-
$\mathbf{Q}^{\mathbf{L}}$	Matrix (Pitzer model)	-
$\mathbf{Q}^\phi$	Matrix (Pitzer model)	-
$\boldsymbol{Q_a}$	Source-sink term, where a positive quantity defines the injection of water	[T^{-1}]
$Q_j^{a,a}$	Internal source and sink terms from intra-aqueous kinetic reactions	[mol L^{-3} T^{-1}]
$Q_j^{a,m}$	Internal source and sink terms from kinetically controlled dissolution-precipitation reactions	[mol L^{-3} T^{-1}]
$Q_j^{a,ext}$	External source and sink terms for the aqueous phase	[mol L^{-3} T^{-1}]
$Q_j^{g,ext}$	External source and sink terms for the gas phase	[mol L^{-3} T^{-1}]
$\boldsymbol{r_{decay}}$	Biomass decay rate	[cell L^{-3} T^{-1}]
$\boldsymbol{r_i^p}$	Radius of an average particle	[L]
$\boldsymbol{r_i^r}$	Radius of the unreacted portion of the mineral grain	[L]
$\boldsymbol{r_j}$	Rate of the *j*th microbially mediated reaction	[mol L^{-3} T^{-1}]
R	Ideal gas constant	[M L^2 T^{-2} Θ^{-1} mol^{-1}]
$\boldsymbol{R_i^a}$	Reaction rate of the i^{th} kinetically controlled intra-aqueous reaction	[mol L^{-3} H_2O T^{-1}]
$\boldsymbol{R_i^{a,ir}}$	Reaction rate of the i^{th} irreversible kinetically controlled	[mol L^{-3} H_2O T^{-1}]

	intra-aqueous reaction	
$\boldsymbol{R_i^m}$	Dissolution-precipitation rate for the i^{th} mineral	[mol L^{-3} bulk T^{-1}]
$\boldsymbol{R_i^{ms}}$	Reaction rate for the i^{th} surface-controlled dissolution-precipitation reaction	[mol L^{-3} bulk T^{-1}]
$\boldsymbol{R_i^{mt}}$	Reaction rate for the i^{th} transport-controlled dissolution-precipitation reaction	[mol L^{-3} bulk T^{-1}]
$\boldsymbol{S_a}$	Saturation of the aqueous phase	[-]
$\boldsymbol{S_{ea}}$	Effective saturation of the aqueous phase	[-]
S_g	Saturation of the gaseous phase	[-]
$\boldsymbol{S_i}$	Reactive surface area of the mineral phase A_i^m	[L^2 mineral L^{-3} bulk]
$\boldsymbol{S_i^0}$	Initial reactive surface area of the mineral phase A_i^m	[L^2 mineral L^{-3} bulk]
$\boldsymbol{S_p}$	Intrinsic specific storage coefficient	[M^{-1} L T^2]
$\boldsymbol{S_{ra}}$	Residual saturation of the aqueous phase	[-]
$\boldsymbol{S_s}$	Specific storage coefficient	[L^{-1}]
t	Time	[T]
T	Temperature	[Θ]
$\mathbf{T_f}$	Temperature of a fluid	[K]
T^*	temperatures for the external water	[Θ]
$\mathbf{T_j}$	Total component concentration	[mol L^{-3} H_2O]
T_j^a	Total aqueous component concentration for the component A_j^c	[mol L^{-3} H_2O]
T_j^g	Total gaseous concentration for the component A_j^c	[mol L^{-3} gas]
T_j^s	Total sorbed component concentration for the component A_j^c	[mol L^{-1} bulk]

$\boldsymbol{TDS}$	Concentration of the total dissolved solids	[M L^{-3}]
$\boldsymbol{V}$	Total volume of the solution that contains 1 kg of water	[L^3]
$\boldsymbol{V}$	Total volume of gas	[L^3]
$\bar{\boldsymbol{V}}_{\boldsymbol{i}}^{\boldsymbol{o}}$	Standard partial volume of the solute i	[L^3 mol^{-1}]
$\boldsymbol{V_{id}}$	Ideal volume based on the molar volume of solutes	[L^3]
$\boldsymbol{V_{ex}}$	Total excess volume of a multicomponent electrolyte solution	[L^3]
$V_{f,j}^{m}$	Volume fraction for the j^{th} mineral	[L^3 mineral L^{-3} bulk]
V_{j}^{m}	Molar volume of the j^{th} mineral	[L^3 mineral mol^{-1}]
$\mathbf{z}$	Elevation with respect to datum	[L]
$\mathbf{z}$	Vector of electric charge	[-]
$\mathbf{z^2}$	Vector of squared electric charge	[-]
$\mathbf{z}_2^{\mathbf{t}}$	Transpose of the square electric charge vector	[-]
$\mathbf{z}_{\mathbf{abs}}^{\mathbf{t}}$	Transpose of the absolute electric charge vectors	[-]
z_c	Charge of ions	[-]
$\mathbf{1}_{\mathbf{N_{aq}}}^{\mathbf{t}}$	unity vector of dimension N_{aq}	-
$\boldsymbol{\alpha}$	Soil hydraulic function parameters (van Genuchten model)	[-]
$\boldsymbol{\alpha_l}$	Longitudinal dispersivity of the porous medium	[L]
$\boldsymbol{\alpha_t}$	Transverse dispersivity of the porous medium	[L]
γ	Vector of activity coefficients	[-]
γ_A	Vector of activity coefficients of anions	[-]
γ_C	Vector of activity coefficients of cations	[-]

γ_{DH}	Modified Debye-Hückel activity coefficient	[-]
$\boldsymbol{\gamma_{H_2O}}$	Activity coefficient of water	[-]
$\boldsymbol{\gamma_i^d}$	Activity coefficient for charged dissolved species A_i^d	[-]
$\boldsymbol{\gamma_j}$	Activity coefficient of the *j*th component	[-]
$\boldsymbol{\gamma_j^c}$	Activity coefficient for the component A_j^c as species in solution	[-]
$\boldsymbol{\gamma_i^x}$	Activity coefficient for the aqueous complex	[-]
$\boldsymbol{\delta_{kl}}$	Kronecker delta	
ζ	One-dimensional loading efficiency coefficient	[-]
$\boldsymbol{\lambda}$	Thermal conductivity tensor for the porous medium	[LM T^{-3} Θ^{-1}]
λ_w	Fluid thermal conductivity	[LM T^{-3} Θ^{-1}]
λ_s	Solid thermal conductivity	[LM T^{-3} Θ^{-1}]
μ_a	Dynamic viscosity	[M L^{-1} T^{-1}]
μ_f	Dynamic viscosity for reference conditions	[M L^{-1} T^{-1}]
$\boldsymbol{\mu_j}$	The specific rate constant	[mol $cell^{-1}$ T^{-1}]
$\boldsymbol{\nu_{ij}^a}$	Stoichiometric coefficient of the j^{th} component in the i^{th} intra-aqueous dissolution-precipitation reaction	[-]
ν_{ij}^g	Stoichiometric coefficients for the j^{th} component in the i^{th} gas species	[-]
ν_{ij}^s	Stoichiometric coefficients for the j^{th} component in the i^{th} ion-exchanged or sorbed species	[-]
$\boldsymbol{\nu_{ij}^m}$	Stoichiometric coefficient of the j^{th} component in the i^{th} mineral dissolution-precipitation reaction	[-]
$\boldsymbol{\nu_{ij}^{mc}}$	Stoichiometric coefficient of of the j^{th} component in the i^{th} transport-controlled dissolution-precipitation reaction – with respect to components as species in solution	[-]

$\boldsymbol{\nu_{ij}^{mt}}$	Stoichiometric coefficient of of the j^{th} component in the ith transport-controlled dissolution-precipitation reaction – with respect to total aqueous component concentrations	[-]
$\boldsymbol{\nu_{ij}^{mx}}$	Stoichiometric coefficient of of the j^{th} aqueous complex in the ith transport-controlled dissolution-precipitation reaction	[-]
ν_{ij}^{x}	Stoichiometric coefficients for the j^{th} aqueous component in the i^{th} aqueous complex	[-]
$\boldsymbol{\nu_{jk}^{e}}$	Stoichiometric coefficients of the primary species in the catabolic pathways for the *j*th reaction	[-]
$\boldsymbol{\nu_{jk}^{s}}$	Stoichiometric coefficients of the primary species in the anabolic pathways for the *j*th reaction	[-]
$\boldsymbol{\nu_{jk}^{b}}$	Stoichiometric coefficients of the averall redox reactions	[-]
$\boldsymbol{\nu_{lj}}$	Number of moles of the *j*th primary species in *l*th gas reaction	[-]
ρ^*	External fluid density	[M L^{-3}]
$\boldsymbol{\rho_0}$	Reference density (e.g. density of pure water at 25 ^{o}C)	[M L^{-3}]
$\boldsymbol{\rho_a}$	Aqueous phase density	[M L^{-3}]
$\rho_{a,f}$	Aqueous phase density (freshwater)	[M L^{-3}]
$\Delta\rho_C$	Density change due to concentration	[M L^{-3}]
ρ_s	Solid density	[M L^{-3}]
$\Delta\rho_T$	Density change due to temperature	[M L^{-3}]
σ_{zz}	Vertical stress	[M L^{-1} T^{-2}]
$\boldsymbol{\tau_a}$	Aqueous phase tortuosity	[-]
$\boldsymbol{\tau_g}$	Gaseous phase tortuosity	[-]
υ_W	Specific volume of pure water	[L^3 M^{-1}]

$\boldsymbol{\phi}$	Porosity	[-]
ϕ	Osmotic coefficient	[-]
$\boldsymbol{\varphi_l}$	Fugacity coefficient	[-]
$\boldsymbol{\psi_a}$	Aqueous-phase pressure head	[L]
ω	Solute mass fractions in the fluid for the actual viscosity	[-]
ω_f	Solute mass fractions in the fluid for the reference viscosity	[-]

A.2. NOMENCLATURE FOR SECTION 2.2

Symbol	Definition	Unit
$\boldsymbol{A_k}$	Surface area of the boundary cell	[L^2]
$\boldsymbol{A_{kl}}$	Interfacial area between the control volumes k and l	[L^2]
$\boldsymbol{\Delta C_i^c}$	Update for the primary unknown C_i^c	[mol L^{-3}]
$\boldsymbol{C_j^{c,N+1,I}}$	Concentration of the j^{th} primary species at the current time level and previous iteration level	[mol L^{-3}]
$\boldsymbol{C_j^{c,N+1,I+1}}$	Concentration of the j^{th} primary species at the current time level and previous iteration level	[mol L^{-3}]
$\boldsymbol{C_i^{m,N}}$	Concentration of the ith mineral at the previous time level	[L^3 mineral L^{-3} bulk]
$c_{s,k}$	Heat capacity for solid phase in the k^{th} control volume	[L^2 T^{-2} $^oC^{-1}$]
$\boldsymbol{d_{kl}}$	Distance between the centroids of the control volumes k and l.	[L]
$D_{a,kl}$	effective dispersion coefficient in the aqueous phase between control volumes k and l	[L^2 T^{-1}]
$\boldsymbol{h_k^{N+1}}$	Hydraulic head in the k^{th} control volume at the current time level	[L]
$\boldsymbol{h_l^{N+1}}$	Hydraulic head in the l^{th} control volume at the current time level	[L]
k	Refers to the k^{th} control volume	[-]
$\boldsymbol{K_{kl}}$	Representative hydraulic conductivity used for the flux calculation between control volumes k and l	[L T^{-1}]
$\boldsymbol{k_{ra,kl}}$	Representative relative permeability used for the flux calculation between control volumes k and l	[-]
$\boldsymbol{l}$	Refers to the l^{th} control volume	[-]
$\boldsymbol{N}$	The previous time level	[-]
$\boldsymbol{N+1}$	The current time level	[-]

$\boldsymbol{N_v}$	Number of control volumes in the solution domain	[-]
$P_{a,k}$	Aqueous phase pressure in the kth control volume	[M L^{-1} T^{-2}]
$\boldsymbol{P_{a,k}^{N}}$	Fluid pressure of the k^{th} control volume at the current time level	[M L^{-1} T^{-2}]
$\boldsymbol{P_{a,k}^{N+1}}$	Fluid pressure of the k^{th} control volume at the current time level	[M L^{-1} T^{-2}]
$\boldsymbol{P_{a,k}^{N+1,i+1}}$	Fluid pressure of the k^{th} control volume at the current time level and current Picard iteration	[M L^{-1} T^{-2}]
$\boldsymbol{P_{a,l}^{N+1}}$	Fluid pressure of the l^{th} control volume at the current time level	[M L^{-1} T^{-2}]
$\boldsymbol{P_{a,l}^{N+1,i+1}}$	Fluid pressure of the l^{th} control volume at the current time level and current Picard iteration	[M L^{-1} T^{-2}]
$q_{a,kl}$	Volumetric fluid flux between control volumes k and l used for the advective flux calculations across the interface between the control volumes k and l	[L^{3} T^{-1}]
$Q*$	Volumetric flux per unit of surface area at the boundary	[L^{3} L^{-2} T^{-1}]
$\boldsymbol{Q_{a,k}^{N+1}}$	Aqueous phase source-sink term in the k^{th} control volume at the current time level	[T^{-1}]
$\boldsymbol{Q_{j,k}^{a,a,N+1}}$	Internal source and sink terms in the k^{th} control volume from intra-aqueous kinetic reactions at the current time level	[mol L^{-3} T^{-1}]
$\boldsymbol{Q_{j,k}^{a,m,N+1}}$	Internal source and sink terms from kinetically controlled dissolution-precipitation reactions in the k^{th} control volume at the current time level	[mol L^{-3} T^{-1}]
$\boldsymbol{Q_{j,k}^{a,ext,N+1}}$	External source and sink terms for the aqueous phase of the k^{th} control volume at the current time level	[mol L^{-3} T^{-1}]
$\boldsymbol{Q_{j,k}^{g,ext,N+1}}$	External source and sink terms for the gas phase in the k^{th} control volume at the current time level	[mol L^{-3} T^{-1}]
$\boldsymbol{R_{j}^{m,N+1}}$	Dissolution-precipitation rate for the j^{th} mineral at the current time level	[mol L^{-3} T^{-1}]
$\boldsymbol{S_{a,k}^{N}}$	Saturation of the aqueous phase in the k^{th} control volume at the previous time level	[-]

$S_{a,k}^{N+1}$	Saturation of the aqueous phase in the k^{th} control volume at the current time level	[-]
$S_{a,kl}^{N+1}$	Harmonic average aqueous phase saturation between control volumes k and l at the current time level	[-]
$S_{g,k}^{N}$	Saturation of the gaseous phase in the k^{th} control volume at the previous time level	[-]
$S_{g,k}^{N+1}$	Saturation of the gaseous phase in the k^{th} control volume at the current time level	[-]
S_{p}^{N+1}	Intrinsic specific storage coefficient at the current time level	[M^{-1} L T^{2}]
$S_{p}^{N+1,i}$	Intrinsic specific storage coefficient at the current time level and previous Picard iteration	[M^{-1} L T^{2}]
$S_{s,k}$	Specific storage coefficient of the k^{th} control volume	[L^{-1}]
T	Temperature	[Θ]
T *	External temperature when fluid mass flux is entering/leaving the system	[Θ]
T_{k}^{N}	Temperature of the k^{th} control volume at the previous time level	[Θ]
T_{k}^{N+1}	Temperature of the k^{th} control volume at the current time level	[Θ]
$T_{j,k}^{a,N}$	Total aqueous concentration of the j^{th} component in control volume k at the previous time level	[mol L^{-3} H_2O]
$T_{j,k}^{a,N+1}$	Total aqueous concentration of the j^{th} component in control volume k at the current time level	[mol L^{-3} H_2O]
$T_{j,l}^{a,N+1}$	Total aqueous concentration of the j^{th} component in control volume l at the current time level	[mol L^{-3} H_2O]
$T_{j,kl}^{a,N+1}$	Total aqueous component concentrations used for the advective flux calculations across the interface between the control volumes k and l	[mol L^{-3} H_2O]
$T_{j,k}^{g,N}$	Total gaseous concentration of the j^{th} component in control volume k at the previous time level	[mol L^{-3} gas]

$T_{j,k}^{g,N+1}$	Total gaseous concentration of the j^{th} component in control volume k at the current time level	[mol L^{-3} gas]
$T_{j,l}^{g,N+1}$	Total gaseous concentration of the j^{th} component in control volume l at the current time level	[mol L^{-3} gas]
$T_{j,k}^{s,N}$	Total sorbed concentration of the j^{th} component in control volume k at the previous time level	[mol L^{-3} bulk]
$T_{j,k}^{s,N+1}$	Total sorbed concentration of the j^{th} component in control volume k at the current time level	[mol L^{-3} bulk]
$T_{k}^{N+1,i}$	Temperature of the k^{th} control volume at the current time level and previous Picard iteration	[Θ]
T_{kl}^{N+1}	Temperature at the interface of the control volumes k and l at the current time level	[Θ]
ΔT_{kl}^{N+1}	Temperature difference between the control volumes k and l at the current time level	[Θ]
$V_{f,j}^{m,N}$	Volume fraction of the j^{th} mineral at the previous time level	[L^3 mineral L^{-3} bulk]
$V_{f,j}^{m,N+1}$	Volume fraction of the j^{th} mineral at the current time level	[L^3 L^{-3}]
V_k	Volume of the k^{th} control volume	[L^3]
z_0	Elevation at the top of the interval	[L]
z_k	Elevation of the k^{th} control volume	[L]
z_l	Elevation of the l^{th} control volume	[L]
Δt	Time increment	[T]
$\gamma_{a,kl}^{d}$	Influence coefficients for the dispersive flux in the aqueous phase	[L^3 T^{-1}]
$\gamma_{g,kl}^{d}$	Influence coefficients for the dispersive flux in the gaseous phase	[L^3 T^{-1}]
$\gamma_{kl}^{c,N+1}$	Influence coefficient for the conductive heat flux at the current time level	[M L^2 T^{-3} $^oC^{-1}$]
$\gamma_{kl}^{c,N+1}$	Influence coefficient for the dispersive heat flux at the current time level	[L^5T^{-3} $^oC^{-1}$]

$\boldsymbol{\varepsilon}$	Prescribed tolerance	[-]
$\boldsymbol{\zeta_k}$	One-dimensional efficiency loading coefficient of the k^{th} control volume	[-]
$\boldsymbol{\eta_k}$	Number of adjacent control volumes, which can vary from one for the boundary control volume in case of a 1D problem to six for an internal control volume (assuming blocks) in the case of 3D spatial discretization.	[-]
λ_k	Thermal conductivity of control volumes *k*	[M L T^{-3} $^oC^{-1}$]
λ_l	Thermal conductivity of control volumes *l*	[M L T^{-3} $^oC^{-1}$]
λ_s	Thermal conductivity of solid	[M L T^{-3} $^oC^{-1}$]
λ_w	Thermal conductivity of water	[M L T^{-3} $^oC^{-1}$]
λ_{kl}	Representative thermal conductivity used for the flux calculation between control volumes *k* and *l*	[M L T^{-3} $^oC^{-1}$]
$\boldsymbol{\mu_{a,kl}^{N+1}}$	Representative aqueous phase viscosity used for the flux calculation between control volumes *k* and *l* at the current time level	[M L^{-1} T^{-1}]
$\boldsymbol{\mu_{a,kl}^{N+1,i}}$	Representative aqueous phase viscosity used for the flux calculation between control volumes *k* and *l* at the current time level and at the previous Picard iteration	[M L^{-1} T^{-1}]
$\boldsymbol{\rho_{a,k}^{N}}$	Aqueous phase density of the k^{th} control volume at the previous time level	[M L^{-3}]
$\boldsymbol{\rho_{a,k}}$	Aqueous phase density of the k^{th} control volume	[M L^{-3}]
$\boldsymbol{\rho_{a,k}^{N+1,i}}$	Aqueous phase density of the k^{th} control volume at the current time level and the previous Picard iteration	[M L^{-3}]
$\boldsymbol{\rho_{a,s}}$	Aqueous phase density of external sources/sinks	[M L^{-3}]
$\boldsymbol{\rho_{a,kl}^{N+1}}$	Representative aqueous phase density used for the flux calculation between control volumes *k* and *l* at the current time level	[M L^{-3}]
$\boldsymbol{\rho_{a,kl}^{N+1,i}}$	Representative aqueous phase density used for the flux calculation between control volumes *k* and *l* at the	[M L^{-3}]

	current time level and the previous Picard iteration	
$\rho_{s,k}$	Solid phase density of the k^{th} control volume	[M L^{-3}]
$\boldsymbol{\sigma_{zz}^{N}}$	Vertical stress at the previous time level	[M L^{-1} T^{-2}]
$\boldsymbol{\sigma_{zz}^{N+1}}$	Vertical stress at the current time level	[M L^{-1} T^{-2}]
$\boldsymbol{\phi_k}$	Porosity of the k^{th} control volume	[-]
$\boldsymbol{\phi_k^N}$	Porosity of the k^{th} control volume at the previous time level	[-]
$\boldsymbol{\phi_k^{N+1}}$	Porosity of the k^{th} control volume at the current time level	[-]
$\boldsymbol{\phi_{kl}}$	Harmonic averaged porosity between control volumes k and l	[-]
ψ_k	Pressure head at the k^{th} control volume	[L]

APPENDIX B: PITZER MODEL AND PITZER VIRIAL COEFFICEINTS DATABASE FOR MODEL VERIFICATION

B PITZER MODEL AND PITZER COEFFICIENTS

The calculation of aqueous speciation and mineral solubilities in brines requires the evaluation of activity coefficients that are valid under high ionic strength conditions. In addition, empirical relationships to calculate fluid densities as a linear function of Total Dissolved Solids (TDS) break down for these concentrated solutions, and more sophisticated approaches are needed. This appendix describes the formulations used to calculate activity coefficients and the solution density based on the Pitzer equations (1973) and documents the Pitzer database as implemented in MIN3P-THCm.

B.1. ACTIVITY COEFFICIENT CALCULATIONS BASED ON PITZER EQUATIONS

The vector of species molalities ($\mathbf{m}$) is the input for this algorithm. The vector of activity coefficients ($\boldsymbol{\gamma}$) is computed according to:

$$\ln \boldsymbol{\gamma} = \left(\ln \gamma_{DH} + q'\right)\mathbf{z^2} + q^c\mathbf{z} + \left(2\mathbf{Q} + Z\mathbf{C}\right)\mathbf{m} + \mathbf{m}^t\mathbf{T}\mathbf{m} \qquad \textbf{Equation B-1}$$

$\mathbf{z}$ and $\mathbf{z^2}$ are the vectors of electric charge and squared electric charge, respectively. The modified Debye-Hückel terms (γ_{DH}), in Equation B-1, are defined according to Harvie et al. (1984):

$$\ln \gamma_{DH} = -A^{\phi}\left[\frac{\sqrt{I}}{1+b\sqrt{I}} + \frac{2}{b}\ln\left(1+b\sqrt{I}\right)\right] \qquad \textbf{Equation B-2}$$

where A^{ϕ} is the one third Debye-Hückel slope (A^{ϕ}=0.392 at 25ºC, Pitzer and Mayorga, 1973), I is ionic strength, and b is a Debye-Hückel parameter (for all electrolytes b=1.2).

The activity of water (a_w) is computed from the osmotic coefficient ϕ (Felmy and Weare, 1986):

$$\ln a_w = -\phi MW \qquad \textbf{Equation B-3}$$

where W is the molecular weight of water [kg mol^{-1}]. The osmotic coefficient is defined as:

$$\phi = \frac{2}{M}\left(f'(I) + q^{\phi} + Zq^c + q^L + t\right) + 1 \qquad \textbf{Equation B-4}$$

Ionic strength (I) and Z account for the effect of the electric charge in the electrolytic solution and are computed according to:

$$I = \frac{1}{2}\mathbf{z}_2^t\mathbf{m} \qquad \textbf{Equation B-5}$$

$$Z = \mathbf{z}_{abs}^t\mathbf{m} \qquad \textbf{Equation B-6}$$

where $\mathbf{z}_2^t$ and $\mathbf{z}_{abs}^t$ are the transpose of the square and absolute electric charge vectors, respectively. The total molar mass of solutes (M) in the water activity expression in Equation B-3 is calculated as:

$$M = \mathbf{1}_{N_{aq}}^t\mathbf{m} \qquad \textbf{Equation B-7}$$

where $\mathbf{1}_{N_{aq}}^t$ is the unity vector of dimension N_{aq}. Scalars q', q^{ϕ}, q^c and q^L in Equation B-1 and Equation B-4 represent the contributions of binary interactions. They are computed from:

$$q' = \mathbf{m}^t\mathbf{Q}'\mathbf{m} \qquad \textbf{Equation B-8}$$

$$q^{\phi} = \mathbf{m}^t\mathbf{Q}^{\phi}\mathbf{m} \qquad \textbf{Equation B-9}$$

$$q^c = \mathbf{m}^t\mathbf{C}\mathbf{m} \qquad \textbf{Equation B-10}$$

$$q^L = \mathbf{m}^t\mathbf{Q}^{\mathbf{L}}\mathbf{m} \qquad \text{Equation B-11}$$

The last term in Equation B-1 and the scalar t in Equation B-4 account for ternary interactions. The scalar t is given by:

$$t = \mathbf{m}^t\mathbf{T}\mathbf{m} \qquad \textbf{Equation B-12}$$

Matrices $\mathbf{Q}$, $\mathbf{Q}'$, $\mathbf{Q}^{\phi}$, $\mathbf{Q}^{\mathbf{L}}$ and $\mathbf{C}$ are square and symmetric [$N_{aq} \times N_{aq}$].These matrices include submatrices for interactions between cations (c), anions (a) and neutral species (n):

$$\mathbf{Q}(\mathrm{I}) = \begin{bmatrix} \mathbf{\Phi}_{cc`} & \frac{1}{2}\mathbf{B}_{ca}^t & \frac{1}{2}\mathbf{L}_{nc}^t \\ \frac{1}{2}\mathbf{B}_{ca} & \mathbf{\Phi}_{\grave{a}a`} & \frac{1}{2}\mathbf{L}_{na}^t \\ \frac{1}{2}\mathbf{L}_{nc} & \frac{1}{2}\mathbf{L}_{na} & 0 \end{bmatrix} \qquad \textbf{Equation B-13}$$

$$\mathbf{Q}'(\mathrm{I}) = \begin{bmatrix} \mathbf{\Phi}'_{cc`} & \frac{1}{2}\mathbf{B}^{t}_{ca} & 0 \\ \frac{1}{2}\mathbf{B}'_{ca} & \mathbf{\Phi}'_{\grave{a}a`} & 0 \\ 0 & 0 & 0 \end{bmatrix}$$

Equation B-14

$$\mathbf{Q}^{\phi}(\mathrm{I}) = \begin{bmatrix} \mathbf{\Phi}^{\varphi}_{cc'} & \frac{1}{2}\mathbf{B}^{\varphi t}_{ca} & 0 \\ \frac{1}{2}\mathbf{B}^{\varphi}_{ca} & \mathbf{\Phi}^{\phi}_{aa'} & 0 \\ 0 & 0 & 0 \end{bmatrix}$$

Equation B-15

$$\mathbf{Q}^{\mathbf{L}} = \begin{bmatrix} 0 & 0 & \frac{1}{2}\mathbf{L}^{t}_{nc} \\ 0 & 0 & \frac{1}{2}\mathbf{L}^{t}_{na} \\ \frac{1}{2}\mathbf{L}_{nc} & \frac{1}{2}\mathbf{L}_{na} & 0 \end{bmatrix}$$

Equation B-16

$$\mathbf{C} = \begin{bmatrix} 0 & \mathbf{C}^{t}_{ca} & 0 \\ \mathbf{C}_{ca} & 0 & 0 \\ 0 & 0 & 0 \end{bmatrix}$$

Equation B-17

Submatrices **B** in Equation B-13, Equation B-14, and Equation B-15 account for ionic interactions between ions of opposite charge. Submatrices **Φ** represent interactions between ions with the same electric charge. **L** accounts for interactions between neutral and charged species, while submatrices **C** account for ternary interactions (Pitzer and Mayorga, 1973).

The elements of submatrices **B** in Equation B-13, Equation B-14, and Equation B-15 are defined as (Pitzer, 1973):

$$\mathbf{B}_{ca} \Rightarrow B_{ij} = \beta^{(0)}_{ij} + \beta^{(1)}_{ij} g\left(\alpha_1\sqrt{I}\right) + \beta^{(2)}_{ij} g\left(\alpha_2\sqrt{I}\right)$$

Equation B-18

$$\mathbf{B}'_{ca} \Rightarrow B'_{ij} = \beta^{(1)}_{ij} \frac{g'\left(\alpha_1\sqrt{I}\right)}{I} + \beta^{(2)}_{ij} \frac{g'\left(\alpha_2\sqrt{I}\right)}{I}$$

Equation B-19

$$\mathbf{B}^{\varphi}_{ca} \Rightarrow B^{\phi}_{ij} = \beta^{(0)}_{ij} + \beta^{(1)}_{ij} e^{-\alpha_1\sqrt{I}} + \beta^{(2)}_{ij} e^{-\alpha_2\sqrt{I}}$$

Equation B-20

where $\beta^{(0)}_{ij}$, $\beta^{(1)}_{ij}$, $\beta^{(2)}_{ij}$ are experimental coefficients. They are read from the virial

coefficients database.

The functions g and g' in Equation B-18 and B-19 are a function of the ionic strength:

$$g(x) = 2\frac{\left(1-(1+x)e^{-x}\right)}{x^2} \qquad \textbf{Equation B-21}$$

$$g'(x) = -2\frac{\left(1-\left(1+x+\frac{x^2}{2}\right)e^{-x}\right)}{x^2} \qquad \textbf{Equation B-22}$$

with $x = \alpha_1\sqrt{I}$ or $x = \alpha_2\sqrt{I}$. When either ion in the couple ij is monovalent $\alpha_1 = 2$. For 2−2 or higher valence pairs, $\alpha_1 = 1.4$. For all electrolytes $\alpha_2 = 12$.

Higher-order ionic interactions are accounted by the submatrices $\mathbf{\Phi}$ in Equation B-13, Equation **B-14** and Equation B-15. These matrices account for the effect of unsymmetrical mixing solutions between ions of the same charge (i.e. + + or − −) and are computed according to Pitzer (1975):

$$\mathbf{\Phi}^{\phi}_{\mathbf{cc'}}, \mathbf{\Phi}^{\phi}_{\mathbf{aa'}} \Rightarrow \phi^{\phi}_{ij} = \theta_{ij} + \theta^{E}_{ij}(I) + I\theta^{E'}_{ij}(I) \qquad \textbf{Equation B-23}$$

$$\mathbf{\Phi}_{\mathbf{cc'}}, \mathbf{\Phi}_{\mathbf{aa'}} \Rightarrow \phi_{ij} = \theta_{ij} + \theta^{E}_{ij}(I) \qquad \textbf{Equation B-24}$$

$$\mathbf{\Phi}^{'}_{\mathbf{cc'}}, \mathbf{\Phi}^{'}_{\mathbf{aa'}} \Rightarrow \phi^{'}_{ij} = \theta^{E'}_{ij}(I) \qquad \textbf{Equation B-25}$$

where θ_{ij} are experimentally determined parameters, and $\theta^{E}_{ij}(I)$ and $\theta^{E'}_{ij}(I)$ are a function of ionic strength and the electrolyte pair type:

$$\theta^{E}_{ij}(I) = \left(\frac{z_i z_j}{4I}\right)\left(J(X_{ij}) - \frac{1}{2}J(X_{ii}) - \frac{1}{2}J(X_{jj})\right) \qquad \textbf{Equation B-26}$$

$$\theta^{E'}_{ij}(I) = -\left(\frac{\theta^{E}_{ij}(I)}{I}\right) + \left(\frac{z_i z_j}{8I^2}\right)\left(J'(X_{ij}) - \frac{1}{2}J'(X_{ii}) - \frac{1}{2}J'(X_{jj})\right) \qquad \textbf{Equation B-27}$$

where $X_{ij} = 6z_i z_j A^{\phi}\sqrt{I}$ and z_i and z_j are the electric charge of ith and jth ion, respectively. To evaluate the functions J in Equation B-26, we can use two polynomial approximations presented by Pitzer (1975) for a broad range of X_{ij} values ($0.1 \le X_{ij} \le 80$):

$$J(X_{ij}) = -\frac{1}{6} X_{ij}^2 \ln(X_{ij}) e^{-10X_{ij}^{\frac{1}{2}}} + \frac{1}{\sum_{k=1}^{6} \frac{C_k}{X_{ij}^k}}$$ **Equation B-28**

For $X_{ij} > 80$, Pitzer (1975) suggests:

$$J(X_{ij}) = \frac{X_{ij}}{4 + \frac{C_1}{X_{ij}^{C_2}} e^{-C_3 X_{ij}^{C_4}}}$$ **Equation B-29**

For the definition of the parameters C_k, we refer to Pitzer (1975). $J'(X_{ij})$ in Equation B-27 is the derivative of $J(X_{ij})$ as defined by Equation B-28 and Equation B-29 ($J'(X_{ij}) = dJ(X_{ij})/dX_{ij}$).

The elements of submatrix $\mathbf{C_{ca}}$ in Equation B-17 do not depend on ionic strength and are defined as (Pitzer and Mayorga, 1973):

$$\mathbf{C_{ca}} \Rightarrow C_{ij} = \frac{C_{ij}^{\phi}}{2\sqrt{|z_i z_j|}}$$ **Equation B-30**

where C_{ij}^{ϕ} are experimentally determined coefficients. **T** in Equation B-1 is a third order tensor [$N_{aq} \times N_{aq} \times N_{aq}$] with the following structure:

$$\mathbf{T} = \begin{bmatrix} \mathbf{T_c} \\ \mathbf{T_a} \\ \mathbf{T_n} \end{bmatrix} = \begin{bmatrix} 0 & 0 & 0 \\ 0 & \boldsymbol{\Psi}_{\mathbf{aa'ci}} & 0 \\ 0 & 0 & 0 \\ \cdot & \cdot & \cdot \\ \cdot & \cdot & \cdot \\ \boldsymbol{\Psi}_{cc'a\mathbf{i}} & 0 & 0 \\ 0 & 0 & 0 \\ 0 & 0 & 0 \\ \cdot & \cdot & \cdot \\ \cdot & \cdot & \cdot \\ \boldsymbol{\Psi}_{cc'n\mathbf{i}} & 0 & 0 \\ 0 & \boldsymbol{\Psi}_{\mathbf{aa'}n\mathbf{i}} & 0 \\ 0 & 0 & 0 \end{bmatrix}$$ **Equation B-31**

Submatrices **Ψ** contain experimental information and are read from a virial coefficient data base.

B.2. SCALED MACINNES CONVENTION

Individual ion activities and activity coefficients cannot be determined separately.

Individual ion activities and activity coefficients have a meaning only in a relative sense and individual values depend on a particular choice of scale convention. A common approach is the MacInnes convention (MacInnes, 1919). For example, the activity coefficient of Cl^- in KCl solution is defined as being equal to the mean activity coefficient of KCl in a KCl solution of equivalent ionic strength, $\gamma_{Cl}^{M} \equiv \gamma_{\pm KCl}^{M}$. The scaling factor (f_i^M) for the ith ion in KCl solution is computed from:

$$f_i^M = \left[\frac{\gamma_{\pm KCl}}{\gamma_{\pm KCl} M} \right]^{\frac{1}{z_i}}$$ **Equation B-32**

The scaled activity coefficient for the ith species (γ_i^M) is computed as:

$$\gamma_i^M = \gamma_i f_i^M$$ **Equation B-33**

where γ_i is the activity coefficient for the ith species.

B.3. DENSITY CALCULATIONS BASED ON PITZER EQUATIONS

The density of the aqueous phase is a key parameter in the modelling of mass transfer processes in a sedimentary basin. Solution density is commonly estimated by empirical relationships that derive the fluid density as a function of ionic strength, but independent of the fluid composition (e.g. Henderson et al., 2009). A more rigorous alternative that is based on the Pitzer equations is provided by Monnin (1994). Monnin (1994) determined the solution density based on the concentrations of the major ions in natural waters: Na, K, Ca, Mg, Cl, SO_4, HCO_3, and CO_3.

The total volume of the solution (which contains 1000 g of water) is:

$$V = V_{id} + V_{ex} = 1000\,\upsilon_w + \sum_i m_i \overline{V}_i^o + V_{ex}$$ **Equation B-34**

where υ_W is the specific volume of pure water (cm^3 g^{-1}), and $\overline{V}_i^o$ is the standard partial volume of the solute i (cm^3 mol^{-1}). The term V_{ex} in Equation B-34 represents the total excess volume of a multicomponent electrolyte solution. It can be expressed as a virial expansion of the solute molalities:

$$\frac{V_{ex}}{RT} = f_{DH}^{v}(I) + 2\sum_c \sum_a m_c m_a \left(B_{ca}^{v} + \left(\sum_c m_c z_c \right) C_{ca}^{v} \right)$$ **Equation B-35**

In this expression, R is the ideal gas constant and T the absolute temperature, m_c is the

molality of cation c (of charge z_c), and m_a that of anion a. $f_{DH}^{v}(I)$ is the Debye-Hückel term:

$$f_{DH}^{v}(I) = \frac{A_v}{RT}\frac{I}{1.2}\ln\left(1+1.2\sqrt{I}\right) \qquad \textbf{Equation B-36}$$

in which I is the ionic strength and A_v the Debye-Hückel slope. B_{ca}^{v} is the second virial coefficients for the volume, depending on ionic strength (equivalent to Equation B-18 with slightly modified notation):

$$B_{ca}^{v} = \beta_{ca}^{(0),v} + \beta_{ca}^{(1),v} g\left(\alpha_1\sqrt{I}\right) + \beta_{ca}^{(2),v} g\left(\alpha_2\sqrt{I}\right) \qquad \textbf{Equation B-37}$$

The parameters α_1 and α_2 depend on the type of the electrolyte and are equal to 2.0 and 0.0, respectively for 1-1, 1-2 and 2-1 salts, and to 1.4 and 12.0 for 2-2 salts. $\beta_{ca}^{(0),v}$, $\beta_{ca}^{(1),v}$, $\beta_{ca}^{(2),v}$ and C_{ca}^{v} are empirical parameters specific to each salt. The functions g within Equation B-37 are defined by Equation B-21. The density of the solution (ρ) is computed according to:

$$\rho = \frac{1000 + \sum_i m_i W_i}{V} \qquad \textbf{Equation B-38}$$

where m_i and W_i are the molality and molecular weight (g mol^{-1}) of the ith solute, respectively.

B.4. PITZER VIRIAL COEFFICIENTS

This section presents the Pitzer virial coefficients used in the reactive transport verification example described in **the verification report in section 1.1.4 '**Pitzer equation – Chemical speciation of Dead Sea water**'**. The coefficients are based on the work from Harvie et al. (1984) and Greenberg and Möller (1989).

Table B-1: Pitzer Virial Coefficients Used for Model Verification – Part 1

Cation	Anion	$\beta^{(0)}$	$\beta^{(1)}$	$\beta^{(2)}$	C^{φ}
Na^+	Cl^-	0.07456	0.27524	-	0.00077
K^+	Cl^-	0.04778	0.21551	-	-0.00037
Mg^{2+}	Cl^-	0.35114	1.65325	-	0.00231
Ca^{2+}	Cl^-	0.30382	1.70143	-	0.00042
$CaCl^+$	Cl^-	0.35684	4.81235	-	-0.00339
$MgOH^+$	Cl^-	-0.10000	1.65800	-	-
H^+	Cl^-	0.17700	0.29292	-	0.00018
Na^+	SO_4^{2-}	0.01206	1.11538	-	0.00232
K^+	SO_4^{2-}	0.05554	0.79638	-	-0.00665
Mg^{2+}	SO_4^{2-}	0.22282	3.37713	-35.25878	0.00609
Ca^{2+}	SO_4^{2-}	0.15000	3.00000	-	-
H^+	SO_4^{2-}	0.09862	0.00000	-	0.02097
Na^+	HSO_4^-	0.07343	0.29994	-	-0.00231
K^+	HSO_4^-	-0.00030	0.17350	-	-
Mg^{2+}	HSO_4^-	0.47460	1.72880	-	-
Ca^{2+}	HSO_4^-	0.21450	2.52750	-	-
H^+	HSO_4^-	0.20909	0.44092	-	-
Na^+	OH^-	0.08834	0.24442	-	0.00200
K^+	OH^-	0.12980	0.32000	-	0.00205
Ca^{2+}	OH^-	-0.17470	-0.23030	-5.72000	-
Na^+	HCO_3^-	0.02800	0.04401	-	-
Mg^{2+}	HCO_3^-	0.03300	0.84980	-	-
K^+	HCO_3^-	-0.01070	0.04780	-	-
Ca^{2+}	HCO_3^-	0.40000	2.97700	-	-
Na^+	CO_3^{2-}	0.03620	1.51207	-	0.00184
K^+	CO_3^{2-}	0.12880	1.43330	-	0.00018

Table B- 2: Pitzer Virial Coefficients Used for Model Verification – Part 2

Ion	Ion	θ	Ion	Ion	θ
K^+	Na^+	-0.0032	K^+	$CaCl^+$	0.0000
Mg^{2+}	Na^+	0.0700	K^+	$MgHCO_3^+$	0.0000
Ca^{2+}	Na^+	0.0500	K^+	$CaOH^+$	0.0000
H^+	Na^+	0.0360	Na^+	$MgOH^+$	0.0000
Ca^{2+}	K^+	0.1156	Na^+	$CaCl^+$	0.0000
H^+	K^+	0.0050	Na^+	$MgHCO_3^+$	0.0000
Ca^{2+}	Mg^{2+}	0.0070	Na^+	$CaOH^+$	0.0000
H^+	Mg^{2+}	0.1000	Ca^{2+}	$MgOH^+$	0.0000
H^+	Ca^{2+}	0.0920	Ca^{2+}	$CaCl^+$	0.0000
SO_4^{2-}	Cl^-	0.0703	Ca^{2+}	$MgHCO_3^+$	0.0000
HSO_4^-	Cl^-	-0.0060	Ca^{2+}	$CaOH^+$	0.0000
HSO_4^-	SO_4^{2-}	-0.1168	CO_3^{2-}	HSO_4^-	0.0000
OH^-	Cl^-	-0.0500	Mg^{2+}	$MgOH^+$	0.0000
HCO_3^-	Cl^-	0.0359	Mg^{2+}	$CaCl^+$	0.0000
CO_3^{2-}	Cl^-	-0.0920	Mg^{2+}	$MgHCO_3^+$	0.0000
OH^-	SO_4^{2-}	-0.0130	Mg^{2+}	$CaOH^+$	0.0000
HCO_3^-	SO_4^{2-}	0.0100	HSO_4^-	OH^-	0.0000
CO_3^{2-}	SO_4^{2-}	0.0200	HSO_4^-	HCO_3^-	0.0000
CO_3^{2-}	OH^-	0.1000	OH^-	HCO_3^-	0.0000
CO_3^{2-}	HCO_3^-	-0.0400	$MgOH^+$	$CaCl^+$	0.0000
H^+	$MgOH^+$	0.0000	$MgOH^+$	$MgHCO_3^+$	0.0000
H^+	$CaCl^+$	0.0000	$MgOH^+$	$CaOH^+$	0.0000
H^+	$MgHCO_3^+$	0.0000	$CaCl^+$	$MgHCO_3^+$	0.0000
H^+	$CaOH^+$	0.0000	$CaCl^+$	$CaOH^+$	0.0000
K^+	Mg^{2+}	0.0000	$MgHCO_3^+$	$CaOH^+$	0.0000
K^+	$MgOH^+$	0.0000			

Table B-3: Pitzer Virial Coefficients Used for Model Verification – Part 3

Ion	Neutral species	λ
Cl^-	$CO_2(aq)$	-0.0050
Na^+	$CO_2(aq)$	0.11544
K^+	$CO_2(aq)$	0.11544
Ca^{2+}	$CO_2(aq)$	0.23088
Mg^{2+}	$CO_2(aq)$	0.23088
SO_4^{2-}	$CO_2(aq)$	0.09386
HSO_4^-	$CO_2(aq)$	0.00300

Table B-4: Pitzer Virial Coefficients Used for Model Verification – Part 4

Ion	Ion	Ion	ψ	Ion	Ion	Ion	ψ
Na^+	K^+	Cl^-	-0.0037	Cl^-	SO_4^{2-}	Mg^{2+}	-0.008
Na^+	K^+	SO_4^{2-}	0.00732	Cl^-	HSO_4^-	Na^+	-0.006
Na^+	K^+	HCO_3^-	-0.003	Cl^-	HSO_4^-	H^+	0.013
Na^+	K^+	CO_3^{2-}	0.003	Cl^-	OH^-	Na^+	-0.006
Na^+	Ca^{2+}	Cl^-	-0.003	Cl^-	OH^-	K^+	-0.006
Na^+	Ca^{2+}	SO_4^{2-}	-0.012	Cl^-	OH^-	Ca^{2+}	-0.025
Na^+	Mg^{2+}	Cl^-	-0.012	Cl^-	HCO_3^-	Na^+	-0.0143
Na^+	Mg^{2+}	SO_4^{2-}	-0.015	Cl^-	HCO_3^-	Mg^{2+}	-0.096
Na^+	H^+	Cl^-	-0.004	Cl^-	CO_3^{2-}	Na^+	0.016
Na^+	H^+	HSO_4^-	-0.0129	Cl^-	CO_3^{2-}	K^+	0.004
K^+	Ca^{2+}	Cl^-	-0.0432	SO_4^{2-}	HSO_4^-	Na^+	0.01437
K^+	Mg^{2+}	Cl^-	-0.022	SO_4^{2-}	HSO_4^-	K^+	-0.0677
K^+	Mg^{2+}	SO_4^{2-}	-0.048	SO_4^{2-}	HSO_4^-	Mg^{2+}	-0.0425
K^+	H^+	Cl^-	-0.011	SO_4^{2-}	HSO_4^-	H^+	0.02781
K^+	H^+	SO_4^{2-}	0.197	SO_4^{2-}	OH^-	Na^+	-0.0091
K^+	H^+	HSO_4^-	-0.0265	SO_4^{2-}	OH^-	K^+	-0.05
Ca^{2+}	Mg^{2+}	Cl^-	-0.012	SO_4^{2-}	HCO_3^-	Na^+	-0.005
Ca^{2+}	Mg^{2+}	SO_4^{2-}	0.024	SO_4^{2-}	HCO_3^-	Mg^{2+}	-0.161
Ca^{2+}	H^+	Cl^-	-0.015	SO_4^{2-}	CO_3^{2-}	Na^+	-0.005
Mg^{2+}	$MgOH^+$	Cl^-	0.028	SO_4^{2-}	CO_3^{2-}	K^+	-0.009
Mg^{2+}	H^+	Cl^-	-0.011	OH^-	CO_3^{2-}	Na^+	-0.017
Mg^{2+}	H^+	HSO_4^-	-0.0178	OH^-	CO_3^{2-}	K^+	-0.01
Cl^-	SO_4^{2-}	Na^+	-0.0091	HCO_3^-	CO_3^{2-}	Na^+	0.002
Cl^-	SO_4^{2-}	K^+	-0.0016	HCO_3^-	CO_3^{2-}	K^+	0.012
Cl^-	SO_4^{2-}	Ca^{2+}	-0.018				

APPENDIX C: MIN3P-THCM ASSOCIATED PUBLICATIONS

C MIN3P-THCM ASSOCIATED PUBLICATIONS

C.1. INTERNAL PUBLICATIONS

C.1.1. Journal papers

1. Forde, O.N., K.U. Mayer, A.G. Cahill, B. Mayer, J.A. Cherry, and B.L. Parker, (2018). Vadose Zone Gas Migration and Surface Effluxes Following a Controlled Natural Gas Release into an Unconfined Shallow Aquifer, Vadose Zone Journal, accepted, July 2018

2. Pedretti, D., K. U. Mayer and R. D. Beckie, (2017). Effective neutralizing capacity of mineralogically heterogeneous waste rock piles: a stochastic multicomponent reactive transport analysis, Journal of Contaminant Hydrology, 201:30-38

3. Espeleta, J. F., Z. G. Cardon, K. U. Mayer, and R. B. Neumann, (2016). Nutrient hotspots in the rhizosphere generated by diel oscillation in rhizosphere water flow and soil cation exchange, Plant and Soil, doi:10.1007/s11104-016-3089-5

4. Sihota, N.J., J. Trost, B. A. Bekins, A. Berg, G. Delin, B. Mason, E. Warren, and K. U. Mayer, (2016). Seasonal variability in vadose zone biodegradation at a crude oil pipeline rupture site, Vadose Zone Journal, doi: 10.2136/vzj2015.09.0125

5. Harrison, A.L., G.M. Dipple, I.M. Power, and K.U. Mayer, (2016). The impact of evolving mineral-water-gas interfacial areas on mineral-fluid reaction rates in unsaturated porous media, Chemical Geology, 421:65-80

6. Wilson, S. A.; #A. L Harrison; G. M Dipple; I. M Power; S. L Barker; K. U. Mayer; S. J. Fallon; M. Raudsepp; G. Southam, (2014). Offsetting of CO2 emissions by air capture into mine tailings at the Mount Keith Nickel Mine, Western Australia: Rates, controls and prospects for carbon neutral mining International Journal of Greenhouse Gas Control, 25, 121–140, doi: 10.1016/j.ijggc.2014.04.002

7. Bea, S. A, D. Su, K. U. Mayer, and K.T.B. MacQuarrie, (2018). Evaluation of the potential for dissolved oxygen ingress into deep sedimentary basins during a glaciation event, Geofluids, https://doi.org/10.1155/2018/9475741

8. Su, D., K.U. Mayer and K. T. B. MacQuarrie, 2017. Parallelization of MIN3P-THCm: a high performance computational framework for subsurface flow and reactive transport simulation, Environmental Modelling and Software, 95:271-289

9. Bea, S.A. K.U. Mayer, K.T.B. MacQuarrie, 2016, Coupling of thermo-hydro-chemical and mechanical processes in deep sedimentary basins: Model development, verification and illustrative example, Geofluids,

doi:10.1111/gfl.12148

10. Steefel, C. I., S. B. Yabusaki, and K. U. Mayer, 2015. Editorial: Reactive transport benchmarks for subsurface environmental simulation, Computational Geosciences, Special Issue on: Subsurface Environmental Simulation Benchmarks, 19:439-443, doi:10.1007/s10596-015-9499-2

11. Steefel, C.I., Appelo, C.A.J., Arora, B., Jacques, D., Kalbacher, T., Kolditz, O., Lagneau, V., Lichtner, P.C., Mayer, K.U., Meeussen, J.C.L., Molins, S., Moulton, D., Shao, H., Šimůnek, J., Spycher, N., Yabusaki, S.B., Yeh, G.T. (2014). Reactive transport codes for subsurface environmental simulation, Computational Geosciences, DOI: 10.1007/s10596-014-9443-x

12. Molins, S., J. Greskowiak, C. Wanner and K.U. Mayer. 2015. A benchmark for microbially mediated chromium reduction under denitrifying conditions in a biostimulation column experiment, Computational Geosciences 19(3): 479. doi:10.1007/s10596-014-9432-0

13. Rasouli, P., C.I. Steefel and K.U. Mayer. 2015. Benchmarks for multicomponent diffusion and electrochemical migration, Computational Geosciences 19(3): 523. doi:10.1007/s10596-015-9481-z

14. Alt-Epping, P., C. Tournassat, P. Rasouli, C. I. Steefel, K. U. Mayer, A. Jenni, U. Mäder, S. S. Sengor and R. Fernández. 2015. Benchmark reactive transport simulations of a column experiment in compacted bentonite with multispecies diffusion and explicit treatment of electrostatic effects, Computational Geosciences 19(3): 535. doi:10.1007/s10596-014-9451-x.

15. Şengör, S.S., K.U. Mayer, J. Greskowiak, C. Wanner, D. Su and H. Prommer. 2015. Benchmarks for multicomponent reactive transport across a cement/clay interface, Computational Geosciences 19(3): 569. doi: 10.1007/s10596-015-9480-0

16. Greskowiak, J., J. Gwo, D. Jacques, J. Yin and K. U. Mayer. 2015. A benchmark for multi-rate surface complexation and 1D dual-domain multi-component reactive transport of U(VI), Computational Geosciences 19(3): 585. doi: 10.1007/s10596-014-9457-4

17. Mayer, K.U., P. Alt-Epping, D. Jacques, B. Arora and C. I. Steefel. 2015. Benchmark problems for reactive transport modeling of the generation and attenuation of acid rock drainage, Computational Geosciences 19(3): 599. doi:10.1007/s10596-015-9476-9.

18. Marty, N.C.M., O. Bildstein, P. Blanc, F. Claret, B. Cochepin, E.C. Gaucher, D. Jacques, J.-E. Lartigue, S. Liu, K.U. Mayer, J.C.L. Meeussen, I. Munier, I. Pointeau, D. Su, C.I. Steefel. 2015. Benchmarks for multicomponent reactive transport across a cement/clay interface, Computational Geosciences 19(3): 635. doi:10.1007/s10596-014-9463-6

19. Xie, M., K.U. Mayer, F. Claret, P. Alt-Epping, D. Jacques, C.I. Steefel, Ch. Chiaberge and J. Simunek. 2015. Benchmark of implementation and evaluation of permeability-porosity relationships linked to mineral dissolution-precipitation, Computational Geosciences 19(3): 655 doi:10.1007/s10596-014-9458-3.

20. Perko, J., K.U. Mayer, G. Kosakowski, L. De Windt, J. Govaerts, D. Jacques, D. Su and J.C.L. Meeussen. 2015. Decalcification of cracked cement structures, Computational Geosciences 19(3): 673 doi:10.1007/s10596-014-9467-2.

21. Yin, J., S.-W. Jeen, D. Lee, and K.U. Mayer, 2014. Reactive transport modeling of Sr-90 sorption in reactive sandpacks, Journal of Hazardous Materials, 280:685–695

22. Mayer, K.U. and K. T. B. MacQuarrie. 2010. Solution of the MoMaS reactive transport benchmark with MIN3P - Model formulation and simulation results, Computational Geosciences, 14(3):405-419, doi:10.1007/s10596-009-9158-6

23. Bea, S.A., S.A. Wilson, K.U. Mayer, G.M. Dipple, I.M. Power and P. Gamazo 2011. Reactive transport modeling of natural carbon sequestration in ultra-mafic mine tailings, accepted for publication in Vadose Zone Journal, October 2011.

24. Conlan, M.J.W., K. U. Mayer, R. Blaskovich, and R. D. Beckie. 2012. Solubility controls for molybdenum in neutral rock drainage, Geochemistry: Exploration, Environment, Analysis. 12(1) p. 21-32, doi: 10.1144/1467-7873/10-RA-043.

25. Marica, F., S.A. Bea Jofré, K. U. Mayer, B. J. Balcom, and T. A. Al, 2011. MRI determination of spatially-resolved tracer distributions in porous media: Experiments involving diffusion and advection. Journal of Contaminant Hydrology, 125:47-56.

26. Masue-Slowey, Y. B.D. Kocar, S.A. Bea Jofré, K. U. Mayer, and S. Fendorf, 2011. Transport implications resulting from internal redistribution of arsenic and Iron within constructed soil aggregates, Environmental Science & Technology, 45:582-588.

27. Sihota, N.J., O. Singurindy, and K. U. Mayer, 2011. CO2 efflux measurements for evaluating source zone natural attenuation rates in a petroleum hydrocarbon contaminated aquifer, Environmental Science & Technology, 45:482-488.

28. Sihota, N.J. and K.U. Mayer, 2012. Characterizing vadose zone hydrocarbon biodegradation using CO2-effluxes, isotopes, and reactive transport modeling, Vadose Zone Journal, 11, doi:10.2136/vzj2011.0204.

29. Loomer, D, T. A. Al, V. J. Banks, B. L. Parker, and K. U. Mayer, 2011. Manganese and trace metal mobility under reducing conditions following in situ oxidation of TCE by KMnO4: A laboratory column experiment, Journal of Contaminant Hydrology, 119:13-24.

30. Loomer, D., T. A. Al, V. Banks, B.L. Parker, and K. U. Mayer, 2010. Manganese Valence in Oxides Formed from in situ Chemical Oxidation of TCE by KMnO4, Environmental Science & Technology, 44:5934-5939.

31. Carrayrou J., J. Hoffmann, P. Knabner, S. Kräutle, C. de Dieuleveult, J. Erhel, J. Van der Lee, V. Lagneau, K. U. Mayer, and K.T.B. MacQuarrie, 2010. Comparison of numerical methods for simulating strongly non-linear and heterogeneous reactive transport problems – the MoMaS benchmark case, Computational Geosciences,14:483-502, doi: 10.1007/s10596-010-9178-2.

32. Mayer, K. U. and K. T. B. MacQuarrie, 2010. Solution of the MoMaS reactive transport benchmark with MIN3P - Model formulation and simulation results, Computational Geosciences, 14:405-419, doi:10.1007/s10596-009-9158-6.

33. MacQuarrie, K. T. B., K. U. Mayer, B. Jin, and S. M. Spiessl, 2010. The importance of conceptual models in the reactive transport simulation of oxygen ingress in sparsely fractured crystalline rock, Journal of Contaminant Hydrology, 112:64-76.

34. Carrayrou J., J. Hoffmann, P. Knabner, S. Kräutle, C. de Dieuleveult, J. Erhel, J. Van der Lee, V. Lagneau, K. U. Mayer, and K.T.B. MacQuarrie, 2010. Comparison of numerical methods for simulating strongly non-linear and heterogeneous reactive transport problems – the MoMaS benchmark case, Comput. Geosci.,14:483-502, doi: 10.1007/s10596-010-9178-2

35. Molins, S., K. U. Mayer, R. T. Amos, and B. A. Bekins, 2010. Vadose zone attenuation of organic compounds at a crude oil spill site - Interactions between biogeochemical reactions and multicomponent gas transport, Journal of Contaminant Hydrology, 112:15-29.

36. Tufano, K.J., S.G. Benner, K. U. Mayer, M. A. Marcus, P. S. Nico, S. Fendorf. 2009. Aggregate-scale heterogeneity in iron (hydr)oxide reductive transformations. Vadose Zone Journal, 8:1004–1012, doi:10.2136/vzj2008.0090.

37. Oiffer, A. J. F. Barker, F. M. Gervais, K. U. Mayer, C. J. Ptacek, D. L. Rudolph, 2009. A Detailed Field-Based Evaluation of Naphthenic Acid Mobility in Groundwater, Journal of Contaminant Hydrology, 108:89-106.

38. Henderson, T.H., K. U. Mayer, B. L. Parker, and T.A. Al., 2009. Three-dimensional density-dependent flow and multicomponent reactive transport modeling of chlorinated solvent oxidation by potassium permanganate, Journal of Contaminant Hydrology, 106:183-199.

39. Miller G.R., Y. Rubin, K.U. Mayer, and P.H. Benito, 2008. Modeling vadose zone processes during land application of food-processing waste water in California's Central Valley. Journal of Environmental Quality, 37:S-43-S-57.

40. Gerard, F. K. U. Mayer, M. J. Hodson, and J. Ranger. 2008, Modelling the

biogeochemical cycle of silicon in soils: application to a temperate forest ecosystem, Geochimica et Cosmochimica Acta, 72:741-758.

41. Spiessl, S.M., K.T.B. MacQuarrie, and K.U. Mayer, 2008. Identification of key parameters controlling dissolved oxygen migration and attenuation in fractured crystalline rocks, Journal of Contaminant Hydrology, 95:141-153.

42. Molins, S., K. U. Mayer, C. Scheutz, and P. Kjeldsen, 2008. Role of transport mechanisms in the attenuation of landfill gas in cover soils: A multicomponent modelling study. Journal of Environmental Quality, 37:459-468.

43. Molins, S. and K. U. Mayer, 2007. Coupling between geochemical reactions and multicomponent gas diffusion and advection – A reactive transport modeling study, Water Resources Research, 43, W05435, doi:10.1029/2006WR005206.

44. Jeen, S.-W., K. U. Mayer, R. W. Gillham and D. W. Blowes, 2007. Reactive transport modeling of trichloroethene treatment with declining reactivity of iron. Environmental Science & Technology, 41:1432-1438.

45. Cavé, L., N. Hartog, T. Al, B. L. Parker, K. U. Mayer, and S. Cogswell, 2007. Electrical monitoring of in situ chemical oxidation by permanganate, Groundwater Monitoring & Remediation, 27:77-84.

46. Williams, R. L., K. U. Mayer, R. T. Amos, D.W. Blowes, C. J. Ptacek, and J. Bain, 2007. Using dissolved gas analysis to investigate the performance of an organic carbon permeable reactive barrier for the treatment of mine drainage, Appl. Geochem., 22:90-108.

47. Al, T. A. V. Banks, D. Loomer, B. L. Parker and K. U. Mayer, 2006. Metal mobility during in-situ chemical oxidation of TCE by KMnO4, Journal of Contaminant Hydrology, 88:137-152.

48. Amos, R. T. and K. U. Mayer, 2006. Investigating ebullition in a sand column using dissolved gas analysis and reactive transport modelling, Environmental Science & Technology, 40:5361-5367.

49. Brookfield., A. D. W. Blowes, and K. U. Mayer, 2006. Integration of field measurements and reactive transport modelling to evaluate contaminant transport at a sulfide mine tailings impoundment, Journal of Contaminant Hydrology, 88:1-22.

50. Amos, R. T. and K. U. Mayer, 2006. Investigating the role of gas bubble formation and entrapment in contaminated aquifers: Reactive transport modeling, Journal of Contaminant Hydrology, 87:123-154.

51. Nowack, B., K. U. Mayer, S. E. Oswald, W. Van-Beinum, C. A. J. Appelo, D. Jacques, P. Seuntjens,F. Gérard, B. Jaillard, A. Schnepf, T. Roose, 2006. Verification and intercomparison of reactive transport codes to describe root-

uptake, Plant Soil, 285:305-321.

52. Mayer, K.U., S. G. Benner, and D. W. Blowes, 2006. Process-based reactive transport modeling of a permeable reactive barrier for the treatment of mine drainage, Journal of Contaminant Hydrology, 85:195-211.

53. MacQuarrie, K. T. M. and K. U. Mayer, 2005. Reactive transport modeling in fractured rock: a state-of-the-science review. Earth Sci. Rev., 72:189-227.

54. Amos, R. T., K. U. Mayer, B. A. Bekins, G. N. Delin, and R. L. Williams. 2005. Use of dissolved and vapor phase gases to investigate methanogenic degradation of petroleum hydrocarbon contamination in the subsurface, Water Resources Research, 41, W02001, doi:10.1029/2004WR003433.

55. Jurjovec, J., D. W. Blowes, C. J. Ptacek, and K. U. Mayer, 2004, Multicomponent reactive transport modelling of acid neutralization reactions in mill tailings. Water Resour Res., 40, W11202, doi:10.1029/2003WR002233.

56. Gérard, F., M. Tinsley, and K. U. Mayer, 2004. Preferential flow revealed by hydrologic modeling based on predicted hydraulic properties and intensive water content monitoring, Soil Sci Soc. Am. J., 68:1526-1538.

57. Amos, R. T., K. U. Mayer, D. W. Blowes, and C. J. Ptacek, 2004. Reactive transport modeling of column experiments for the remediation of acid mine drainage, Environmental Science & Technology, 38:3131-3138.

58. Watson, I. A., S. E. Oswald, K. U. Mayer, Y. Wu, and S. A. Banwart, 2003. Modeling kinetic processes controlling hydrogen and acetate concentrations in an aquifer-derived microcosm, Environmental Science & Technology, 37:3910 – 3919.

59. Romano, C. G., K. U. Mayer, D. W. Blowes, D. R. Jones, and D. A. Ellerbroek, 2003. Effectiveness of various cover scenarios on the rate of sulfide oxidation, Journal of Hydrology, 271:171-187.

60. Mayer, K. U., E. O. Frind, and D. W. Blowes, 2002. Multicomponent reactive transport modeling in variably saturated porous media using a generalized formulation for kinetically controlled reactions, Water Resources Research, 38, 1174, doi: 10:1029/2001WR000862.

61. Benner, S. G., D. W. Blowes, C. J. Ptacek and K. U. Mayer, 2002. Rates of sulfate reduction and sulfide mineral precipitation in a permeable reactive barrier, Appl. Geochem., 17, 301-320.

62. Mayer, K. U., D. W. Blowes, and E. O. Frind, 2001. Reactive transport modelling of groundwater remediation by an in-situ reactive barrier for the treatment of hexavalent chromium and trichloroethylene, Water Resources Research, 37:3091-3103.

63. Mayer, K. U., S. G. Benner, E. O. Frind, S. F. Thornton, and D. L. Lerner, 2001. Reactive transport modeling of processes controlling the distribution and natural attenuation of phenolic compounds in a deep sandstone aquifer, Journal of Contaminant Hydrology, 53:341-368.

64. Bain, J. G., K. U. Mayer, J. W. H. Molson, D. W. Blowes, E. O. Frind, R. Kahnt and U. Jenk, 2001. Assessment of the suitability of reactive transport modelling for the evaluation of mine closure options, Journal of Contaminant Hydrology, 52:109-135.

65. Leeming, G. J. S., K. U. Mayer and R. B. Simpson, 1998. Effects of chemical reactions on iterative methods for implicit time stepping, Adv. Water Res., 22:333-347.

C.1.2. Refereed Conference Proceedings

1. Pedretti, D. R. Beckie, K.U. Mayer, 2017. Risk assessment of acidic drainage from waste rock piles using stochastic multicomponent reactive transport modeling, In: Wolkersdorfer, C.; Sartz, L.; Sillanpää, M. & Häkkinen, A.: Mine Water & Circular Economy (Vol I). – p. 696 – 703; Lappeenranta, Finland (Lappeenranta University of Technology).

2. Javadi, M., #Peterson, H., #Blackmore, S., Mayer, K.U., Beckie, R.D., Smith, L., 2012. Evaluating preferential flow in an experimental waste rock pile using unsaturated flow and solute transport modeling. The 9th International Conference on Acid Rock Drainage, May 20-26, 2012, Ottawa, ON, Canada.

3. Bea, S.A., K.U. Mayer, K.T.B. MacQuarrie, 2011. Modeling of reactive transport in a sedimentary basin affected by a glaciation/deglaciation event. Waste Management, Decommissioning and Environmental Restoration for Canada's Nuclear Activities, Canadian Nuclear Society, Toronto, Sep 11 - Sep 14.

4. Bay, D. S., H. E. Peterson, O. Singurindy, C. Aranda, J.W. Dockrey, F. Sifuentes Vargas, K. U. Mayer, L. Smith, B. Klein, and R. D. Beckie, 2009. Assessment of Neutral pH Drainage from Three Experimental Waste-Rock Piles at the Antamina Mine, Peru, In conference proceedings of "Securing the Future and 8th ICARD, June 23-26, 2009, Skellefteå, Sweden.

5. Aranda, C. A., B. Klein, R. D. Beckie, and K. U Mayer, 2009. Assessment of waste rock weathering characteristics at the Antamina mine based on field cells experiment, In conference proceedings of "Securing the Future and 8th ICARD, June 23-26, 2009, Skellefteå, Sweden.

6. Ellis, S. R., K.U. Mayer, and T. A. Al., 2007. Three dimensional diffusive transport in sedimentary rock: Numerical modeling based on non-destructive imaging, In: Conference Proceedings of OttawaGeo2007, 60th Canadian Geotechnical Conference and the 8th Joint CGS/IAH-CNC Groundwater Conference, Ottawa, Ontario, October 21-25.

7. Marica, F., B. J. Balcom, K. U. Mayer, and T. Al, 2007. MRI determination of spatially resolved tracer distributions in a rock matrix diffusion experiment. In: Conference Proceedings of OttawaGeo2007, 60th Canadian Geotechnical Conference and the 8th Joint CGS/IAH-CNC Groundwater Conference, Ottawa, Ontario, October 21-25.

8. Freed, R., R. Dickin, K. U. Mayer, and A. Mitchell, 2007. Effect of saline groundwater on migration of trace metal contaminants, High Lake Mine, Nunavut, In: Conference Proceedings of OttawaGeo2007, 60th Canadian Geotechnical Conference and the 8th Joint CGS/IAH-CNC Groundwater Conference, Ottawa, Ontario, October 21-25.

9. Romano, C. G. K. U. Mayer, and D. W. Blowes, 2006. Reactive transport modeling of AMD release and attenuation at the Fault lake Tailings Area, Falconbridge, Ontario, In: Conference Proceedings of 7th ICARD, March 26-30, St. Louis MO, Eds.: R. Barnhisel, Published by AS MR, 31334 Montavesta Rd., Lexington, KY 40502.

10. Henderson, T.H., K.U. Mayer, B.L. Parker and T. A. Al, 2005. Numerical simulation of density-driven permanganate oxidation of trichloroethylene DNAPL in a sandy aquifer In GQ 2004 Conference Proceedings: Bringing Groundwater Quality Research to the Watershed Scale, Eds.: Barker, J. F. et al., IAHS Publication no. 297:525-530.

11. Williams, R. L., K. U. Mayer, R. T. Amos, D. W. Blowes, and C. J. Ptacek, 2005. Investigation of the performance of organic carbon permeable reactive barriers using dissolved gas analysis. In GQ 2004 Conference Proceedings: Bringing Groundwater Quality Research to the Watershed Scale, Eds.: Barker, J. F. et al., IAHS Publication no. 297:383-388.

12. Mayer, K. U. and E. O. Frind, 2003. Reactive transport modeling for variably saturated groundwater systems – The state of the art. Chapter 32 in: Geochemical Processes in Soil and Groundwater, Measurement – Modelling – Upscaling. Eds.: H. D. Schulz and A. Hadeler, Wiley VCH, Weinheim, Germany, 468-482.

13. Geistlinger, H., D. Lazik, A. Beckmann, D. Eisermann, G. Krauss, and K. U. Mayer, 2003. Experimental and theoretical investigations of oxygen release by a trapped gas phase. Chapter 2 in: Geochemical Processes in Soil and Groundwater, Measurement – Modelling – Upscaling. Eds.: H. D. Schulz and A. Hadeler, Wiley VCH, Weinheim, Germany, 19-36.

14. Geistlinger, H., D. Eisermann, D. Lazik, G. Krauss, A. Beckmann, and K. U. Mayer, 2002. Experimental and theoretical investigations of oxygen release through a trapped gas phase, Acta Universitas Carolinae - Geologica 46 (2/3), 458 - 461.

15. Mayer, K. U., S. G. Benner, E. O. Frind, S. F. Thornton, and D. N. Lerner, 2002. Multicomponent reactive transport modeling of natural attenuation at the Four

Ashes Research Site, UK, in GQ 2001 Conference Proceedings: Groundwater Quality: Natural and enhanced restoration of groundwater pollution, Eds.: Thornton, S. F. and Oswald, S. E., IAHS Publication no. 275, 479-484.

16. Benner, S.G., D. W. Blowes, C. J. Ptacek, and K. U. Mayer, 2000. A permeable reactive wall for treatment of mine drainage: Long-term results. In: ICARD 2000, Proceedings from the Fifth International Conference on Acid Rock Drainage, Sponsored by the Society of Economic Geologists, Denver, Colorado, May 21-24, 1221-1225.

17. Mayer, K. U., D. W. Blowes and E. O. Frind, 2000. Numerical Modeling of acid mine drainage generation and subsequent reactive transport. ICARD 2000, Proceedings from the Fifth International Conference on Acid Rock Drainage, Sponsored by the Society of Economic Geologists, Denver, Colorado, May 21-24,Vol. 1, 135-142.

18. Mayer, K. U., S. G. Benner, D. W. Blowes and E. O. Frind, 1999. The reactive transport model MIN3P: Application to acid mine drainage generation and treatment – Nickel Rim Mine Site, Sudbury, Ontario. In: Sudbury '99, Conference on Mining and the Environment, Sudbury, Ontario, Vol. 1, 145-154.

C.2. SELECTED EXTERNAL PUBLICATIONS

1. Al, T. A., I. D. Clark, L. Kennell, M. Jensen and K. G. Raven (2015). Geochemical Evolution and Residence Time of Porewater in Low-permeability Rocks of the Michigan Basin, Southwest Ontario. Chemical Geology. DOI: 10.1016/j.chemgeo.2015.03.005

2. Anawar, H. Md. (2013) Impact of climate change on acid mine drainage generation and contaminant transport in water ecosystems of semi-arid and arid mining areas – Review article, Physics and Chemistry of the Earth, Parts A/B/C, 58–60, 13-21.

3. Richard T. Amos, David W. Blowes, Brenda L. Bailey, David C. Sego, Leslie Smith, A. Ian M. Ritchie (2014) Waste-rock hydrogeology and geochemistry – Review, Applied Geochemistry, Doi: 10.1016/j.apgeochem.2014.06.020.

4. Bilardi, S., Amos, R.T., Blowes, D.W., Calabro, P.S., Moraci, N. (2013). Reactive Transport Modeling of ZVI Column Experiments for Nickel Remediation. Ground Water Monitoring and Remediation, 33, 97-104. DOI: 10.1111/j.1745-6592.2012.01417.

5. Broholm, M.M., M. Christophersen, U. Maier, E. H. Stenby, P. Höhener and P. Kjeldsen. (2005). Compositional Evolution of the Emplaced Fuel Source in the Vadose Zone Field Experiment at Airbase Værløse, Denmark, Environmental Science & Technology 39, 8251–8263.

6. Clifton, L.M., P. R. Dahlen and P. C. Johnson (2014). Effect of Dissolved Oxygen Manipulation on Diffusive Emissions from NAPL-Impacted Low Permeability Soil Layers. Environmental Science & Technology 48, 5127–5135.

7. De Biase, C., A. Carminati, S. E. Oswald and M. Thullner (2013) Numerical modeling analysis of VOC removal processes in different aerobic vertical flow systems for groundwater remediation, Journal of Contaminant Hydrology, 154, 53-69.

8. De Biase, C., Maier, U., Baeder-Bederski, O., Bayer, P., Oswald, S., Thullner, M. (2012): Removal of volatile organic compounds in vertical flow filters: predictions from reactive transport modeling, Ground Water Monit. Remediat. 32 (2), 106 – 121

9. De Biase, C., Reger, D., Schmidt, A., Jechalke, S., Reiche, N., Martínez-Lavanchy, P.M., Rosell, M., van Afferden, M., Maier, U., Oswald, S.E., Thullner, M. (2011): Treatment of volatile organic contaminants in a vertical flow filter: relevance of different removal processes, Ecol. Eng. 37 (9), 1292 – 1303.

10. Gibson, B., Amos, R.T., Blowes, D.W. (2011) Reactive transport modeling of isotope fractionation in permeable reactive barriers. Environmental Science & Technology 45, 2863–2870.

11. Grathwohl, P., Rügner, H., Wöhling, T., Osenbrück, K., Schwientek, M., Gayler, S., Wollschläger, U., Selle, B., Pause, M., Delfs, J.-O., Grzeschik, M., Weller, U., Ivanov, M., Cirpka, O.A., Maier, U., Kuch, B., Nowak, W., Wulfmeyer, V., Warrach-Sagi, K., Streck, T., Attinger, S., Bilke, L., Dietrich, P., Fleckenstein, J.H., Kalbacher, T., Kolditz, O., Rink, K., Samaniego, L., Vogel, H.-J., Werban, U., Teutsch, G. (2013): Catchments as reactors: a comprehensive approach for water fluxes and solute turnover, Environmental Earth Sciences 69 (2), 317 – 333.

12. Höhener, P., N. Dakhel, M. Christophersen, M. Broholm and P. Kjeldsen (2006). Biodegradation of hydrocarbons vapors: Comparison of laboratory studies and field investigations in the vadose zone at the emplaced fuel source experiment, Airbase Værløse, Denmark, Journal of Contaminant Hydrology, 88(3–4), 337-358.

13. Jamieson-Hanes, J.H., Amos, R.T., Blowes, D.W. (2012). Chromium Isotope Fractionation During Reduction of Cr(VI) Under Saturated Flow Conditions. Environmental Science & Technology, 46, 13311–13316.

14. Jamieson-Hanes, J.H., Amos, R.T., Blowes, D.W. (2012). Reactive Transport Modeling of Chromium Isotope Fractionation during Cr(VI) Reduction. Environmental Science & Technology, 46, 13311–13316.

15. Jamieson-Hanes, J.H., Lentz, A. M., Amos, R.T., C. J. Ptacek and Blowes, D.W. (2014). Examination of Cr(VI) treatment by zero-valent iron using in situ, real-time X-ray absorption spectroscopy and Cr isotope measurements. Geochimica et Cosmochimica Acta, 142, 299-313.

16. Jeen, S.-W., Amos, R.T., Blowes, D.W. (2012). Modeling Gas Formation and Mineral Precipitation in a Granular Iron Column. Environmental Science & Technology, 46, 6742–6749.

17. Maier, U., Flegr, M., Rügner, H., Grathwohl, P. (2013): Long-term solute transport and geochemical equilibria in seepage water and groundwater in a catchment cross section, Environmental Earth Sciences 69 (2), 429 – 441

18. Maier, U. and Grathwohl, P. (2006): Numerical experiments and field results on the size of steady state plumes, Journal of Contaminant Hydrology, 85(1–2), 33-52.

19. Maier, U., H. Rügner and P. Grathwohl (2007) Gradients controlling natural attenuation of ammonium, Applied Geochemistry, 22(12), 2606-2617

20. suk O, J., S.-W. Jeen, R. W. Gillham and L. Gui (2009) Effects of initial iron corrosion rate on long-term performance of iron permeable reactive barriers: Column experiments and numerical simulation, Journal of Contaminant Hydrology, 103(3–4), 145-156.

21. Trauth, N., Schmidt, C., Maier, U., Vieweg, M., Fleckenstein, J.H. (2013): Coupled 3-D stream flow and hyporheic flow model under varying stream and ambient groundwater flow conditions in a pool-riffle system, Water Resources Research 49 (9), 5834 – 5850

22. Trauth, N., Schmidt, C., Vieweg, M., Maier, U., Fleckenstein, J.H. (2014): Hyporheic transport and biogeochemical reactions in pool-riffle systems under varying ambient groundwater flow conditions, Journal of Geophysical Research 119 (5), 910 – 928

23. Wanner, C., Druhan, J.L., Amos, R.T., Alt-Epping, P., Steefel, C.I. (2014). Benchmarking the simulation of Cr isotope fractionation. Computational Geosciences, DOI: 10.1007/s10596-014-9436-9.

24. Watson, I., S. E. Oswald, S. A. Banwart, R. S. Crouch, and S. F. Thornton (2005). Modeling the Dynamics of Fermentation and Respiratory Processes in a Groundwater Plume of Phenolic Contaminants Interpreted from Laboratory- to Field-Scale, Environmental Science & Technology, 39, 8829–8839.

25. Weber, A., Ruhl, A.S., Amos, R.T. (2013). Investigating dominant processes in ZVI permeable reactive barriers using reactive transport modeling. Journal of Contaminant Hydrology, 151, 68-82.

26. Ying, S.C., B. D. Kocar, S. D. Griffis, and S. Fendorf (2011). Competitive Microbially and Mn Oxide Mediated Redox Processes Controlling Arsenic Speciation and Partitioning. Environmental Science & Technology, 45, 5572–5579.

27. Ying, S.C., B. D. Kocar and S. Fendorf (2012). Oxidation and competitive retention of arsenic between iron- and manganese oxides. Geochimica et Cosmochimica Acta, 96, 294-303.

REFERENCES

Bea, S.A., J. Carrera, C. Ayora and F. Batlle. (2010). Pitzer Algortithm: Efficient implementation of Pitzer equations in geochemical and reactive transport models. Computers & Geosciences, 36, 526-538.

Bea, S.A., K.U. Mayer and K.T.B. MacQuarrie (2016). Reactive transport and thermo-hydro-mechanical coupling in deep sedimentary basins affected by glaciation cycles: model development, verification, and illustrative example, Geofluids (2016), 16, 279–300

Harvie, C.E., N. Moller and J.H. Weare (1984). The prediction of mineral solubilities in natural waters: The Na-K-Mg-Ca-H-Cl-SO_4-OH-HCO_3-CO_3-CO_2-H_2O system to high ionic strengths at 25^{o}C. Geochimica et Cosmochimica Acta, 48, 723-751.

Greenberg, J.P. and N. Moller (1989). The prediction of mineral solubilities in natural-waters - A chemical-equilibrium model for the Na-K-Ca-Cl-SO_4-H_2O system to high-concentration from 0^o to 250^{o}C. Geochimica et Cosmochimica Acta, 53, 2503-2518.

MacInnes, D.A., (1919). The activities of the ions of strong electrolytes: Journal American Chemical Society, 41, 1086-1092.

Pitzer, K.S. and Mayorga, G. (1973). Thermodynamics of electrolytes. II. Activity and osmotic coefficients for strong electrolytes with one or both ions univalent, Journal of Physical Chemistry, 77 (19), 2300–2307.